Development of an elongational-flow microprocess for the production of size-controlled nanoemulsions : application to the preparation of composite and hybrid polymeric microparticles

Wei Yu

UNIVERSITÉ DE STRASBOURG

ÉCOLE DOCTORALE ED182

[ICS, Institut Charles Sadron-UPR 22 CNRS]

THÈSE présentée par :

Wei YU

soutenue le : **25 Novembre 2015**

pour obtenir le grade de : **Docteur de l'université de Strasbourg**

Discipline/ Spécialité : Chimie de matériaux/Génie des procédés d'émulsification et de polymérisation

Développement d'un microprocédé discontinu et continu pour la production de nanoémulsions de tailles contrôlées : application à la préparation de microparticules de polymère composites et hybrides

THÈSE dirigée par :	Christophe SERRA	Professeur, Université de Strasbourg
RAPPORTEURS :	Elodie Bourgeat-Lami	Directrice de Recherche, CNRS
	Michele Giordano	Chercheur, CNR (Italie)
AUTRES MEMBRES DU JURY :	Abraham Chemtob	Maître de conférences, Université de Haute Alsace

RESUME DE THESE

Développement d'un microprocédé pour la production de nanoémulsions de tailles contrôlées : application à la préparation de microparticules de polymère composites et hybrides

1 Introduction

Les émulsions de tailles nanométriques, ou nanoémulsions, sont très largement employées depuis des décennies dans des secteurs industriels tels que les industries laitières, agroalimentaires, pharmaceutiques, la cosmétique, l'agriculture etc. Les méthodes conventionnelles de préparation de ces nanoémulsions peuvent être classées selon le niveau d'énergie nécessaire à la dispersion sous forme de gouttelettes nanométriques d'une phase liquide dans une autre immiscible. Les méthodes dites à hautes énergies reposent sur l'emploi principalement d'une énergie d'origine mécanique. Ainsi trouve-t-on l'homogénéiseur à haute pression (~2000 bars), les mélangeurs à cisaillement de type rotor-stator, les mélangeurs statiques et les dispositifs à ultrasons et ceux à membrane. Les nanogouttelettes sont obtenues par transfert d'énergie pour rompre les gouttelettes les plus grosses en plus petites en présence d'un surfactant dont le but est d'abaisser la tension superficielle et faciliter ainsi la rupture des gouttelettes. A l'opposé, les méthodes dites à faible énergie tirent avantage de la réduction du potentiel chimique de la phase dispersée sous forme de nanogouttelettes pour promouvoir l'émulsification. Cette dernière s'opère généralement quand la composition des phases ou leurs propriétés variées brusquement ; ainsi parle-t-on d'émulsification spontanée, d'inversion de phase sous l'effet d'un changement de composition ou de température. L'existence d'une tension superficielle très faible est alors un prérequis indispensable qui est généralement atteint par le choix judicieux de la composition de l'émulsion. Cependant ces deux types de méthodes souffrent généralement d'un mauvais contrôle de la taille et d'une large distribution de tailles des nanogouttelettes.

Dans ces travaux de thèse, une nouvelle méthode à basse énergie basée sur un procédé microfluidique fut développée afin de produire des nanoémulsions polymérisables (à base de MMA[1]) de tailles contrôlées entre 50 et 500 nm. Ce procédé, représenté sur la Figure 1A, est composé de deux pousses seringues moyenne pression, deux seringues en acier, des tubes en PTFE[2] et d'un micromélangeur à flux élongationnel en PEEK[3] de différentes

[1] méthyl méthacrylate

[2] polytétrafluoroéthylène

[3] polyétheréthercétone

géométries Figure 1B. Le principe opératoire de ce nouveau procédé repose sur le transfert alternatif de l'émulsion d'une seringue à l'autre au travers de la restriction du micromélangeur (c.-à-d. du microcanal de diamètre 150, 250 ou 500 µm). De par sa géométrie particulière, ce micromélangeur induit un fort écoulement élongationnel au passage du microcanal qui, selon la théorie développée par Grace[4], est bien plus efficace qu'un écoulement de cisaillement pur pour rompre une gouttelette en des gouttelettes plus petites. Le mouvement d'un va-et-vient des deux pousse seringue est assimilé à un cycle. Les deux phases liquides composant l'émulsion sont chargées sans prémélange directement dans l'une des seringues (volume total 5mL). La phase dispersée comprenait le MMA, un agent réticulant (monomère acrylate bifonctionnel, TPGDA[5]), un agent anti murissement d'Ostwald (Hexadécane) et un amorceur de polymérisation thermique (AIBN[6]) ou un photoamorceur (HCPK[7]). Quant à la phase continue, elle était composée d'eau distillée et d'un surfactant (SDS[8]). Puis les deux pousses seringue sont allumés et forcés à travailler en opposition de phase à un débit donné *via* leur logiciel de contrôle. Après un certain nombre de cycles, l'opération est arrêtée et l'émulsion est déchargée et analysée par diffusion de la lumière pour en connaître la taille moyenne des nanogouttelettes et leur distribution en tailles (PDI). Une valeur du PDI inférieure à 0.2 est communément admise comme le reflet d'une émulsion monodisperse. Ce microprocédé tel que décrit fonctionne en mode dit discontinu. L'influence des paramètres opératoires, composés des paramètres de procédé (nombres de cycles, débit au travers du micromélangeur), des paramètres géométriques du micromélangeur (angle, taille du microcanal) et des paramètres de composition (concentration en surfactant et en MMA, fraction volumique de MMA dans l'émulsion, rapport des viscosités de la phase dispersée et de la phase continue), ont été scrupuleusement étudiés. Les nombreux résultats expérimentaux furent utilisés afin de déterminer une équation empirique entre nombres adimensionnels permettant de prédire la taille des nanogouttelettes en fonction des paramètres opératoires. A titre de comparaison, une nanoemulsion de même composition fut également produite à l'aide d'un dispositif rotor-stator (Ultraturrax) ce qui a permis de montré la très grande efficacité du microprocédé développer puisque les nanoémulsions obtenues furent plus fines (tailles plus petites) et sensiblement plus monodisperses.

[4] Grace, H. P., Dispersion phenomena in high viscosity immiscible fluid systems and application of static mixers as dispersion devices in such systems. *Chemical Engineering Communications* **1982,** *14* (3-6), 225-277.

[5] tri(propylene glycol) diacrylate

[6] azobisisobutyronitrile

[7] 1-hydroxycyclohexyl phenyl ketone

[8] sodium dodecyl sulfate

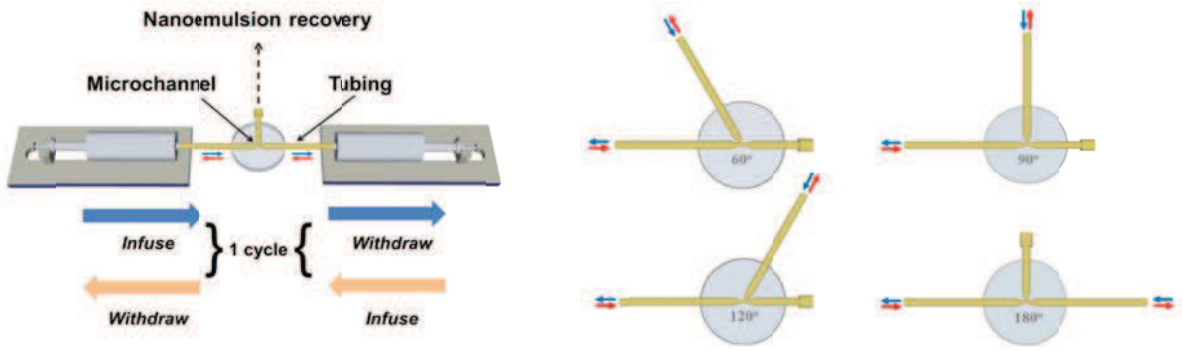

A) B)

Figure 1. A): schéma du microprocédé (non à l'échelle); B) 4 micromélangeurs à flux élongationnel de différents angles

Fort du succès et de l'efficacité du microprocédé discontinu développé, nous l'avons modifié pour une production continue (Figure 2). Deux pousses seringue supplémentaires ont été utilisés pour alimenter le procédé en phase continue (water phase) et en phase dispersée (MMA, oil phase). Le micromélangeur présentait alors 4 ports (un de plus que dans la version discontinue) : un pour l'alimentation, un pour la sortie et deux pour l'écoulement élongationnel alternatif. Tous ces ports furent reliés entre eux par 4 microcanaux. L'adjonction d'une vanne antiretour sur la ligne d'alimentation et d'une vanne de contrôle de la pression sur la ligne de sortie fut nécessaire pour éviter d'une part un retour dans les pousses seringue d'alimentation et d'autre part pour ajuster le débit de sortie à celui imposé en entrée. La faisabilité d'une opération continue fut alors démontrée avec des débits de production d'émulsions de tailles contrôlées allant jusqu'à 0.75 mL/min soit environ une 1 L d'émulsion produite par jour.

Par la suite les nanoémulsions produites ont été converties en suspension colloïdales de nanoparticules de polymère après qu'elles eurent été polymérisées par voie thermique (Figure 3A) ou par irradiation UV (Figure 3B). Après avoir été produites, les nanoémulsions furent chargées soit dans un bécher qui fut placé dans l'enceinte fermée d'un four à 70°C pendant une nuit complète (12h) ou dans la seringue d'un pousse seringue et injectées dans un tube en PTFE (1.06 mm de diamètre interne) irradié par une lampe UV (temps de résidence de 16 min). La taille des nanoparticules de poly(MMA) obtenus après polymérisation fut analysée par diffusion de la lumière en fonction du taux de dilution. Seul le procédé thermique permit d'obtenir des nanoparticules de tailles sensiblement identiques à celle des nanogouttelettes de départ.

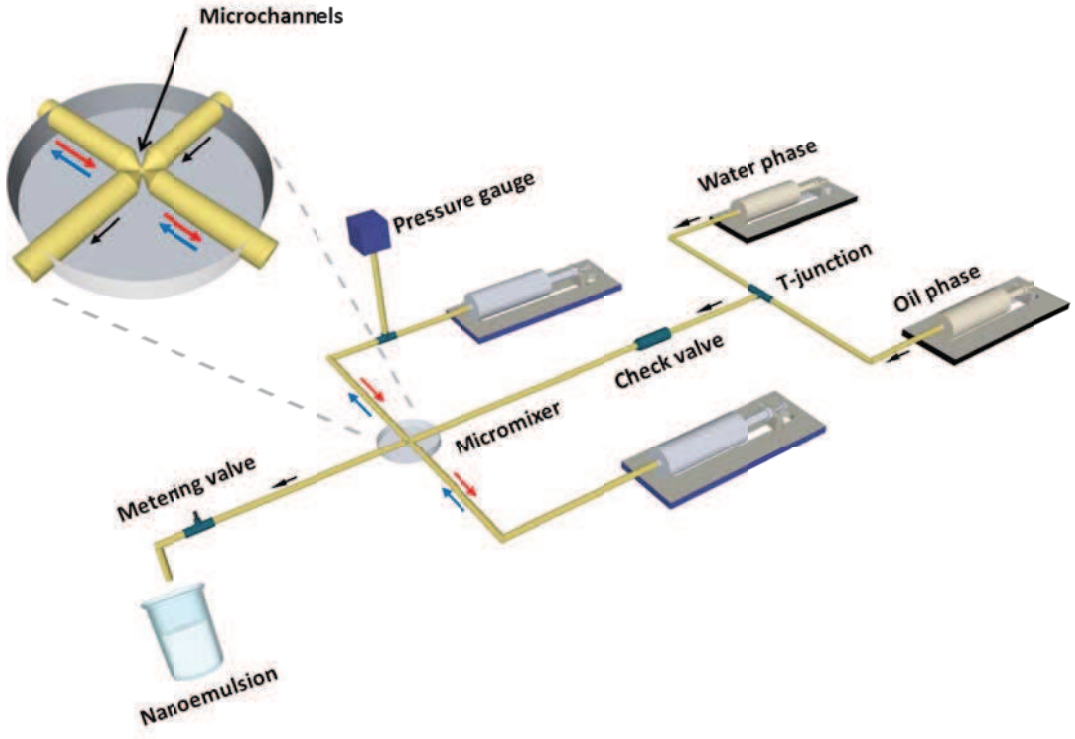

Figure 2. Schéma du microprocédé à flux élongationnel pour la production de nanoémulsions en continu

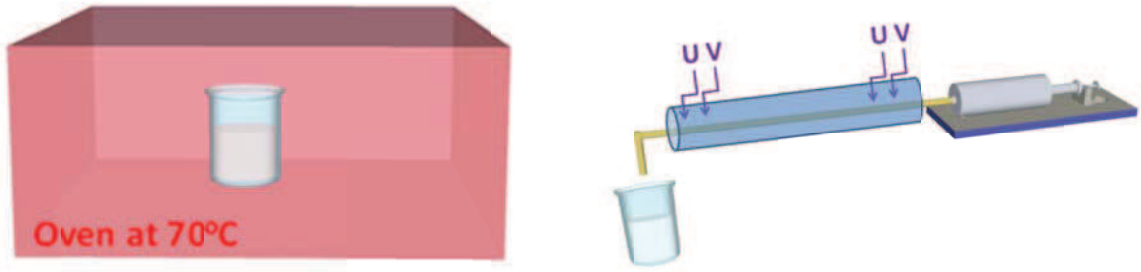

A) B)

Figure 3. Schémas (non à l'échelle) des différentes méthodes de polymérisation des nanoémulsions : A) polymérisation thermique; B) polymérisation par irradiation UV.

Une fois produites selon le microprocédé discontinu à flux élongationnel précédemment décrit, des suspensions colloïdales de nanoparticules de poly(MMA-co-TPGDA) furent utilisées dans des dispositifs microfluidiques à un ou deux capillaires pour produire des microparticules de polymère composites simples ou de type cœur-écorce (Figure 4). Du monomère acrylamide, un agent de réticulation (N,N'-Methylene-bisacrylamide) et un photoamorceur hydrophile (DMHA[9]) furent ajoutés à la phase aqueuse de ces suspensions

[9] Genocure photoiniator

colloïdales pour les rendre polymérisables. Puis la solution résultante fut utilisée comme phase dispersée (Figure 4A) ou comme phase interne (Figure 4B) et injectée dans les dispositifs au moyen d'un capillaire de très faible diamètre (typiquement 50-150 µm de diamètre interne). Pour la production de microparticules simples, la phase dispersée était une huile de silicone. Au contact de cette dernière (à l'extrémité du capillaire), des microgouttelettes de la phase dispersée sont spontanément formées. Elles furent par la suite, une fois détachées du capillaire, polymérisées par irradiation UV en ligne pour donner lieu à des microparticules de poly(acrylamide) contenant des milliers de nanoparticules de poly(MMA-co-TPGDA). Pour la production de microparticules coeur-écorce, la suspension colloïdale polymérisable fut utilisée comme phase interne alors qu'une solution de TPGDA et d'un photoamorceur (phase intermédiaire) fut injectée dans un second capillaire entourant le premier. A l'extrémité des deux capillaires et au contact d'une phase continue composée d'eau distillée viscosifiée avec de la méthyle cellulose se forma des gouttelettes doubles qui furent polymérisées par irradiation UV en ligne pour donner lieu à des microparticules composées d'un cœur en poly(acrylamide) contenant des milliers de nanoparticules de poly(MMA-co-TPGDA) et d'une écorce en poly (TPGDA).

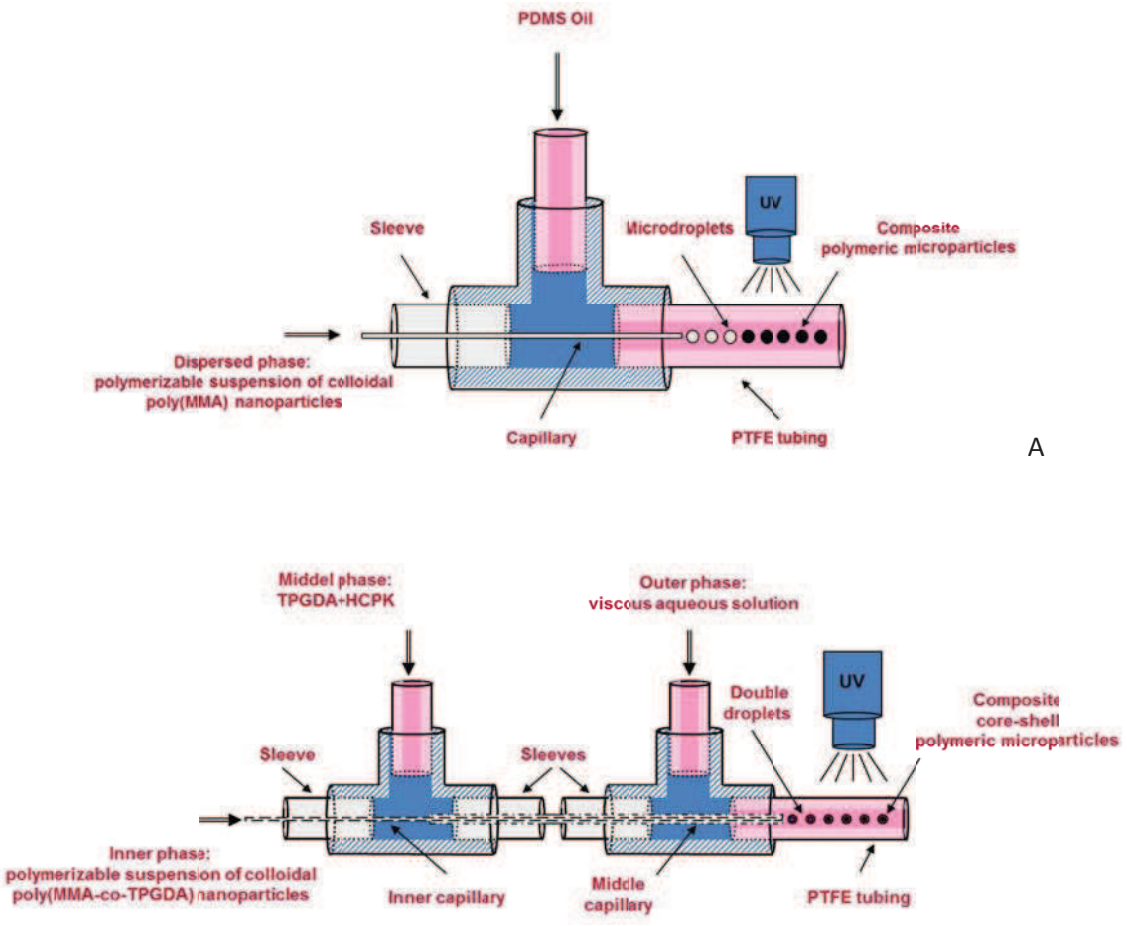

Figure 4. Schémas des dispositifs microfluidiques à capillaires utilisés pour la production de microparticules de polymère composite simple (A) ou cœur-écorce (B)

Outre ces deux morphologies différentes de microparticules de polymère composites, une structure bien plus complexe a été préparée à partir de ces suspensions colloïdales polymérisables. En partant du dispositif de la Figure 4B et en ajoutant un sel d'or (HAuCl4) dans la phase interne et une solution de sel d'argent ($AgNO_3$) et de DEG[10] dans la phase intermédiaire, des microparticules polymères hybrides multi-échelle et multi-domaine ont été préparées comportant des nanoparticules d'or et de poly(MMA) dans le cœur et des nanoparticules d'argent dans et à la surface de l'écorce. La morphologie de telles microparticules a été caractérisée par MEB[11] et par EDXS[12] en mode compo pour localiser les atomes lourds (Ag et Au).

2 Résultats choisis

2.1 Production de nanoemulsions en mode discontinu

Les effets combinés du diamètre du microcanal et du débit sont représentés dans la Figure 5. Plus le débit est élevé ou lorsque la restriction est plus petite, plus le diamètre obtenu est petit. Dans une géométrie telle que celle du micromélangeur étudié, il est attendu que la vitesse de déformation élongationnelle soit importante. Or la théorie de Grace prévoit que la rupture d'une goutte s'opère quand, à rapport de viscosité constant, le nombre Capillaire (Eq. 1) atteint une valeur critique. Pour un écoulement élongationnel, ce nombre est directement proportionnel à la vitesse de déformation élongationnelle ($\dot{\varepsilon}$). Cette dernière peut, par analogie avec les écoulements de polymères fondus au travers d'une filière (approche de Cogswell[13]), en considérant de plus la correction de Bagley[14] et en supposant que l'émulsion se comporte comme un fluide newtonien en écoulement laminaire, s'écrire selon l'Eq. 2.

3.1 **Eq. 1**

$$\mathrm{Ca} = \frac{\eta\,\dot{\varepsilon}\,D_d}{2\,\sigma}$$

3.2 **Eq. 2**

$$\dot{\varepsilon} = \frac{K_f\,\rho\,q^2}{3\,\pi^2\,\mu\,L_h{}^2\,D_h{}^2}$$

[10] diéthylène glycol

[11] microcopie électronique à balayage

[12] spectroscopie de rayons X à dispersion d'énergie

[13] Cogswell, F. N., Converging flow of polymer melts in extrusion dies. *Polymer Engineering & Science* **1972,** *12* (1), 64-73.

[14] Paradkar, A.; Kelly, A.; Coates, P.; York, P., Shear and extensional rheology of hydroxypropyl cellulose melt using capillary rheometry. *Journal of Pharmaceutical and Biomedical Analysis* **2009,** *49*

On constate ainsi que plus le débit (q) est élevé et le diamètre de la restriction (D_h) petit, plus $\dot{\varepsilon}$ est élevé ce qui induit selon l'Eq. 1 à des diamètres de nanogouttelettes (D_d) plus faibles comme expérimentalement observé. Par ailleurs, la variation du diamètre des nanogouttelettes en fonction du nombre de cycles présente une décroissance pour atteindre une valeur plateau à haut nombre de cycles. Ce plateau est atteint d'autant plus rapidement que le débit est grand et le diamètre de la restriction petit. Cela montre qu'il faut un certain temps pour que le diamètre minimum de gouttelettes soit atteint. Ceci est dû au profile de vitesse dans la restriction qui fait que toutes les gouttelettes passant dans cette restriction ne subissent pas la même la vitesse de déformation élongationnelle. Il faut ainsi plusieurs passages pour qu'*in fine* toutes les gouttelettes atteignent la même taille. On notera que dans la gamme 30 – 500 nm, toutes les nanogouttelettes obtenues étaient monodisperses, c.-à-d. que le PDI était inférieur à 0.2.

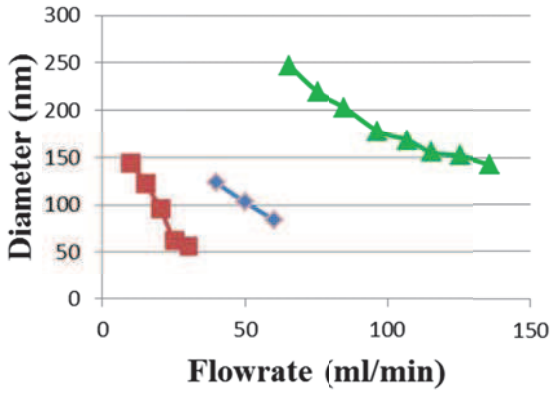

Figure 5. Variation du diamètre des nanogouttelettes en fonction du débit pour différents diamètres du microcanal (▲-: 150 µm, -♦-: 250 µm, -■-: 500 µm). Tous les autres paramètres étant fixés à leur valeur de référence (angle de 180°, 800 cycles, 15% en volume de MMA, 2.4 % en masse/MMA de SDS et 4% en masse/MMA de hexadécane)

La Figure 6 présente les variations du diamètre des nanogouttelettes en fonction de la concentration massique de SDS par rapport au MMA pour différents débits et nombres de cycles. Comme attendu plus la concentration de SDS augmente plus la taille des nanogouttelettes diminue pour atteindre une valeur limite Cela correspond à la diminution de la tension superficielle avec l'augmentation de la concentration de SDS et la valeur constante de celle-ci lorsque la surface de toutes les gouttelettes est recouverte de surfactant. On observe également que pour de faibles concentrations de SDS (par exemple 1% en masse/MMA), des nanogouttelettes monodisperses de taille variables peuvent être facilement obtenus en faisant varier le nombre de cycles et le débit. Cela représente un avantage indéniable de notre microprocédé par rapport aux procédés plus conventionnels pour lesquels les paramètres de procédé ont en généralement peu d'influence ; la taille des

gouttelettes étant « réglée » au moyen de la quantité de surfactant ajouté.

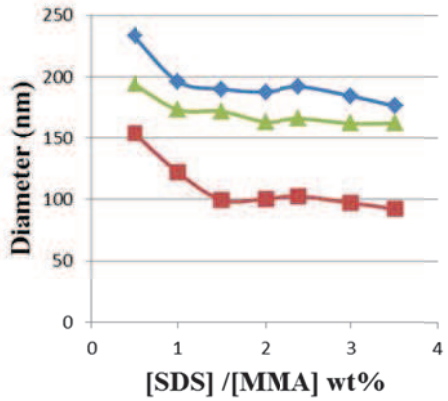

Figure 6. Variation du diamètre des nanogouttelettes en fonction de la concentration massique de SDS par rapport au MMA pour différents débits et nombres de cycles (-♦-: 40 mL/min et 100 cycles, -▲-: 50 mL/min et 100 cycles, -■-: 50 mL/min et 800 cycles). Tous les autres paramètres étant fixés à leur valeur de référence (angle de 180°, diamètre du microcanal 250 µm, 15% en volume de MMA et 4% en masse/MMA de hexadécane)

Des nombreux résultats expérimentaux, une équation reliant le diamètre normalisé (D^*_{th}) des nanogouttelettes (par apport au diamètre de la seringue, D_s) en fonction des nombres de Reynolds et de Weber, de la fraction volumique de MMA dans l'émulsion (ϕ), du rapport des viscosités de la phase dispersée et de la phase continue (η_d/η_c) et du facteur de contraction (rapport de la section des seringues utilisée et du microcanal, CF) fut trouvée (Eq. 3). Elle prédit avec un excellent accord la taille des nanogouttelettes dans la gamme 50 – 300 nm (Figure 7).

3.3 Eq. 3 $$D^*_{th} = 2.56\text{x}10^{-11}\ Re^{-9/4}\ \eta_d/\eta_c^{1/3}\ \phi^{1/2}\ We^{-3/2}\ CF^{1/3}$$

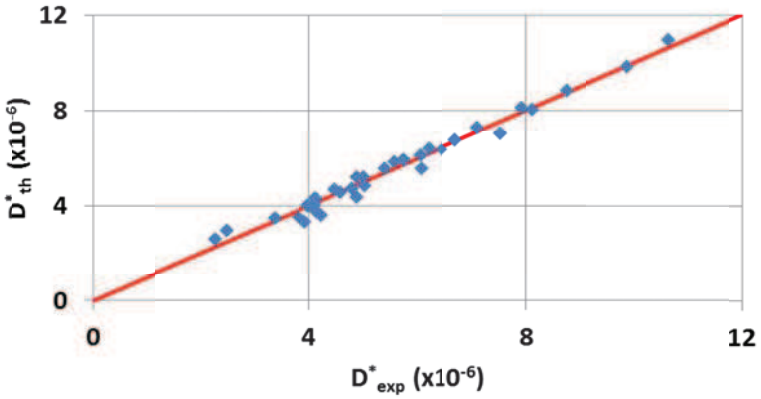

Figure 7. Variation du diamètre normalisé des nanogouttelettes calculé selon l'Eq. 3 en fonction du diamètre expérimental sur 36 points expérimentaux (erreur résiduelle = $7.43\text{x}10^{-2}$)

2.2 Production de nanoémulsions en mode continu

La faisabilité d'une production continue de nanogouttelettes monodisperses de taille contrôlable sur la base de notre microprocédé à flux élongationnel a été démontrée. La Figure 8 présente ainsi les variations du diamètre des nanogouttelettes pour deux restrictions et plusieurs débits d'alimentation différents. On observe que les tailles des nanogouttelettes obtenues en procédé continu sont systématiquement plus grandes que celles obtenues dans les mêmes conditions mais avec un débit d'alimentation nul (c.-à-d. en procédé discontinu) et qu'elles augmentent lorsque le débit d'alimentation augmente. On observe également que l'effet du nombre de cycles est quasi négligeable en procédé continu. Ce dernier est un point important car il signifie qu'une production continue et de qualité constante peut être envisagée. Ces résultats montrent également que la taille des nanogouttelettes peut être facilement contrôlée en jouant sur le rapport débit élongationnel sur débit d'alimentation. Plus ce rapport est élevé, plus les gouttelettes sont petites et se rapprochent de celles obtenues en procédé discontinu.

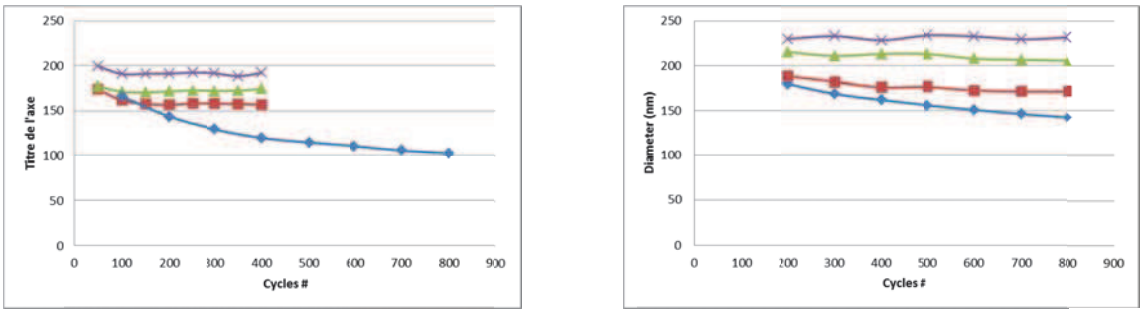

A) B)

Figure 8. Variation du diamètre des nanogouttelettes en fonction du nombre de cycles (c.-à-d. du temps) pour une restriction de 250 µm (A) et de 500 µm (B) et pour différent débits d'alimentation (-x- : 0.75 mL/min, -▲-: 0.5 mL/min, -■-: 0.25 mL/min, -♦-: 0 mL/min). Tous les autres paramètres étant fixés à leur valeur de référence (angle de 180°, débit élongationnel de 50 mL/min, 15% en volume de MMA, 2.4% de SDS/MMA et 4% en masse/MMA de hexadécane) excepté le débit élongationnel pour la restriction de 500 µm qui fut fixé à 136 mL/min

2.3 Production de microparticules de polymère composites multi-domaine

Avant de synthétiser les microparticules de polymère composites, la nanoémulsion de référence fut polymérisée pour obtenir des nanoparticules de polymère. Deux techniques de

polymérisation - l'une thermique, l'autre par irradiation UV - furent employées. La taille des nanoparticules ainsi obtenues fut comparée à celle des nanogouttelettes d'origine en fonction du taux de dilution de la nanoémulsion (Figure 9). Il apparait ainsi que les nanoparticules obtenues par irradiation UV de la nanoémulsion non diluée présentent une taille sensiblement plus grande que celle des nanogouttelettes d'origine (130 nm *vs* 56 nm). Toutefois en augmentant le taux de dilution, cette taille diminue et rejoint celle des nanogouttelettes pour un taux de 95%. Il est probable que la forte concentration de nanogouttelettes diffuse la lumière UV et empêche donc sa pénétration au cœur de la solution. Ainsi seules les nanogouttelettes situées à la périphérie du tube PTFE sont irradiées et peuvent polymériser. Les autres nanogouttelettes servant de réservoir à celles qui polymérisent compte tenu du fait que le MMA est légèrement soluble dans l'eau. Pour une polymérisation thermique de la nanoémulsion non diluée, la différence de taille est encore plus grande (184 nm *vs* 56 nm) et est attribuée à une déstabilisation (coalescence) de la nanoémulsion lors de l'augmentation de la température jusqu'à 70°C. Une dilution autorise la réduction de cet écart mais dans l'intervalle de taux de dilution testés ne permet de recouvrir la taille originale des nanogouttelettes.

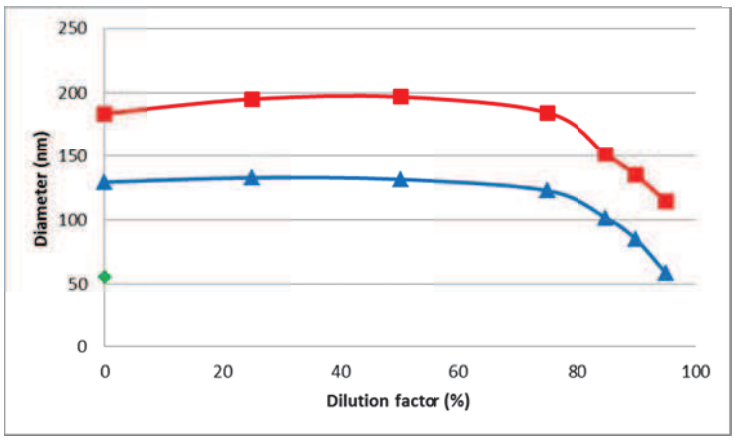

Figure 9. Variation du diamètre des nanoparticules (poly(TPGDA-co-MMA) en fonction du taux de dilution de la nanoémulsion originale (-♦-), polymérisée par irradiation UV (-▲-) ou thermiquement (-■-)

Une fois obtenues ces nanoparticules furent employées avec succès pour la synthèse de microparticules de polymère composites préparées avec le dispositif microfluidique de la Figure 4A. La Figure 10 présente ainsi des clichés MEB de microparticules de poly(acrylamide) dopées avec des nanoparticules de Poly(MMA-co-TPGDA) à différents pourcentages de TPGDA. Des microparticules de morphologie plus complexe, de type coeur-écorce, ont également été obtenues grâce au dispositif microfluidique de la Figure 4B. Les clichés MEB de la Figure 11 montrent très clairement la structure cœur-écorce et la présence de nombreuses nanoparticules de poly(MMA-co-TPGDA) dans le cœur.

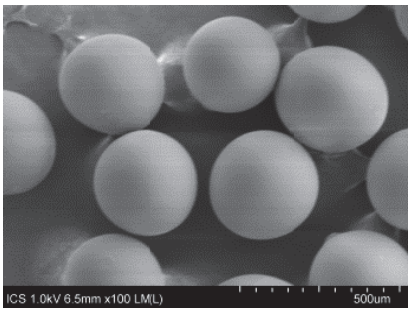

A)

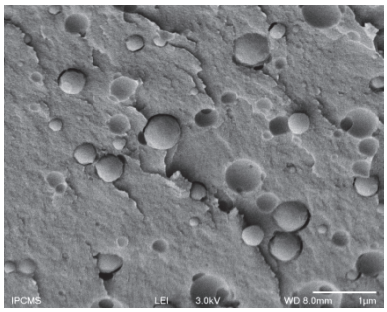

B)

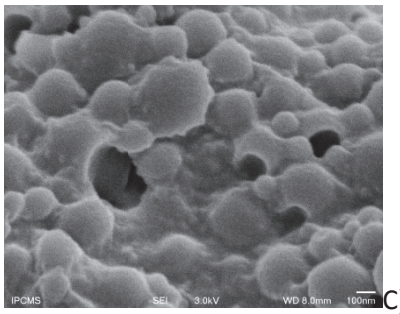

C)

Figure 10. Clichés de microcopie électronique à balayage de microparticules de poly(acrylamide) (A), de leur matrice montrant la présence de nombreuses nanoparticules de poly(TPGDA) (B) et de la surface dans le cas du dopage avec des nanoparticules de poly(MMA-co-TPGDA) à 50:50 (C)

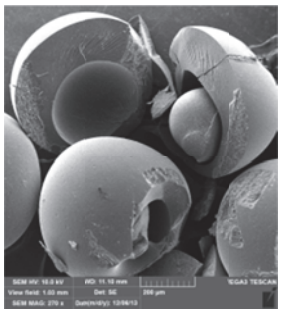

A)

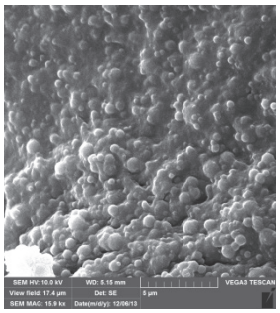

B)

Figure 11. Clichés de microcopie électronique à balayage d'une microparticule coupée de structure cœur-écorce (poly(acrylamide)– poly(TPGDA))(A) et de l'intérieur de sa matrice montrant des nanoparticules de poly(MMA-co-TPGDA) à 50:50 (B). Débit de la phase continue, 130 µL/min, de la phase intermédiaire (écorce), 4 µL/min et de la phase interne (cœur), 1.5 µL/min.

2.4 Production de microparticules polymères hybrides multi-échelle et multi-domaine

En s'appuyant sur les procédés microfluidiques développés pour la synthèse de micro- et

nanoparticules de polymère (cf. Figure 1, Figure **3**, Figure **4**) nous avons pu préparer des matériaux polymères encore plus complexes dans leur morphologie que ceux présentés au paragraphe précèdent. En effet, en ajoutant des sels d'or et d'argent respectivement dans les phases composant le cœur et l'écorce et après une réduction *in situ* déclenchée par l'irradiation UV (dont le but était également de polymériser les gouttelettes doubles), nous avons obtenus des microparticules hybrides organique/inorganiques de structure cœur-écorce (Figure 12B) présentant de multiples échelles. Une échelle de la dizaine de nanomètres avec les nanoparticules d'or (Figure 12F) et d'argent (Figure 12D,E), de la centaine de nanomètres avec celles de poly(MMA) (Figure 12C) et de la centaine de micromètres avec le cœur et l'écorce (Figure 12A). Il est a noté que les nanoparticules d'argent présent dans l'écorce ont été observées au voisinage des trous laissés par l'évaporation du DEG. En effet, le sel d'argent utilisé comme précurseur du métal argent fut dissout dans le DEG afin de pouvoir le mélanger avec le monomère de l'écorce (TPGDA).

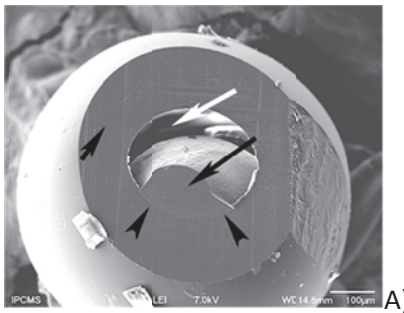
A)

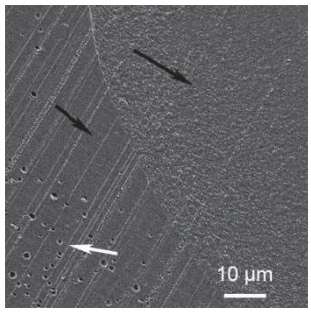

B)

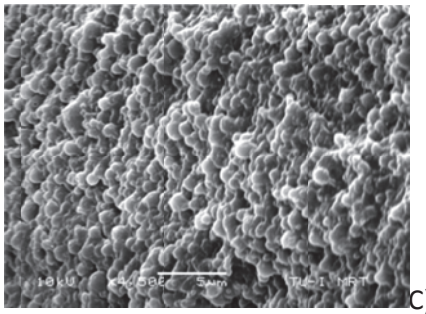
C)

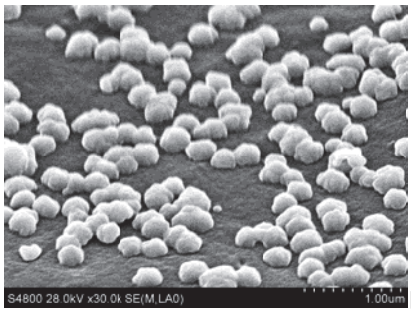

D)

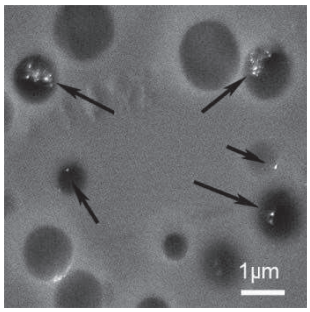

E)

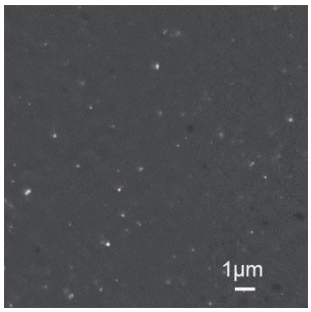

F)

Figure 12. Clichés de microcopie électronique à balayage d'une microparticule polymère hybride de structure cœur-écorce (A), d'un grossissement de l'interface cœur- écorce [poly(acrylamide) – poly(TPGDA)] (B), des nanoparticules de poly(MMA) présents dans le cœur (C), des nanoparticules d'argent présent à la surface de l'écorce après renforcement. Clichés EDXS en mode compo des nanoparticules d'argent (points brillants) dans l'écorce (E) et des nanoparticules d'or supposées dans matrice du coeur (points brillants) (F). Débit de la phase continue, 130 µL/min, de la phase intermédiaire (écorce), 4 µL/min et de la phase interne (cœur), 1.5 µL/min.

3 Conclusion

Ce travail de thèse a démontré la possibilité de produire des nanoémulsions monodisperses de tailles contrôlées (50 - 300 nm) au moyen d'un dispositif microfluidique discontinu à écoulement élongationnel opérant à très faible pression (<8 bars). Le contrôle de la taille s'effectue simplement par le réglage des paramètres de procédés (débit au travers de la restriction, nombre de cycles) et par les caractéristiques géométriques du micromélangeur à flux élongationnel (angle et diamètre du microcanal) sans avoir recours à un ajustement de la quantité de surfactant. Une analyse dimensionnelle du microprocédé développé a permis de trouver une corrélation entre nombres adimensionnels (Re et We en autres) qui prédit parfaitement la taille des nanogouttelettes en fonction des différents paramètres opératoires - ceux précédemment cités ainsi que la fraction volumique de la phase dispersée (jusqu'à 50%), le rapport de la viscosité de la phase dispersée et celle de la phase continue (de $3x10^{-2}$ à 14) et le facteur de contraction.

Moyennant quelques aménagements, le microprocédé précédemment développé a pu produire en continu des nanoémulsions de tailles également contrôlées.

L'emploi d'un monomère comme phase dispersée autorisa la production de nanoparticules de polymère après que les nanoémulsions produites furent polymérisées soit par polymérisation thermique ou par irradiation UV en mode discontinu et continu.

Ces nanoparticules de polymères ont ensuite été utilisées pour préparer à l'aide de dispositifs microfluidiques à capillaires des microparticules de polymères composites simples ou de structure cœur-écorce ainsi que des microparticules de polymères hybrides organique/inorganique multi-échelle et multi-domaine. De telles morphologies de microparticules sont difficiles à obtenir au moyen des procédés conventionnels mais l'emploi de dispositifs microfluidiques rend leur méthode de fabrication rapide et relativement simple (une seule étape).

Ces travaux de thèse on ainsi montré les voies de préparation de microparticules de polymère de morphologies variées et complexes. Ces microparticules devraient rapidement trouver des applications dans des domaines tels que la délivrance de principes actifs, la théranostique, l'optique ou bien encore la détection de gaz ou de solutés de par leur taille et la possibilité d'y inclure des nanoparticules inorganiques dans des compartiments précis.

Enfin, le microprocédé discontinu à écoulement pourrait être utile pour réaliser des tests sur une phase dispersée onéreuse ou disponible en petite quantité puisque seul 1 mL peut être employé contrairement aux procédés conventionnels qui nécessitent une plus grande quantité. Quant à sa version continue, elle pourrait trouver application dans une petite production d'émulsions à hautes valeurs ajoutées ou bien servir de base au dimensionnement d'une unité de production de plus gros volume.

TABLE OF CONTENT

Chap 3. DEVELOPMENT OF AN ELONGATIONAL-FLOW MICROPROCESS FOR THE PRODUCTION OF SIZE-CONTROLLED NANOEMULSIONS

Chap 4. APPLICATION TO THE SYNTHESIS OF MULTI-SCALE AND MULTI-DOMAIN POLYMERIC MICROPARTICLES

CHAPTER 1

INTRODUCTION

Nanoemulsions are essential for fundamental studies and a number of applications including paint, dairy, cosmetic and pharmaceutical industries. Nanoemulsions are usually formed by applying an external energy to disperse one liquid phase (the dispersed phase) into another immiscible liquid phase (continuous phase) since its free energy is higher than the free energy of the separate phases. That is also the reason why most of nanoemulsions are kinetically stable instead of thermodynamically stable. In order to deliver the external energy into the system, a number of apparatus and methods have been developed including the ultrasound generator, high-pressure homogenizer, rotor-stator mixer, static mixer, membrane, spontaneous emulsification, phase inversion temperature and phase inversion composition. However, each approach has its own drawbacks, which led us to design a novel low input energy microfluidic emulsification device to improve the control over the size of the nanodroplets and to widen the range of formulation that can be emulsified (e.g. highly viscous phases or high solid contents).

Microfluidic devices provide several distinct advantages in comparison to their macroscale counterparts. For instance, they are characterized by improved mass and heat transfers owing to their high surface to volume ratio, operate most of the time in laminar regime and hence provide reproducible conditions, allow mixing miscible fluids in few milliseconds and finally are extremely efficient emulsification devices. In contrast to most of the aforementioned emulsification apparatus which are based on the shearing of the dispersed phase, we have developed an elongational-flow microemulsifier. Elongation flows are known, from the early work of Taylor, to be more efficient, in contrast to shear flow, to rupture dispersed phase droplets into smaller ones even when the dispersed phase is more viscous than the continuous phase. The working principle of the new device is based on the reciprocating flow of a oil-in-water emulsion through an abrupt restriction imposed by the microchannel of a micromixer. As such a predominant elongational strain rate is acting on the dispersed

phase droplets when passing through the microchannel and ultimately leads to the formation of nanodroplets which size ranges from 50 to 300 nm.

When the dispersed phase is composed of a polymerizable liquid, i.e. a monomer admixed with a proper initiator, the obtained nanoemulsion can be easily turned into a colloidal suspension of polymer nanoparticles upon thermal-induced or UV-initiated polymerization.

Not only nanoparticles can be prepared with microfluidic devices but also microparticles. For instance, capillaries-based microfluidic droplet generators were recently found to be quite efficient devices to produce monodispersed polymeric microparticles. Over conventional methods, microfluidic droplet generators offer the effective possibility to control their size, composition, shape and morphology by simply tuning the operating parameters and making slight changes in the design of the droplet generators. Thus spherical, disk- and slug-like particles can be prepared in a straightforward manner as well as plain, core-shell and Janus morphologies.

Composite/hybrid multi-scale and multi-domain polymeric microparticles represent an interesting class of materials. Indeed, their specific structure and composition may confer new properties that could make them suitable for novel applications in varied fields such as drug, cell or gene delivery, functional optical materials and theranostics to name a few. In such objects, polymer and inorganic nanoparticles are selectively embedded into different domains of a polymeric microparticle.

The aim of this PhD thesis was to develop a new facile microfluidic route to the preparation of such composite/hybrid multi-scale and multi-domain polymeric microparticles. To fulfill our goal, a new elongational-flow microemulsifier was developed to produce size-controlled polymer nanoparticles which were in combination with possibly noble metal salts incorporated into selected domains of monomer-based microdroplets. The latter were generated thanks to different

capillaries-based microfluidic droplets generators and finally photopolymerized to give the targeted polymeric microparticles.

This manuscript is composed of 5 chapters. Beside the current one, the 2^{sd} chapter is dedicated to the literature background and comprises two different sections. The first section reviews the conventional emulsification methods and their corresponding drawbacks. The second section reviews the different microfluidic devices used to produce microdroplets, microparticles, nanodroplets and nanoparticles.

Chapter 3 presents a novel elongational-flow microfluidic device operating in batch mode for the production of size-controlled nanoemulsions. Effect of operating parameters (flow rate through the restriction, number of cycles), micromixer parameters (angle, bore size) and finally composition parameters (weight content and viscosity of the dispersed phase, concentration of the surfactant) on nanodroplets size and size distribution was thoroughly investigated. Upon slight modification of its original design, this elongational-flow microfluidic device was operated in continuous-flow mode. Both effects of the reciprocating flow rate through the restriction of the micromixer and the inlet flow rate across the micromixer were assessed.

Chapter 4 deals with the production of polymer nanoparticles derived from the polymerizable nanoemulsions obtained in previous chapter and investigates different strategies to harden the nanodroplets (thermal-induced or UV-initiated polymerization). Then plain and core-shell composite multi-scale and multi-domain polymeric microparticles embedded with lower scale polymer nanoparticles were produced. In addition, more complex core-shell hybrid multi-scale and multi-domain polymeric microparticles embedded with lower scale polymer nanoparticles and inorganic nanoparticles were also synthesized.

Finally Chapter 5 concludes about the work accomplished during this PhD and gives some perspective for future work.

CHAPTER 2
BACKGROUND LITERATURE

2.1 Conventional emulsification methods

2.1.1 General overview

An emulsion is a two-phase system prepared by combining two immiscible liquids, in which small globules of one liquid (so-called dispersed phase) are dispersed uniformly throughout the other liquid (so-called continuous phase).[1] For several decades, emulsions have been used in a wide range of fields including dairy industry, food, cosmetic, pharmacy, agriculture, bitumen, fuel and so on.[2 3] In order to formulate a stable emulsion, it is necessary to consider well the factors which can influence emulsion's quality. These factors include choosing a proper set of components (dispersed and continuous phases, surfactant or combination of surfactants etc.) and their respective concentration, offering an efficient mechanism that can rupture the bigger droplets into micro- or nanoscale ones and finally selecting a proper order for adding each component. As seen in Figure 1, different types of emulsion are distinguished depending on the physical properties of the phase composing the dispersed medium and the morphology of the dispersed phase globules. Oil-in-water (o/w) usually refers to oil droplets dispersed in an aqueous solution while in water-in-oil (w/o) the dispersed phase is composed of aqueous droplets dispersed in an oil phase. These two emulsion types are also called single emulsions as the dispersed phase globules have the form of single droplets. However double emulsions can be encountered and are characterized by droplets-in-droplet. Thus water-in-oil-in-water (w/o/w) refers to droplets of an aqueous solution encapsulated in a droplet of an oil phase which is turn is dispersed in an (other) aqueous solution; oil-in-water-in-oil (o/w/o) is just the other way around.

Miniemulsions, also referred to as nanoemulsions, are classically defined as aqueous dispersions of oil droplets which size ranges from 50 to 500 nm prepared by shearing a system containing oil, water, a surfactant, and a so-called "cosurfactant".[4] Nanoemulsions are thermodynamically unstable since the free energy of the colloidal

dispersion is higher than the free energy of the separate phases (oil and water). Thus, nanoemulsions are usually formulated such as to be kinetically stable by ensuring that there is a sufficiently large energy barrier between the two states. Microemulsions are defined as dispersions made of water, oil, and surfactant(s) that are thermodynamically stable with dispersed domain diameter varying approximately from 1 to 100 nm but more often from 10 to 50 nm.[5,6]

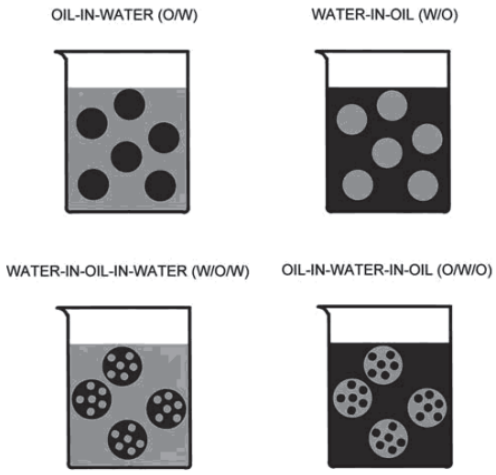

Figure 1 Schematic drawing of the main kinds of single emulsions (top) and two different kinds of double emulsions (bottom).[7]

For the production of nanoemulsions, several requirements should be considered. First, the total insolubility between the dispersed phase and continuous phase is a key factor to ensure the stability of the emulsion over time. However, for practical reasons, it may happen than the dispersed phase be slightly soluble in the continuous phase. In such situation, the emulsion should be formulated such as to avoid the so-called Ostwald ripening phenomenon. The latter occurs in the presence of non-equal size droplets which induce a Laplace pressure difference between small and large droplets. As a consequence the larger droplets grow at the expense of the smaller ones by diffusion of the dispersed phase through the continuous phase. [8] Although suppressing

the Ostwald ripening phenomenon can be achieved by trapping particles inside the droplets that are insoluble in the surrounding fluid or by continuous shearing of the whole emulsion,[9] it is easiest to add in the dispersed phase a molecule (so-called Ostwald ripening inhibitor) completely immiscible with the continuous phase which purpose is to create an osmotic pressure which balances the Laplace pressure. The second requirement is an excess of an ionic surfactant which effect is two-fold. First, it contributes to reduce the interfacial tension between the two phases and thus allows the formation of smaller droplets. Second, it guarantees the efficient coating of the new coming surface of the nanoscale droplets and contributes to the suppression of the shear-induced coalescence by electrostatic repulsion.[10] Generally, the surfactant is dispersed in the continuous phase with the form of micelles. When the new droplets are produced, these micelles dissociate rapidly into single surfactant entities to cover the droplet's surface. The third requirement is choosing the proper surfactant.[11] The fourth requirement is using an emulsification method that allows rupturing the dispersed phase into nanodroplets and thus overcoming the Laplace pressure. The Laplace pressure is the pressure difference between the inside and the outside of a curved surface caused by the surface tension of the interface.[12] The Laplace pressure equation is given as below.

$$\Delta P \equiv P_{\text{inside}} - P_{\text{outside}} = \gamma \left(\frac{1}{R_1} + \frac{1}{R_2} \right)$$

Equation 1 where R_1 and R_2 are the radii of curvature and γ (also denoted as σ) is the surface tension.[13]

Several methods are available for producing nanoemulsions. They can be classified into two categories: high-energy and low-energy methods[14,15] (cf. Table 1) High-energy methods include energy inputs which can be reached by ultrasound generator, high-pressure homogenizer, rotor-stator mixer, static mixer and membrane. By using these emulsification methods, the nanodroplets can be obtained by energy transfer with the presence of surfactant whose function is to decrease the interfacial

tension. Low-energy methods take advantage of the internal chemical potential of the emulsion components to achieve emulsification. They rely on the spontaneous formation of emulsion when either its composition or the surrounding conditions are changed.[16] Example of the main low-energy methods include spontaneous emulsification, phase inversion temperature and phase inversion composition. Very low interfacial tensions are the key factor of these emulsification methods which can be achieved by formulation designs. The details of these emulsification methods will be introduced in the following paragraphs.

Table 1 Classification of emulsification methods accordingly to their energy consumption

High-energy methods	Low-energy methods
• ultrasound generator • high-pressure homogenizer • rotor-stator mixer • static mixer • membrane	▪ spontaneous emulsification ▪ phase inversion temperature ▪ phase inversion composition

2.1.2 Ultrasound generator

Ultrasound generator method for the emulsification was reported firstly by Wood and Loomis in 1927 and patented in 1944.[17] Two mechanisms are considered for this kind of emulsification. Firstly, the application of the acoustic field produces unstable interfacial waves leading to the eruption of the dispersed phase into the continuous phase in the form of droplets. Secondly, the application of low frequency ultrasound results in an acoustic cavitation inducing the formation of microbubbles which then collapse due to the pressure fluctuations of a simple sound wave. The collapse event causes an extreme localized turbulence breaking up the primary droplets of dispersed phase into sub-micro size droplets. High-power ultrasonic devices usually comprise

several components as show in Figure 2.

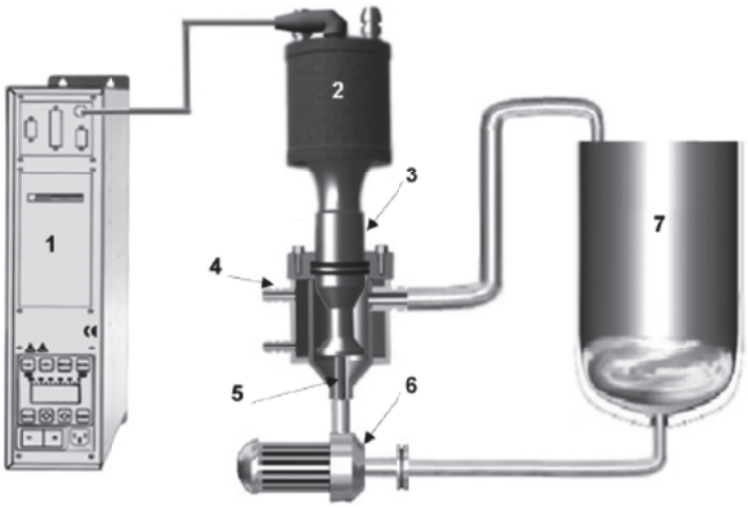

Figure 2 Pilot-scale flow-through process schematic, where (1) 1200W ultrasonic generator, (2) piezoelectric transducer, (3) half-wave Barbell Horn, (4) reactor chamber with water-cooling jacket, (5) liquid delivery tube (used to bring the liquid close to the horn's lower output surface), (6) pump and (7) main storage / mixing beaker.[18]

In most ultrasonic processes, it is necessary to re-circulate the solution close to the horn in order to make all the droplets experience the high-power region because the emitted sound field is inhomogeneous. After many times of the re-circulation, the nanoemulsion can be obtained.

The effect of applied power was investigated by Kentish *et al.*[19] It is supposed that the droplet size decreases while increasing the shear, because it would increase the applied power to the system. However, as shown in Figure 14, the droplet size reaches a minimum value when the applied power is increased. This phenomenon is described as "over-processing" and is due to more coalescence among the droplets at higher applied powers. The ultrasonic radiation force, so-called Bjerknes force, will increase in intensity as applied power increases. Afterwards, the secondary Bjerknes force will

reach the nodes and antinodes of the acoustic field for the droplets in the emulsion. The closer droplets would get more opportunity to coalesce so that "over-processing" phenomenon is produced.

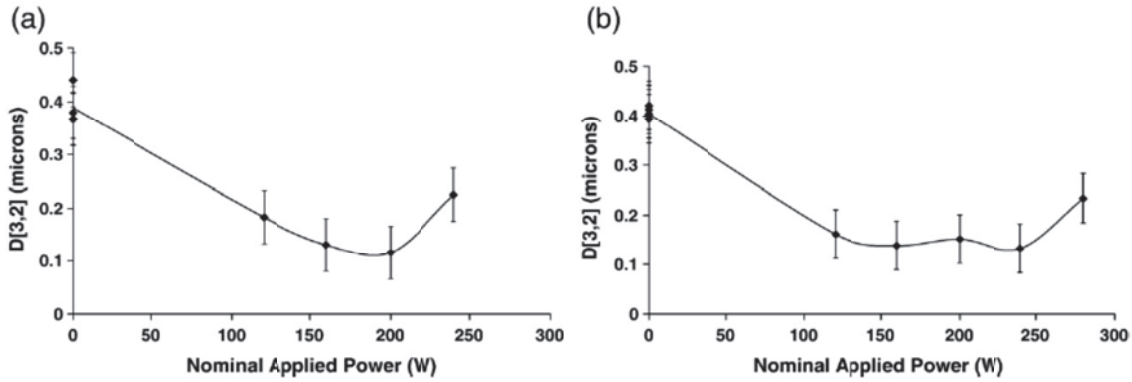

Figure 3 Effect of the nominal applied power in (a) a 50 mL or (b) 75 mL sample size batch cell on the particle size, D[3,2], of 15 vol.% flax seed oil in-water emulsions stabilized by 5.6 vol.% Tween 40. Error bars are based on two standard deviations, calculated from eight replicate unsonicated samples.[19]

A major challenge of the ultrasonic generator in the industry is the effective design of the continuous flow equipment. For instance, one of the most important parameters is the ultrasonic amplitude which is strongly related to the intensity of cavitation-generated shear forces and must be maintained at a sufficiently high level so that the emulsification process can be efficient. So far, it is impossible to significantly increase the size of the ultrasonic horn-based generators without drastically decrease the amplitudes. As a result, scaling up has been selected to increase the ultrasonic amplitude, however, sacrificing the product quality.[18]

2.1.3 High-pressure homogenizer

The high-pressure homogenizer is one of the most important continuously emulsification device in industry to produce commercial monodispersed emulsion. So,

this kind of emulsification method has been in focus for several years.[20] A high-pressure pump and a homogenizing nozzle are essential parts for the high-pressure homogenizers. The pump is used for infusing the solution through the nozzle. The nozzle is used for disrupting the crude droplets into micro- or nanodroplets. Four kinds of nozzle are shown in Figure 4.

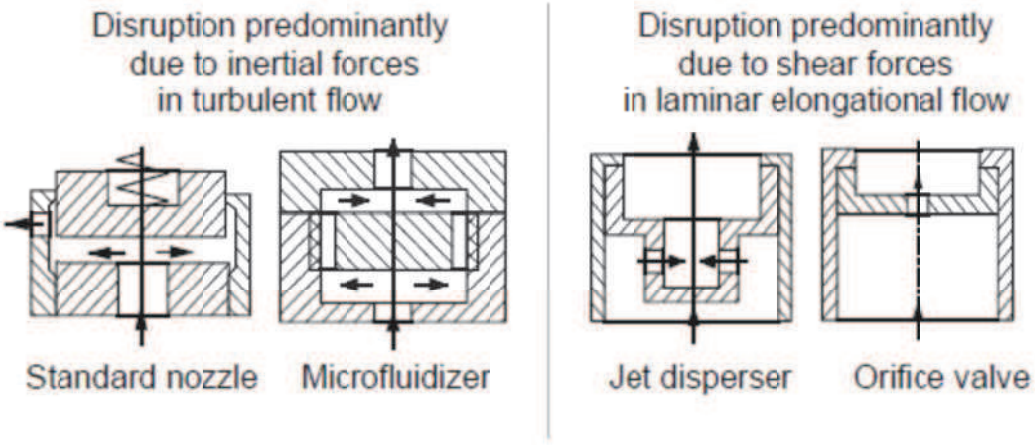

Figure 4 Homogenizer nozzles classified by mechanism of droplet disruption.[21]

Respectively, the standard nozzle is the most widespread homogenizer nozzle. The crude emulsion can be infused into the central bore by the high-pressure pumps, diverted by 90° and will be passed through the radial gap between the valve plug and valve seat. For a given pump throughput the homogenizing pressure is determined by the force acting on the axially movable valve plug and the size of the gap resulting from this.[22] The jet disperser can be described as two or more jets of crude emulsion from opposite bores mixed with each other. The diameter of the bore is typically 0.3-0.5 mm. The orifice plate is the simplest form for the homogenizer nozzle from the construction point of view. The diameter of the bore orifice is the same as in the jet disperser (0.3 to 0.5 mm). However, the diameter of the inlet ahead of the orifice plate is typically 10-60 mm. The microfluidizer involves a small chamber where the

collision plane is formed between the two square inlet jet streams at 180^{o} whose diameter is 0.1-0.5 mm. The characteristic of this chamber is the rapid dissipation of the turbulent kinetic energy where the scale of segregation decreases rapidly.[23] The microfluidizer's square inlet tubing generate a large surface area for shearing with the surrounding fluid in this chamber. Majority of the droplets rupture occurs at the outer regions of the jets and the area where the jets impinge. Subsequent to impinging, the emulsion is forced through one exit tubing typically 0.75 mm diameter, which constrains the turbulence and produces an elongational flow.

It is more reasonable to classify the emulsification devices by the mechanism by which they rupture the droplets instead of their construction characteristics. The turbulent flow is predominant to rupture the droplets in the case of standard nozzles and microfluidizers. But the disruption in the laminar elongational flow is also possible in microfluidizers especially when the viscosity of the emulsion is high. The laminar elongational flow ahead of the bores is predominant to rupture the droplets in the case of jet dispersers and orifice plates.

The advantage of the high-pressure homogenizer is the combination of high-volume throughput of nanoscale droplets at a relatively large solid content ($\phi < 0.6$), monodispersed droplet size distribution (PDI < 0.2) and extremely high peak shear rates. However, the high peak shear rate can be so huge that it may heat the emulsion significantly above the room temperature through viscous dissipation. If such heating is undesired, the area where extreme shear occurs can be cooled using a heat exchanger without affecting the size distribution and stability. Furthermore, the volume rate of production of the nanoemulsion can be as high as several liters per hour. According to the final nanodroplet radius after rupturing, the production rate ranges from 10^{14} to 10^{18} droplets per second.

One kind of such high-pressure homogenizers has been reported to produce silicone oil nanodroplets.[24] It implied a two stage emulsification process. Firstly, a

polydispersed microscale emulsion of silicone oil in an aqueous solution of sodium dodecyl sulfate (SDS) was obtained by means of a shear device (a high-speed dispersing wand, IKA). Then, a high-pressure homogenizer equipped with a jet disperser was employed to rupture these microscale droplets into submicron droplets. This systematic study clearly showed how to control the droplet size by varying the composition and shearing conditions. The silicone oil has a large enough molecular weight whose solubility in the water is so small that it can be neglected.

In a recent work, Lee *et al.* compared the droplet breakup between high-pressure valve homogenizer and a microfluidizer.[25] The effect of pass number and pressures has been specifically investigated. A series of oil-in-water were produced with the following component, 10 wt.% silicone oil (viscosity 0.05 Pa s) and 3 wt.% Tween 20 in the continuous phase. The Tween 20 was used as a surfactant that has a low molecular weight and can be absorbed onto the new interface quickly when in large excess. The emulsions were passed through the microfluidizer and high-pressure valve homogenizers at 50, 100 and 150 MPa for 1-5 times. Results in terms of droplet size achieved are shown in Figure 5 and Figure 6.

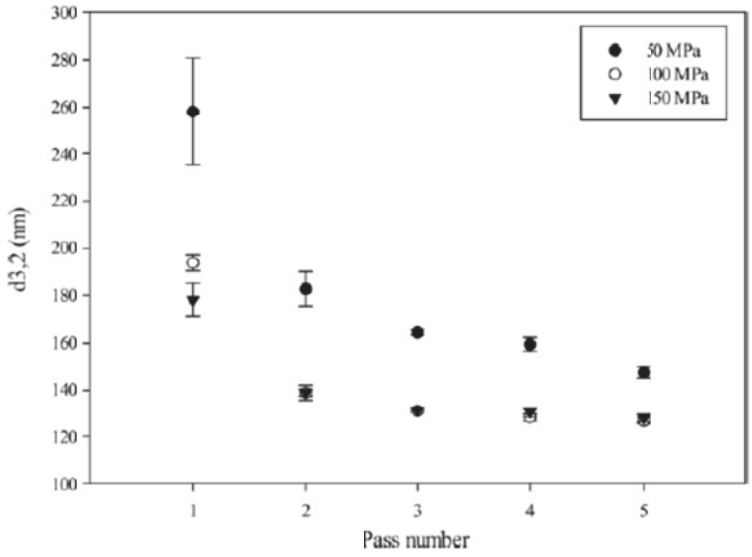

Figure 5 Droplet size with respect to pass numbers for different pressures and 10 wt.% silicone oil and 3 wt.% Tween 20 in a valve homogenizer.[25]

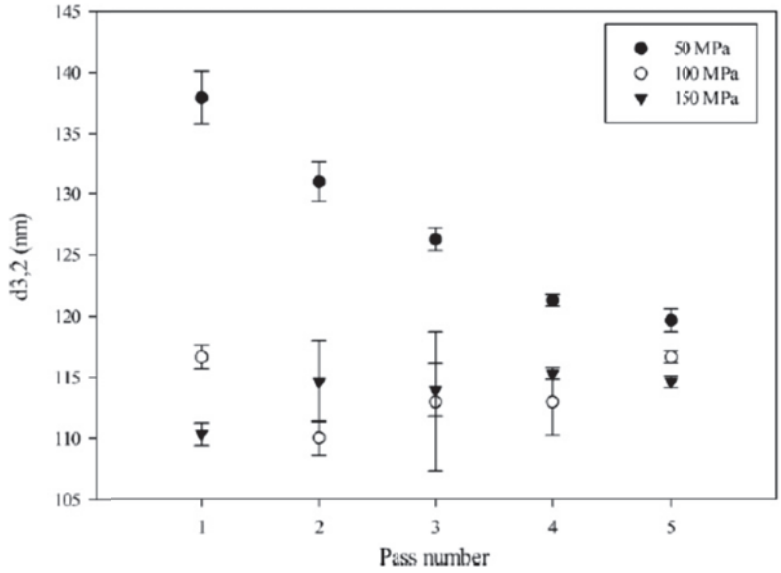

Figure 6 Droplet size with respect to pass numbers for different pressures and 10 wt.% silicone oil and 3 wt.% Tween 20 in microfluidizer.[25]

It is clearly shown that the droplet size decrease with increasing the pressure of the homogenization in both devices, which is in agreement with the previous study from McClements and coll. in 2011.[16] For the lowest pressure (50 MPa), both curves do not reach a plateau value which suggests that smaller droplet size can be achieved by further passes. However, a plateau is observed for the valve homogenizer after three passes for 100 MPa and 150 MPa while the smallest droplet size is reached after one pass for the microfluidizer and 150 MPa. These differences are caused by the different geometries of the two devices. The high-pressure valve homogenizer produces a wide distribution of shearing forces, whereas the microfluidizer produces a narrow distribution. Therefore, the solution flowing through the latter experiences the highest shear force. Furthermore this microfluidizer can eliminate coalescence effectively so that the smallest droplet size with the narrow distribution is obtained after only one pass and 150 MPa. However, this is not the case when the pressure drop is 50 MPa, the

droplet size after the first pass is significantly larger than the droplet size after the fifth one, which indicates there is some bypassing of the highest shear force in the microfluidizer. Bypassing of flow can be confirmed by the droplet size distribution.[25]

2.1.4 Rotor-stator mixers

Rotor-stator devices provide a focused delivery of power, energy and shear to accelerate physical processes such as emulsification, mixing, dissolution and de-agglomeration. The rotor-stator mixer includes a rotor that rotates at high speed inside the stationary stator, which is interchangeable enabling different process requirements. Normally, the stator is cylindrical screen with tiny clearance from the rotor, containing numerous holes or slots where the solution flows. The kinetic energy generated by the rotor which is dissipated in the stator region creates quite high energy dissipation rates due to the small volume, which is able to rupture the solution to emulsion.[26] Nanoemulsions can also be produced by rotor-stator mixer with several hundred nanometers and a narrow size distribution. Besides the nanoemulsion, the rotor-stator mixers were used to produce macroemulsions.[27] Virtishear™ system with the following parameters 24,000 rpm and a rotor diameter of 10 mm resulted in a rotor tip speed of 12.5 m/s for 5min. According to the above parameters, dichlormethane and an aqueous bovine serum albumin solution were turned into a macroemulsion with droplets diameter around 1000 nm. Within one minute, the highest size dispersity was obtained. If the stirring speed is reduced down to 15,000 rpm, the time for the highest dispersity at 1000 nm is delayed by 3 minutes.[28]

One Silverson rotor-stator system was developed for the continuous production of emulsions[29]. Silicone oil with different viscosities and water were emulsified with a rotor tip speed of 36 m/s and a stirring rate of 11,000 rpm. One conclusion from this paper is that low silicone viscosity can form smaller droplet diameters below 3000 nm while higher viscosities or lower stirring speeds produce larger droplet size.

The ART MICCRA D27 rotor-stator system (shown in Figure 7) provides a maximum stirring speed of 36,000 rpm which means 68 m/s for the tip speed. This speed is significantly higher than those achieved by regular rotor-stator systems. As a consequence the shear rate produced by this Miccra homogenizer is significantly higher. So, it is possible to produce emulsions with a wide range of droplets diameter from submicron to nanometer.[30]

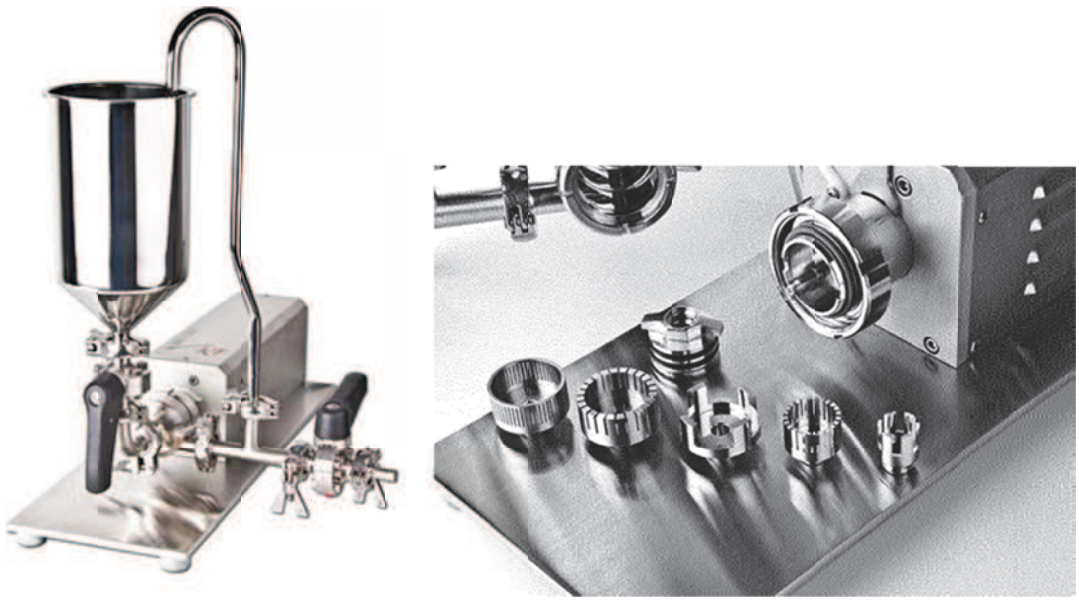

Figure 7 ART MICCRA D27 rotor-stator system (left) and the opened flow-through chamber with various rotors and stators (right).[30]

Steven Hall and coll. observed that the droplet size can be easily varied by changing the dispersed phase viscosity and tip speed[31]. The single pass mean droplet size measured at the same mean residence time (0.45 s) and for three homogenizers of different scales was found to be correlated to the tip speed and Weber number. Thus, Sauter mean droplet diameter follows a power law with respect to the tip speed as illustrated in Figure 8. Whatever the dimension of the homogenizers tested, measured Sauter mean droplet diameters fell onto two distinctive straight lines depending only

on the viscosity of the silicone; bigger droplet sizes being observed for the more viscous silicone oil. The tip speed exponent extracted from the plot matched more or less with the theoretical value of -1.2 for fully developed turbulent flow when the silicon oil viscosity is low whereas it reached -1 for the highest viscosity investigated highlighting a simple shear flow break-up mechanism. These correlations show that the tip speed can be considered as a good scaling parameter. Tip speed was also a good correlating parameter for dispersion/emulsion in stirred vessels.[24]

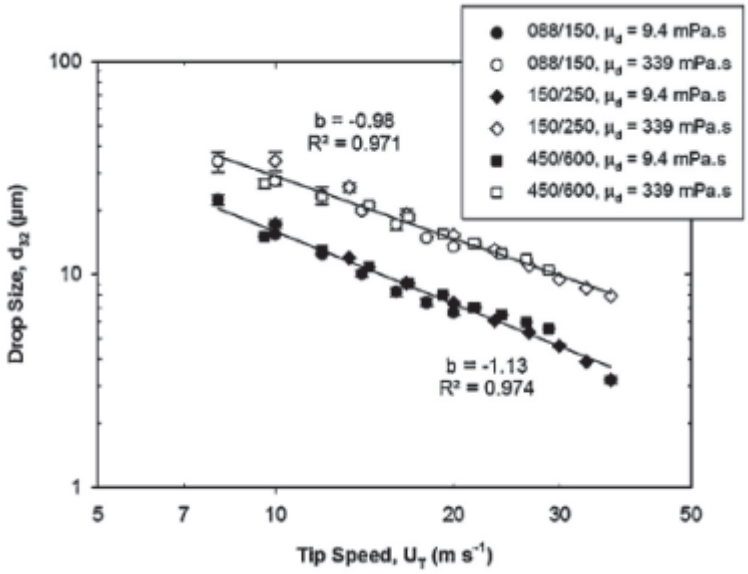

Figure 8 Mean droplet size emulsions containing 1 wt.% of either 9.4 or 339 mPa.s silicone oils (into aqueous solutions) as a function of tip speed for three different mixer scales(Laboratory scale 088/150; Pilot plant scale 150/250; Factory scale 450/600; the figures represent the product model) and a constant residence time of 0.45s.[31]

2.1.5 Static mixer

A static mixer is a precision engineered device for the continuous mixing of fluids.[32] Static mixers have various applications including mass transfer processes, metal extraction, desalting fuels in refineries, saponification in petrochemical plants

and gas-liquid contacting devices, etc. Static mixer can replace the stirred vessel due to very efficient mixing in the radial direction with no back-mixing in axial direction and no dead space and with comparatively less energy dissipation due to non-moving elements.[33] Figure 9 illustrates the comprehensive elements of different commercial static mixers.

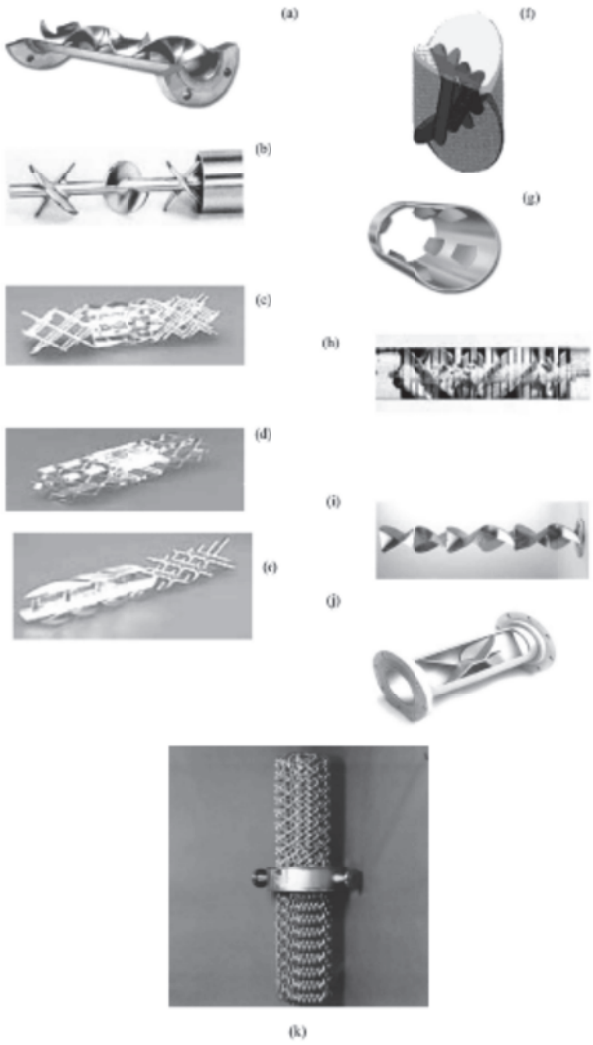

Figure 9 Elements of different commercial static mixers: (a) Kenics (Chemineer Inc.); (b) low pressure drop (Ross Engineering Inc.); (c) SMV (Koch-Glitsch Inc.); (d) SMX (Koch-Glitsch Inc.); (e) SMXL(Koch-Glitsch Inc.); (f) Interfacial Surface Generator-ISG (Ross Engineering Inc.); (g) HEV (Chemineer Inc.);(h) Inliner series 50 (Lightnin Inc.); (i) Inliner series 45 (Lightnin Inc.); (j) Custody transfer mixer (Komax systems Inc.); (k) SMR (Koch-Glitsch, Inc.).[34]

The surfactant is a key factor that strongly influences the droplet diameter in such devices. The surfactant is always used at a low concentration and above its critical micellar concentration (CMC) in order to decrease the surface tension and thus to favor droplet break-up, and to some extend to stabilize them. N. Kiss and coll. used poly(vinyl alcohol) (PVA) as the surfactant to emulsify ethyl acetate and benzyl alcohol in aqueous solution with a static mixer. In their experiments, the flow velocity was 0.0755 m/s, the dispersed phase was kept at 0.14 vol.%. The continuous phase was deionized water with PVA and the dispersed phase was 67 vol.% ethyl acetate, 33 vol.% benzyl alcohol and PLGA (0.11g/mL). The surfactant concentration was varied between 0 to 5 wt.%/Continuous phase. The mean droplet size is reported in Figure 10 and was found to vary from 30 to 184µm when the surfactant concentration increases.[35]

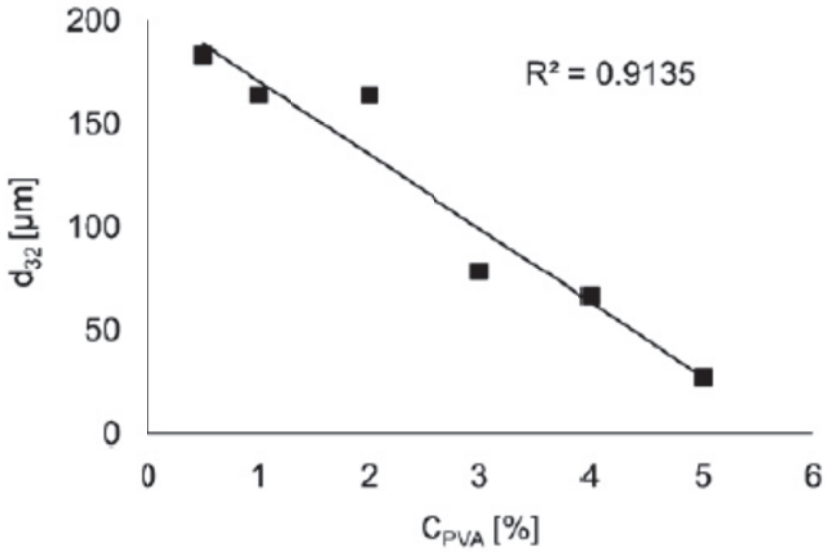

Figure 10 Sauter mean oil droplet diameter with respect to different concentrations of surfactant.[35]

G. Farzi and coll. used a simple in-line static mixer to produce polymerizable methyl methacrylate nanoemulsions. In detail, the continuous phase and dispersed phase were homogenized by causing it to circulate over one or more tubes. Each tube contains 4 static mixer elements with 15cm length and 6.4mm diameter. The mixture of two phases is placed in a reservoir with a magnetic bar and circulated through a tube or tubes containing the static mixer elements. The circle consists of one tube, reservoir and one gear pump. The static mixer is placed between the gear pump and reservoir. The flow rate was fixed at 60.6 mL/s for all the experiments unless otherwise noted. Several operating conditions were investigated to assess their influences on the droplets diameter which ranged from 150 to 300 nm. As expected, the droplet size decreases by increasing the flow rate through the static mixer. It was also shown that higher surfactant concentration led to smaller droplets.[36]

2.1.6 Membrane

The last high-energy method is the membrane emulsification. Its principal is quite simple and consists in pumping the dispersed phase through an uniform pore-size membrane into the continuous phase flowing tangentially on the opposite side of the membrane (Figure 11).[37] The droplets grow due to the applied pressure until a certain size for which they detach from the membrane and flow downstream in the continuous phase. This method is applicable to both oil-in-water and water-in-oil emulsions and consumes lower energy compared to other traditional methods like rotor-stator, homogenizers. The significant feature of this method is such that the droplets size is not dependent on the generation of a turbulent flow for droplet break-up but dependent on the membrane material and pore size. Actually, the droplet size is also strongly determined by the balance among driving pressure, interfacial tension forces, the buoyancy of the droplet and the drag force on the droplet in the flowing continuous phase.[38]

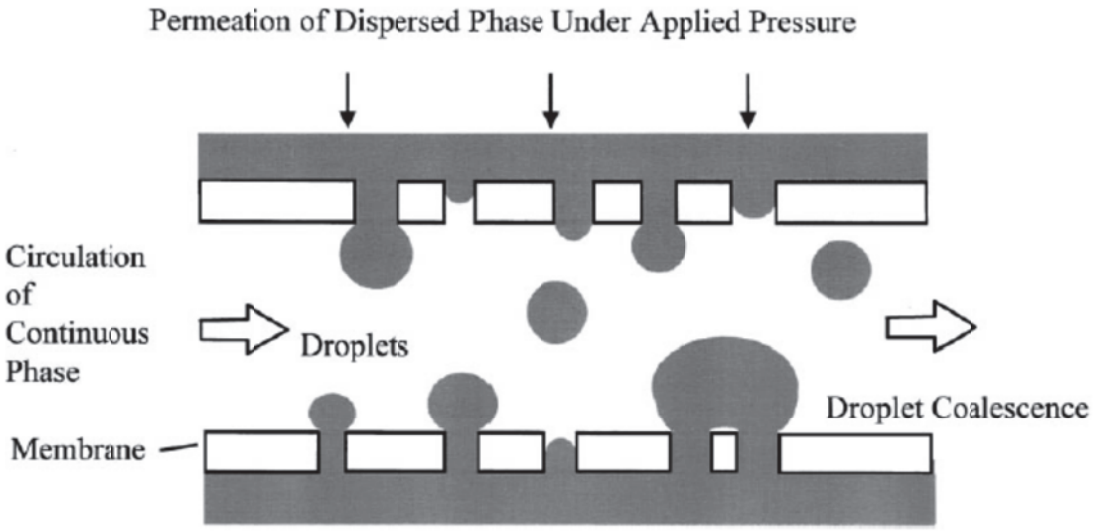

Figure 11 Schematic drawing of the membrane emulsification method.[37]

The newly born droplet in front of the pore tends to adopt a spherical shape due to the interfacial tension, but some distortion may appear, which depends on the flowrate of continuous phase and the contact angle between the membrane surface and the droplet.[39] As mentioned, the final droplet size is determined by the pore size but also by its size distribution and degree of coalescence on the membrane surface and in the bulk solution. The porosity of a membrane determines the distance between two adjacent pores. When this parameter becomes too small, it leads to the coalescence of droplets before they separate from the membrane surface. The flux though the membrane is determined by the emulsification pressure. Higher pressures are necessary for smaller pores to maintain the same droplet size. However, a notable disadvantage of the membrane emulsification is the low flux of the dispersed phase caused by the low hydraulic permeability of most membrane.[40]

2.1.7 Spontaneous emulsification

The spontaneous emulsification method takes advantage of the system's gain in energy when the dispersed phase is mixed with the continuous phase. It usually occurs at constant temperature and without any phase transitions.[41] In order to obtain nanodroplets, a very high solvent/oil ratio is needed for the spontaneous emulsification. The solvent diffusion through the dispersed phase is thus so quick that it generates turbulence leading to the formation of nanodroplets. Indeed, Miller[42] discussed about the diffusion of water-soluble components from the organic phase into the aqueous phase when the emulsion is diluted. Taylor and Ottewill[43] firstly mentioned the formation of nanoemulsion by spontaneous emulsification by dilution of o/w microemulsion with and alcohol as cosurfactant. The alcohol diffuses from the oil droplets into the water since the surfactant concentration is not high enough to maintain the low interfacial tension required for thermodynamic stability. shows the schematic representation proposed mechanism for spontaneous emulsification by dilution of an o/w emulsion.

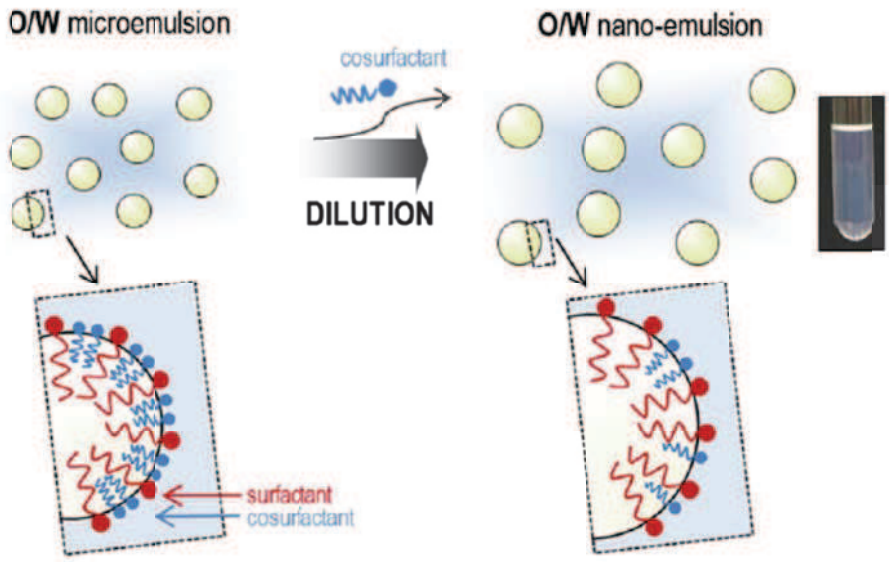

Figure 12 Schematic representation of proposed mechanism for spontaneous emulsification by dilution of an O/W emulsion.[41]

Ouzo effect is also famous for its surfactant-free system. These nanoemulsions are characterized by a high solubility of oil in the water-solvent phase and a rather low interfacial tension due to the presence of a solvent.[44] Ouzo effect is also named spontaneous emulsification. F. Ganachaud and J.L. Katz reviewed how to create nanoparticles and nanocapsules using the Ouzo effect. The emulsion produced by Ouzo effect is kinetically stable, without presenting any surfactant. The droplets produced by Ouzo effect are homogenously sized and are large enough so that the Ostwald ripening phenomenon is greatly delayed. But, they are also small enough so that creaming is slow, especially when the density of the oil is similar to water.[45]

2.1.8 Phase inversion methods

Phase transitions triggered either by changing the temperature or composition are called phase inversion temperature and phase inversion composition methods respectively. Shinoda and Saito[46] were the first to introduce the phase inversion temperature (PIT) in 1968 and showed that it originates from the change in the surfactant spontaneous curvature due to temperature. The schematic PIT working principle is reported in Figure 13. PIT usually involves the controlled transformation of an emulsion from one type to another type through an intermediate bicontinuous phase.[16] Change in the physicochemical properties of the surfactant induced by the temperature is the driving force for the PIT. Due to the hydrophobic effect, surfactant molecules tend to spontaneously associate with each other in water to form monolayers that possesses a curvature that allows the most efficient packing of the molecules.[47] At this optimum curvature, the system free energy is the lowest and any deviation from this situation needs extra energy. The mechanism of surfactant solubility is twofold. When the temperature is low, the head group of a non-ionic surfactant is strongly hydrated so that the surfactant is highly soluble in the water.

When increasing the temperature, the solubility of surfactant decreases in the water as to the head group becomes more and more dehydrated. When the critical temperature is reached, the balance of surfactant solubility in the oil phase and water phase is obtained. Above this critical temperature, the solubility in the oil phase is higher than in the water phase. Kevin Roger and his coworkers[48] re-examined the phase inversion temperature (PIT) emulsification process and highlighted two conditions. First, the mixture must be stirred at low speed throughout the whole process: this allows producing emulsions at surfactant concentrations that are too low to form a thermodynamically stable microemulsion. Second, the stirred mixtures must be heated above a threshold temperature called the clearing boundary (CB) and then quenched to lower temperatures.

Alternatively, the system can also be formed by changing the composition instead of temperature, which is called phase inversion composition (PIC). The typical procedure of PIC to obtain nanoemulsion is progressively adding one component to the pre-formed emulsion mixture. PIC can be preferred when temperature problem occurs. This is the case for large scale production when it is difficult to increase rapidly the temperature of a whole tank. The starting point is similar to PIT: a reverse microemulsion (w/o) that forms spontaneously with low water percentage. Then one adds rapidly water until to a certain amount where the surfactant chains are fully hydrated and their curvature turned toward oil phase. Meanwhile, the solution changes its structure and forms o/w emulsion. The PIC method has significantly attracted industry interest because on a large scale it is easier to change abruptly a composition rather than the temperature. Moreover, it is not necessary to heat the whole composition. However, the comprehensive mechanism of PIC method is not still known so far.[49]

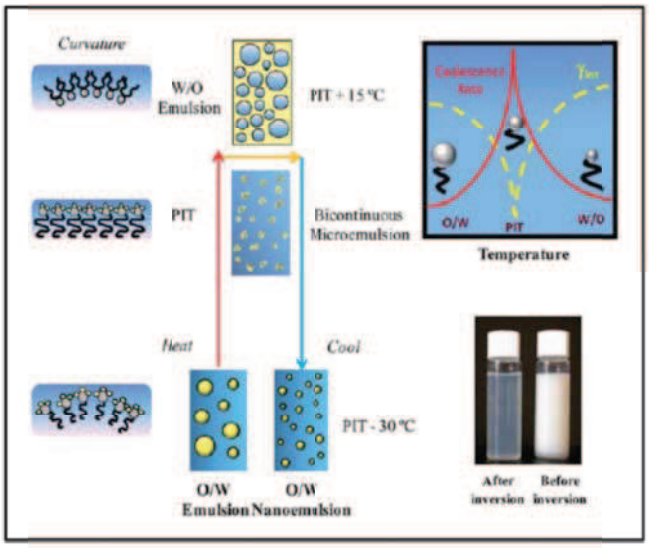

Figure 13 Schematic diagram of the formation of nanoemulsions by the PIT method.[16]

2.1.9 Summary on conventional emulsification methods

If all aforementioned emulsification methods are quite effective to produce nanoemulsions of a given size range, they all suffer from some drawbacks. Ultrasonic devices usually deal with a small amount of fluid and cannot be readily scaled-up for mass production. They also suffer from a limitation in the droplets size when the sound power is increased. High-pressure homogenizers usually operate at very high pressure (ca. 2,000 bars) and thus require an enormous amount of energy to generate the desired droplet size. The preparation of nanoemulsion with an average droplet size less than 100 nm is quite difficult by using rotor-stator mixer and static mixer not to mention the high polydispersity in droplet sizes. The major disadvantage of the membrane emulsification is a moderate productivity due to the extrusion flow rate that should be slow enough to avoid the jetting mode. It is difficult to generate nanoemulsions by phase inversion temperature method for most common ionic and nonionic surfactants whose hydrophilic-lipophilic balance is quite independent of the temperature. It has been noticed that the surfactant and co-surfactant concentrations are rather high when using the phase inversion composition, which make the whole process costly due to

the high price of the chemicals. Finally, the major drawback of the spontaneous emulsification is the ratio of dispersed phase which should be lower than 1 wt.%.[50] Therefore, there is still the need for new methods that can produce monodispersed nanoemulsions with low energy input and whose droplets size can be conveniently varied in a wide range by simply adjusting the process parameters. To this extent, microfluidic devices can be a promising solution.

2.2 Micro- and nanoparticles produced by microfluidics

2.2.1 General overview

Microfluidics is the science and technology of systems that process or manipulate small (10^{-9} to 10^{-18} liters) amounts of fluids, using channels with dimensions of tens to hundreds of micrometres.[51] A number of benefits can be pulled out from microfluidic technologies compared to large scale technologies. It includes that carrying out separations and detections with high resolution and sensitivity by using very small quantity of chemicals or reagents, low cost for reagent, time-saving and tiny footprint for the analytical devices.[52]

2.2.2 Production of microdroplets with microfluidic devices

Droplets microfluidics is a special area of microfluidics dedicated to the production of droplets in microfluidic devices. This area has lately attracted a growing interest due to several benefits brought by microfluidic technologies. Thus, droplets with sizes ranging from few tens of microns up to several hundreds of micrometers can be easily produced with narrow size distribution and generation frequencies from few Hz to several kHz. In contrast to conventional methods, microfluidic methods also allow the production of microdroplets with different shapes and morphologies, like spherical, slug, core-shell or even Janus-like. Droplets are produced one after the other and thus

very small quantities of dispersed phase are required when it comes to study the behavior of few hundreds of droplets if not only one. This is really on edge over conventional methods when the dispersed phase is highly toxic or available in restricted quantities (e.g. synthesized). Moreover, microfluidic devices can be implemented with spectroscopic methods to quantify and/or analyze phenomena at a drop level.[53] In 1997, Nakajima *et al.* firstly developed a PDMS-based microchannel device for the production of micron size sunflower oil droplets in water whose formation was recorded by a micro-scope video system.[54] By now, different microfluidic devices were developed and could be classified as follows: cross-flow devices, flow-focusing devices and co-flow devices. In the following, each category will be discussed.

2.2.2.1 Droplet formation in cross-flow devices

Cross-flow devices (also called T-junction devices) can easily produce droplets whose size is not only limited by the channel width but depends upon the flow rates of the continuous and dispersed phases. J.H. Xu and coll. prepared highly monodispersed microdroplets of n-octane in deionized water from 50 to 500 μm with coefficient of variation of the droplet size distribution lower than 5%, thus considered monodispersed in size Figure 14. Furthermore, a capillary was used to deliver the dispersed phase into the continuous phase. The schematic drawing of this device is shown in Figure 15, the dispersed phase flow direction was perpendicular to the continuous phase flow direction. Authors have investigated the effect of surfactant concentration on droplet size. It has been concluded that the disordered state has been reached at lower surfactant concentration. In the opposite, threads of the dispersed phase were obtained at higher concentration (> 0.05% w/w). This phenomenon was explained by the adsorption of the surfactant to the inner wall surface of the microchannels inducing a change in the wetting property from hydrophobic to hydrophilic. Authors also investigated the effect of the of the two phase flow rates. The

drop diameter decreased with increasing the dispersed phase flow rate (Q_d). Nevertheless, the continuous phase flow rate (Q_c) didn't have any significant influence on the final droplet size. However, by increasing the continuous phase viscosity, te average droplet size decreased.[55]

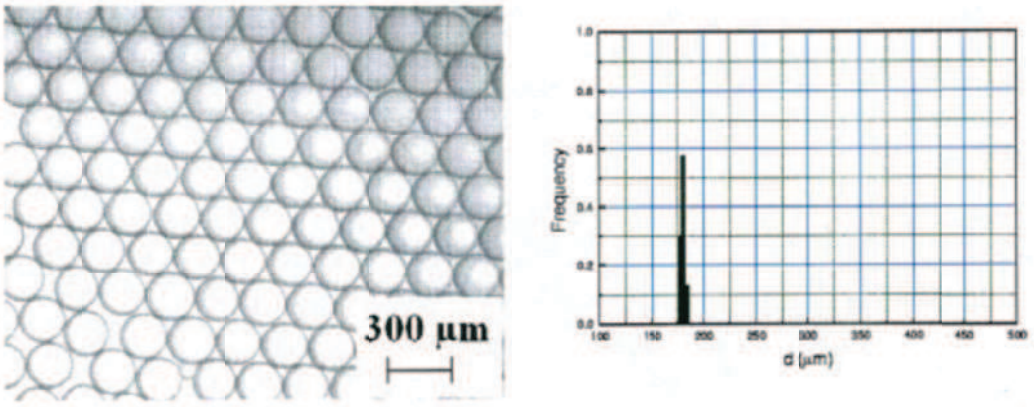

Figure 14 Monodispersed microdroplets and its size distribution.[55]

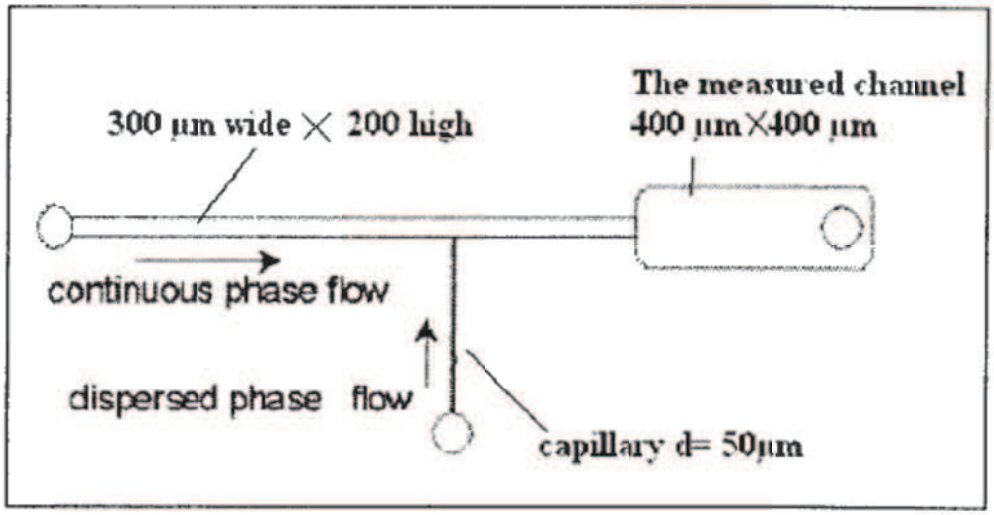

Figure 15 Schematic drawing of the T-junction microfluidic device.[55]

2.2.2.2 Droplet formation in flow-focusing devices

Figure 16 shows the flow-focusing device geometry. In detail, liquid A flows in the

middle channel and immiscible liquid B flows in the two adjacent channels. Afterwards, the two phases were pushed into one tiny orifice which is located downstream of these three channels and in front of the middle channel. Due to the pressure from the adjacent channels, the middle fluid was hydrodynamically focused as a thread nearby the orifice. Subsequently, the thread is broken up into several droplets before or after the orifice, which is really dependent on the combination of the two flow rates and the nature of the liquids. From Figure 16, it can be seen that the flow rate of liquid B was faster than the flow rate of liquid A since the liquid B filled the downstream chamber pass the orifice. Liquid A consisted of 2 wt.% of SDS in water while liquid B was hexadecane. Liquid A thread could be not only broken up in the dripping mode (Figure 16) but also in the jetting mode.[56] When one combines the low flow rate of the continuous phase and low ratio of flow rates of continuous phase to dispersed phase, the dispersed phase will break up behind the orifice and form the bigger droplets in the dripping regime with the weak shear force. With increasing the flow rate of continuous phase and suitable Q_c/Q_d, the dispersed phase thread will be broken upstream or behind the orifice due to the stronger shear force imposed on the dispersed phase thread. The formation of the droplets is still in the dripping regime. However, by continuously increasing the flow rate of the continuous phase and a large ratio of Q_c/Q_d, the formation of droplets will be in the jetting regime. The dispersed phase thread will be elongated up to the downstream channel pass the orifice and experience Rayleigh-Plateau instabilities producing much smaller droplets compared to the former two situations. However, small satellites are to be observed with the main droplets production under such condition. If with T-junction geometry, it is relatively easy to prepare droplets with a wide range of combination of continuous and dispersed phase flow rates, with a flow focusing device, one should optimized hydrodynamic conditions with much more attention in order to generate identical droplets with narrow size distributions and to reduce the satellites as much as possible.[57]

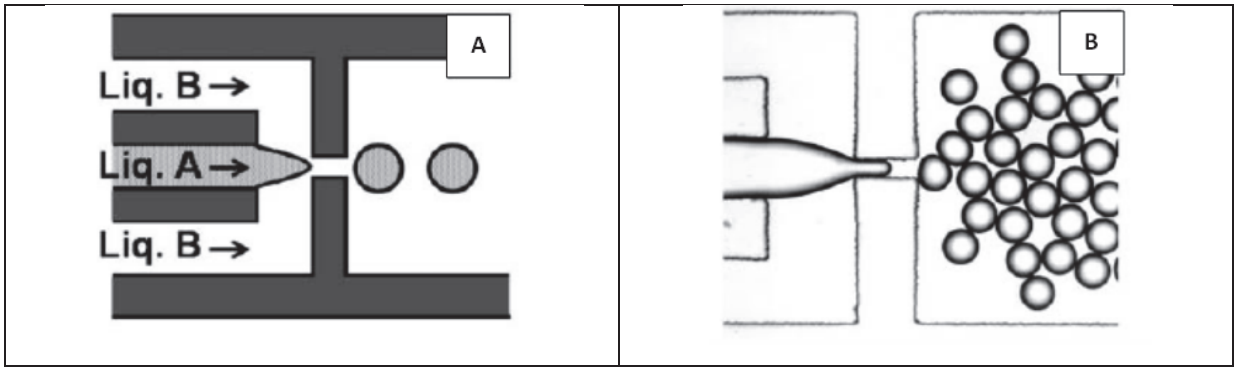

Figure 16 Schematic drawing of droplet formation in a microfluidic flow focusing device (A) and optical micrograph of obtained droplets from the top view (B).[58]

2.2.2.3 Droplet formation in co-flow devices

Compare to the T-junction and flow-focusing devices, co-flow devices are characterized by continuous and dispersed phases flowing parallelly to each other (Figure 17**).** Y. Hong and coll. investigated the flow rates effect on droplet size control in a co-flow microfluidic device.[59] In detail, the formation of droplets in such device is also due to the competition between the surface tension and the shear force induced by the flow of continuous phase on the forming droplet. Some other parameters could also influence the final droplets size, such as the diameter of the capillary or channel, viscosity of the two immiscible fluids, property of the device material and surface tension between the continuous phase and dispersed phase. Hereby, one will only consider the operating parameters. At the beginning, the dispersed phase flows into a fluid at rest in the channel, the supposed dispersed phase becomes larger and larger till it contacts with the wall of the channel and flows downstream by the power from itself. At this stage, no droplet are formed in the channel, in fact, the steady state flow has been reached. Big droplets will be formed by increasing the flow rate of the continuous phase. If this flow rate is further increases; a long elongated thread could be seen in the channel and ultimately break-up into several smaller droplets. Droplet size is not strongly dependent on the flow rate ratio and the size decreases with

increasing the capillary number when $Q_d/Q_c \geq 0.1$. In opposite, the droplet configuration and size are strongly dependent on the flow rate ratio and capillary number when $Q_d/Q_c < 0.1$.[59]

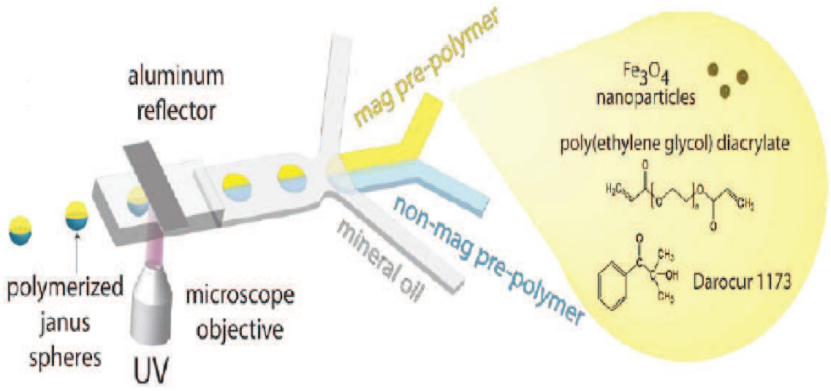

Figure 17 Schematic of Janus droplet and particle synthesis in a co-flow microfluidic device[60]

2.2.3 Preparation of polymeric microparticles from microfluidic emulsification devices

Different kinds of polymeric microparticles can be prepared by microfluidic systems such as plain, core-shell, or Janus particles. They are characterized by narrow particle size distributions for which the coefficient of variation – defined as the standard deviation divided by the average particle diameter – is typically lower than 5%. The size of the final polymeric microparticles is always a little bit smaller than the original microdroplets size by 2-10% due to the higher density of the polymer with respect to the density of its monomer.[61] In the following paragraphs, we will review the most microparticles.

2.2.3.1 Spherical microparticles

S. Sugiura and coll. designed one kind of microchannel-based device where monodispersed microdroplets were prepared by pressurizing the dispersed phase to the continuous phase (Figure 18).

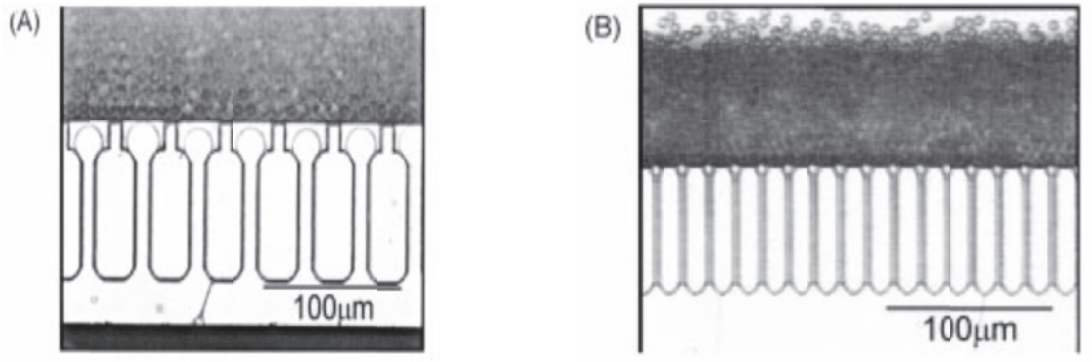

Figure 18 Optical micrographs of the microchannel-based device.[62]

The device had hundreds of microchannels aligned along the main continuous phase (0.2 wt.% SDS in aqueous solution) channel. The divinylbenzene dispersed phase was pumped through the microchannels and fell down on a terrace where the droplets are formed. Afterwards, the monomer emulsion was mixed with a PVA solution which was used as a stabilizer during the polymerization process. The resulting mixture was heated up to 90°C for 2h to promote the polymerization and the microdroplets were converted into polymeric microspheres with 3.4 μm and 9.2 μm diameter.[62]

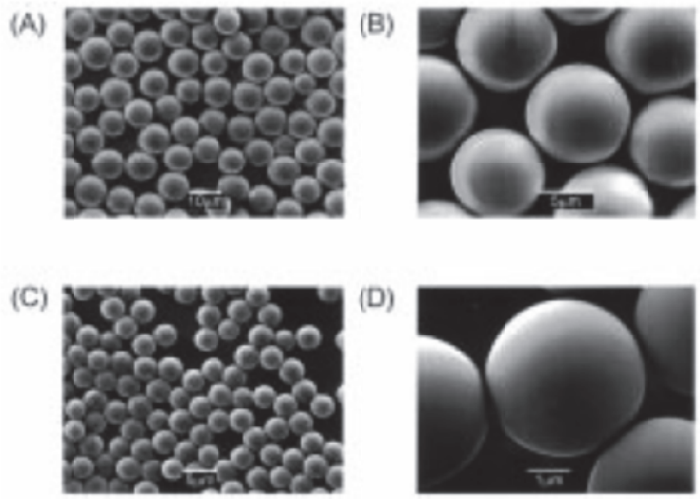

Figure 19 SEM images of polymeric microspheres prepared using microchannel-based device; (A), (B), (C) and(D) are under different magnification and two types of microfluidic channel device.[62]

2.2.3.2 *Janus microparticles*

Janus particles were named after the Roman Janus god because they exhibit two different faces of dissimilar chemical or physical properties, shapes etc. Several approaches are known to prepare Janus microparticles. Using non microfluidic methods, they can be obtained by breaking-up the two-layered wax jets produced in a spinning disk (Figure 20).[63]

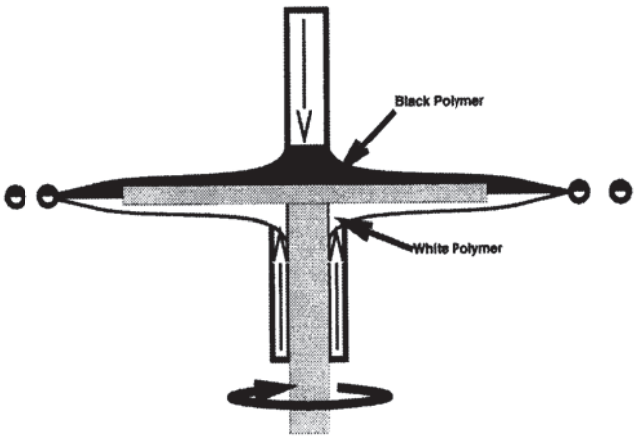

Figure 20 Janus microparticles are produced by introducing pigmented liquids to the top and bottom of a spinning disk.[63]

However the process efficiency is quite low as Janus and non-Janus microparticles are produced at the same time. Hereby, T. Nisisako and coll. successfully produced Janus microparticles from a microchannel-based device which is shown in Figure 21.[64]

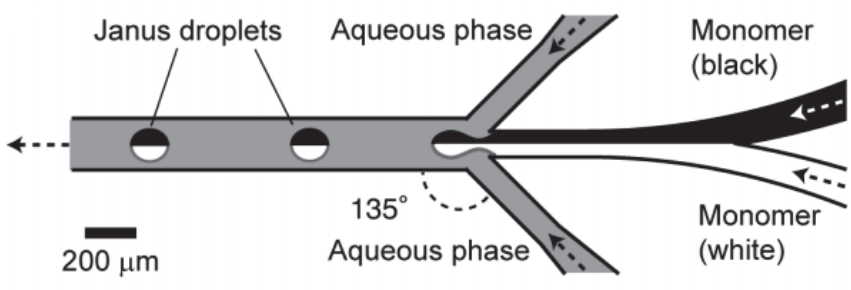

Figure 21 Schematic of the channel and flow configuration to produce Janus microdroplets.[64]

The design of this device comprised two Y-shape channels dry-etched on a planar glass. The representation is shown in Figure 21. Firstly, one Y-shape channel was used to deliver the two monomer phases containing a black and white pigment respectively. Under laminar flow, the two streams of each colored monomer phase left the Y-shape channel to flow side by side in another single channel. Downstream, a second Y-shape channel delivered the continuous phase (0.5 wt.% PVA in aqueous solution)such as to sheath the two dispersed monomer phases. As a result Janus droplets were formed. The monodispersed bicolored spheres were thermally polymerized out of the device at 90°C. From Figure 22, monodispersed Janus microparticles (117 μm, CV = 1.9%) can be seen. 20 μm microparticles presenting the same Janus characteristics were also produced from the satellite droplets formed during the emulsification.

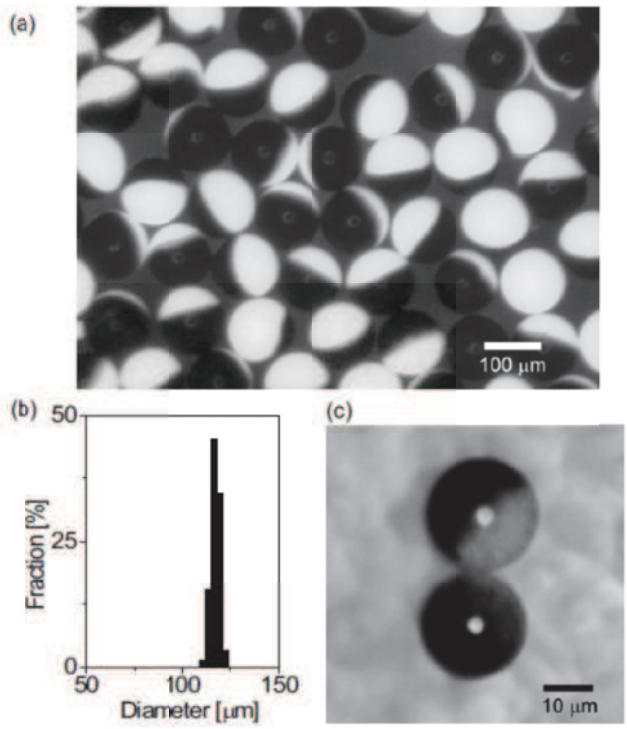

Figure 22 a) Monodispersed bicolored polymeric particles. b) Size distribution of the particles. Mean diameter is 117 µm. CV is 1.9% (n = 427), c) Particles prepared from satellite droplets.[64]

2.2.3.3 Core-shell microparticles

Core-shell or multilayer structured microparticles could be used in optical data storage, coating technologies, security data encryption and spherical dielectric resonators.[65] Z. Nie and coll. used a flow-focusing microfluidic device to produce core-shell microparticles where o/w/o where generated at first and UV-polymerized downstream (Figure 23).[65] The flow rates of the oil, monomer and aqueous phases influenced the entire core-shell microparticles diameter, the core diameter and the shell thickness. By increasing the ratio of flow rates between the water phase/monomer phase or monomer phase/oil phase, the size of the microparticles was smaller which resulted from an increase in the shear forces acting on the monomer phase and oil phase jets. The smallest microparticles were formed by increasing the flow rate of the aqueous phase. Increasing the monomer phase produced smaller core and thicker shell; while any

increase in the oil phase resulted in bigger core. Multiple cores droplets were achieved when the frequency of the break-up of the oil phase thread was above the frequency of the break-up of the monomer phase thread.[65]

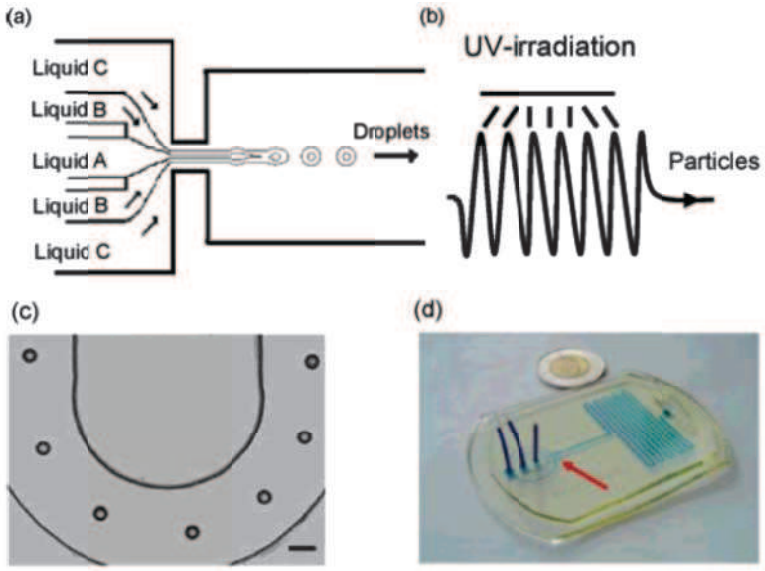

Figure 23 (a) Schematic representation of producing the droplets in MFFD by laminar co-flow of silicone oil (A), monomer (B), and aqueous phase(C). The orifice had a rectangular shape with width and height of 60 and 200 μm, respectively. (b) Schematic of the wavy channel used for photo polymerization of monomer in core-shell droplets. (c) Optical microscopy image of core-shell droplets flowing in the wavy channel used for in situ monomer photo polymerization. The scale bar is 200 μm. (d) Photograph of a real microfluidic system. Polyethylene tubing and microchannels are filled with a dye-labeled aqueous solution for increasing contrast of image. The arrow is pointing to the orifice.[65]

2.2.3.4 Other microparticles morphologies

Polymeric microparticles with high aspect ratios can also be produced in microfluidic devices my means of the so-called projection photolithography technique. This technique developed by *Dendukuri et al.*[66] relies on the UV irradiation, through the objective of an optical microscope, of a polymer solution flowing within a microchannel. Thus a stream of acrylate oligomer (poly(ethylene glycol) diacrylate)

and photo initiator was passed through a rectangular PDMS microfluidic device. The key part to obtain microparticles with high aspect ratios was the use of a mask placed in the field-stop plane of the microscope, which after UV exposure allowed in combination with a rapid polymerization (less than 0.1 s) transferring the pattern to the microparticles. Due to the flowing carrier, the newly formed microparticles will be pushed downstream till the reservoir. Various types of microparticles can be seen in Figure 25, such as triangles, squares, hexagons, colloidal entities, triangular and square cross-sections and non-symmetric or curved objects. The shape of the microparticles in the x-y plane is dependent on the used defined transparency mask. However, the height of the microparticles in the z direction is determined by the height of the channel and the oxygen inhibition layer' thickness.

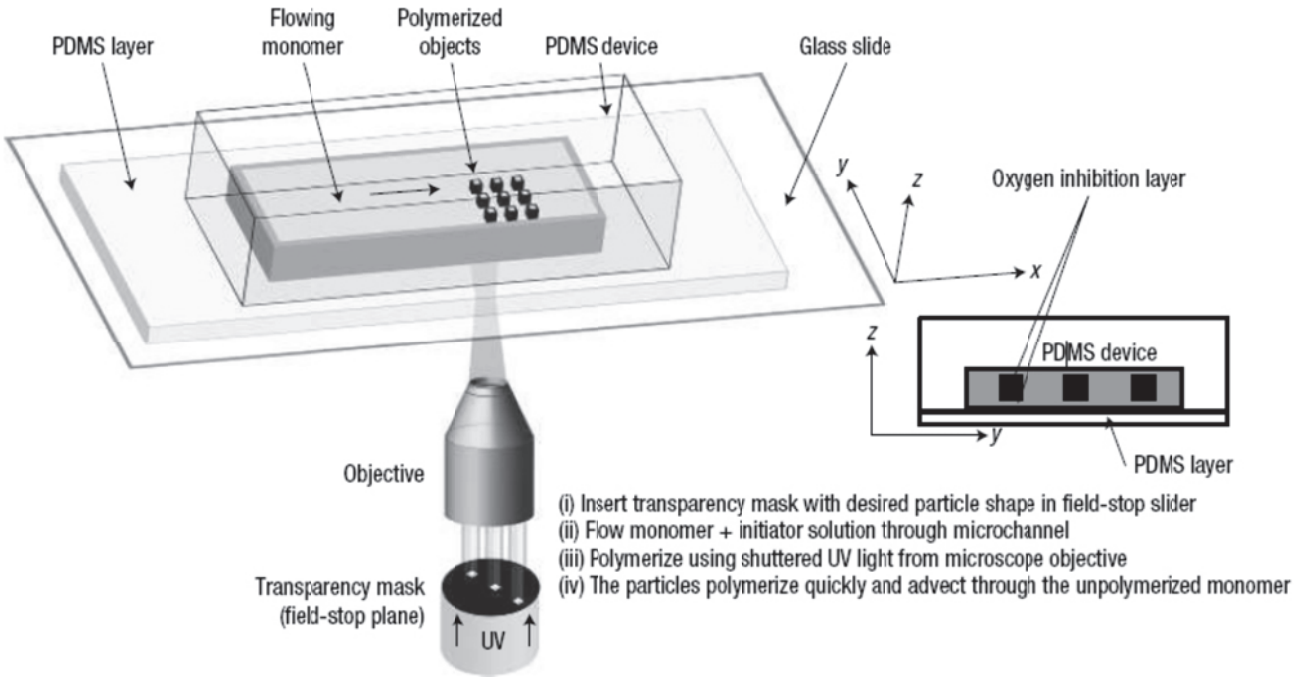

Figure 24 The monomer stream flows through the all-PDMS device in the direction with the arrow. The mask-defined UV light beam polymerizes the monomer, and then, the polymer particles advect within the unpolymerized monomer stream. The side view of the polymerized particles can also be seen from the lower right corner. An oxygen inhibition layer developed near the walls of the device prevents the polymerization and allows the free flow of the polymerized particles.[66]

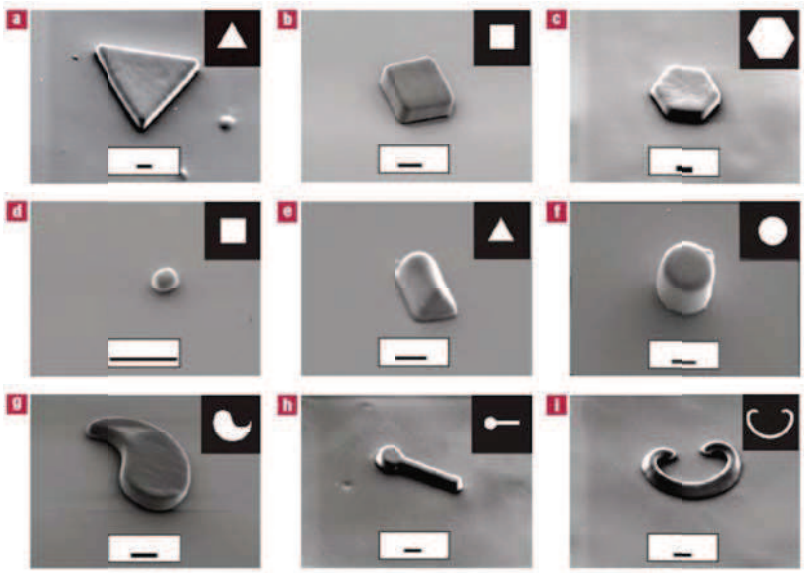

Figure 25 SEM images of different types of microparticles. The scale bar in all the figures is 10μm.[66]

2.2.4 Production of nanodroplets and polymer nanoparticles with microfluidic devices

Microfluidic technology can also be applied for the production of nanodroplets and nanoparticles[67]. Recently, Visaveliya *et al.*[68] investigated how to control the shape and size of polymer nanoparticles aggregates in a single-step microcontinuous flow process. Nanodroplets of the monomer phase were generated by the shear force caused by the tangential flow of a continuous phase at the surface of a microhole plate through which the dispersed phase was pumped (Figure 26).[68] Then downstream upon collection in a heated beaker, the nanodroplets were thermally polymerized. In general, spherical nanoparticles in the size range 50 to 500 nm were synthesized with ionic surfactants (e.g. SDS or CTAB). In the contrast, when polyvinylpyrrolidone (PVP) was dissolved in the continuous phase, flower-like nanoparticles were obtained. The formation of this type of nanoparticles can be explained by the nucleation/assembling mechanism. It was assumed that electrical charges vary during the particle growth as well as the electrostatic repulsion between nanoparticles in the colloidal suspension.

Visaveliya *et al.*[69] also investigated the role of self-polarization during the synthesis of linear and branched polymer nanoparticles. From this paper, linear and branched PMMA nanoparticles have been successfully prepared by via controlling the repulsive interaction using the theory of limited polarization. Different chain lengths of polystyrene sulfonate sodium salt (PSSS) could strongly influence the length and width of the obtained linear assembly of the polymeric nanoparticles. Based on the importance of charge and concentration of PSSS, the branched characteristic can be obtained due to the repulsive effect when the ratio of PSSS to nanoparticles is low.

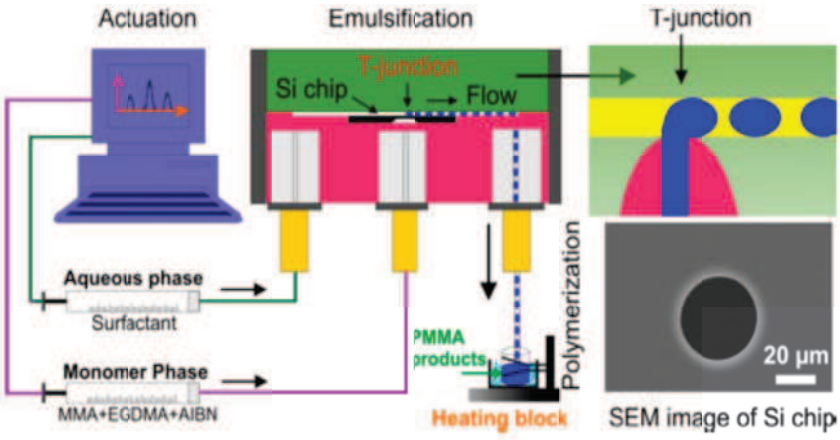

Figure 26 Schematic drawing of the single-step microcontinuous flow process for the synthesis of PMMA nanoparticles.[68]

L.-H. Hung and coll.[70] synthesized 70 nm poly(lactic-co-glycolic acid) (PLGA) nanospheres in a dual microfluidic droplet generator following the solvent extraction approach. PLGA was dissolved into DMSO solvent and resulting mixture was emulsified in the form of microdroplets by a continuous flow of silicon oil in a cross-flow microfluidic device (Figure 27). Another cross-channel allowed producing at the same time microdroplets of an aqueous solution in a dual manner (e.g. alternated with PLGA/DLSO microdroplets). In the downstream widening channel, both PLGA/DMSO and water microdroplets fused. Then DMSO diffused rapidly into the

aqueous solution leaving the PLGA in a supersaturation which induced the precipitation of the polymer chains into nanoparticles.

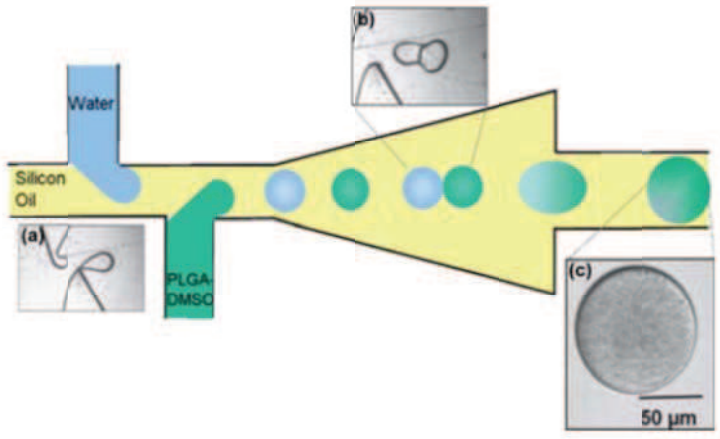

Figure 27 The procedure of how to prepare hundreds of PLGA nanoparticles in one microdroplet by microfluidic system.[70]

F. Bally *et al.*[71] have successfully developed a one-step micromixer-assisted nanoprecipitation process for the preparation of size-tunable polymer nanoparticles in the size range 90 to 200 nm. This technique relies on the solvent displacement method in which a polymer precipitates when its solvent diffuses rapidly in a non-solvent of the polymer. A diluted methacrylate-based polymer solution and an aqueous solution were flowed into an interdigital multilamination micromixer (HPIMM, IMM) through two different inlets (Figure 28). Thus, the nanoprecipitation occurred when both fluids met in the flow-focusing section. By increasing the ratio of the aqueous to polymer solutions flow rate, the nanoparticles size decreased. This is due to an increase in the nuclei formed favored by an even faster diffusion of the polymer solvent into the aqueous solution. Moreover, the concentration of the preformed polymer strongly influences the nanoparticles size, higher concentrated solutions gave bigger nanoparticles. However polymer solutions with a concentration in polymer up to 5 wt.% were successfully nanoprecipitated conversely to the conventional batch process

for which aggregates were formed. Finally CFD simulation highlighted the benefit of chaotic mixing when the overall flow rate through the micromixer was increases as smaller polymer nanoparticles were obtained for a given ratio of the aqueous to polymer solutions flow rate.

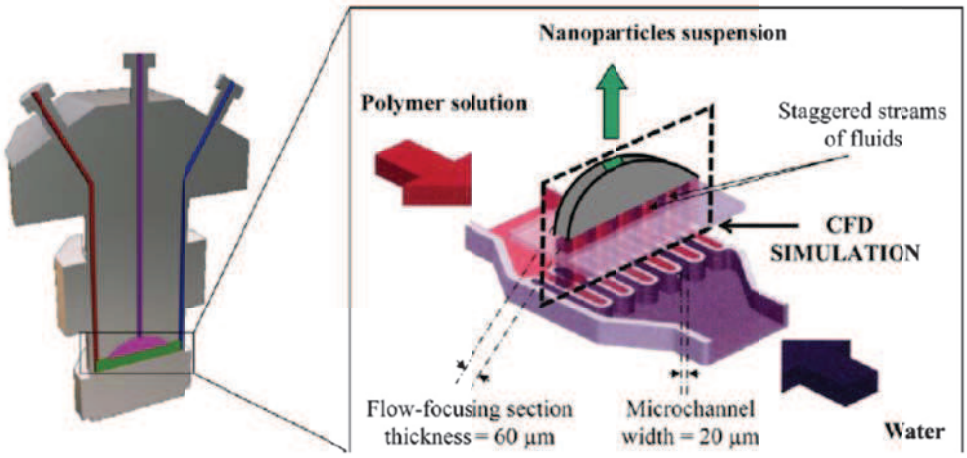

Figure 28 Schematic drawing of the nanoprecipitating micormixer.[71]

2.2.5 Summary on micro- and nanoparticles produced by microfluidics

Microfluidic devices were proved to be quite efficient systems to produce microdroplets with a high control on their size and size distribution. Polymeric microparticles with different shapes (sphere, high aspect ratios particles) and different morphologies (plain, Janus, core-shell) can be easily produced from the thermally-induced or UV-assisted polymerization of above polymerizable microdroplets.

On the other hand, microfluidic devices were also found recently as excellent candidates to produce monodispersed polymeric nanoparticles either from monomer nanodroplets or by nanoprecipitation of a preformed polymer.

Although both "worlds" (microfluidic nanodroplets and microfluidic micropdroplets) allow producing size controlled polymeric particles at the micro- and nanoscale, they

were never readily merged to prepare even more morphologically complex particles like composite/hybrid multi-scale and multi-domain polymeric microparticles. In such objects, polymer nanoparticles and possibly inorganic nanoparticles are selectively embedded into different domains of a polymeric microparticle. However these materials could have strong applications in fields such as sensorics, optical sensors and theranostics.

2.3 Conclusion

Given the aforementioned background literature, this thesis aims at producing composite/hybrid multi-scale and multi-domain polymeric microparticles by merging different microfluidic techniques allowing the production of size-tunable polymer nanoparticles and polymeric microparticles. Thus Chapter 3 will be dedicated to the development of an easy scalable elongational-flow microprocess operating either in batch or continuous-flow mode for the production of size-tunable nanoemulsions. Chapter 4 will investigate the possibility to convert these nanoemulsions into colloidal suspensions of polymer nanoparticles either by thermally-induced or UV-assisted miniemulsion polymerization. Then upon mixing with proper compounds, the obtained nanosuspensions will be used in different capillaries-based microfluidic droplet generators to produce these composite/hybrid multi-scale and multi-domain polymeric microparticles.

2.4 References

1. Remington, J. P.; Troy, D. B.; Beringer, P., Remington: The science and practice of pharmacy. Lippincott Williams & Wilkins: 2006; Vol. 1.

2. Chappat, M., Some applications of emulsions. Colloids and Surfaces A: Physicochemical and Engineering Aspects 1994, 91 (0), 57-77.

3. Debnath, B. K.; Saha, U. K.; Sahoo, N., A comprehensive review on the application of emulsions as an

alternative fuel for diesel engines. Renewable and Sustainable Energy Reviews 2015, 42 (0), 196-211.

4. Landfester, K.; Bechthold, N.; Tiarks, F.; Antonietti, M., Formulation and Stability Mechanisms of Polymerizable Miniemulsions. Macromolecules 1999, 32 (16), 5222-5228.

5. Slomkowski, S.; Alemán, J. V.; Gilbert, R. G.; Hess, M.; Horie, K.; Jones, R. G.; Kubisa, P.; Meisel, I.; Mormann, W.; Penczek, S., Terminology of polymers and polymerization processes in dispersed systems (IUPAC Recommendations 2011). Pure and Applied Chemistry 2011, 83 (12), 2229-2259.

6. McClements, D. J., Nanoemulsions versus microemulsions: terminology, differences, and similarities. Soft matter 2012, 8 (6), 1719-1729.

7. Schramm, L. L., Emulsions, foams, and suspensions: fundamentals and applications. John Wiley & Sons: 2006.

8. Ratke, L.; Voorhees, P. W., Growth and coarsening: Ostwald ripening in material processing. Springer Science & Business Media: 2013.

9. Zwicker, D.; Hyman, A. A.; Jülicher, F., Suppression of Ostwald ripening in active emulsions. Physical Review E 2015, 92 (1), 012317.

10. Ouzineb, K.; Graillat, C.; McKenna, T. F., Study of compartmentalization in the polymerization of miniemulsions of styrene and butyl methacrylate. Journal of Applied Polymer Science 2004, 91 (1), 115-124.

11. Tlusty, T.; Safran, S. A., Microemulsion networks: the onset of bicontinuity. Journal of Physics: Condensed Matter 2000, 12 (8A), A253.

12. Butt, H.-J.; Graf, K.; Kappl, M., Physics and chemistry of interfaces. John Wiley & Sons: 2006.

13. De Gennes, P.-G.; Brochard-Wyart, F.; Quéré, D., Capillarity and wetting phenomena: drops, bubbles, pearls, waves. Springer Science & Business Media: 2013.

14. Solans, C.; Izquierdo, P.; Nolla, J.; Azemar, N.; Garcia-Celma, M. J., Nano-emulsions. Current Opinion in Colloid & Interface Science 2005, 10 (3–4), 102-110.

15. Sajjadi, S., Nanoemulsion Formation by Phase Inversion Emulsification: On the Nature of Inversion. Langmuir 2006, 22 (13), 5597-5603.

16. McClements, D. J., Edible nanoemulsions: fabrication, properties, and functional performance. Soft Matter 2011, 7 (6), 2297-2316.

17. Wood, R. W.; Loomis, A. L., XXXVIII. The physical and biological effects of high-frequency sound-waves of great intensity. The London, Edinburgh, and Dublin Philosophical Magazine and Journal of Science 1927, 4 (22), 417-436.

18. Peshkovsky, A. S.; Peshkovsky, S. L.; Bystryak, S., Scalable high-power ultrasonic technology for the production of translucent nanoemulsions. Chemical Engineering and Processing: Process Intensification 2013, 69 (0), 77-82.

19. Kentish, S.; Wooster, T. J.; Ashokkumar, M.; Balachandran, S.; Mawson, R.; Simons, L., The use of ultrasonics for nanoemulsion preparation. Innovative Food Science & Emerging Technologies 2008, 9 (2), 170-175.

20. Burgaud, I.; Dickinson, E.; Nelson, P. V., An improved high-pressure homogenizer for making fine

emulsions on a small scale. International Journal of Food Science & Technology 1990, 25 (1), 39-46.

21. Stang, M.; Schuchmann, H.; Schubert, H., Emulsification in High-Pressure Homogenizers. Engineering in Life Sciences 2001, 1 (4), 151-157.

22. Sánchez, H. H.; Gutierrez-Lopez, G. F., Food Nanoscience and Nanotechnology. Springer: 2015.

23. Siddiqui, S. W.; Unwin, P. J.; Xu, Z.; Kresta, S. M., The effect of stabilizer addition and sonication on nanoparticle agglomeration in a confined impinging jet reactor. Colloids and Surfaces A: Physicochemical and Engineering Aspects 2009, 350 (1–3), 38-50.

24. Meleson, K.; Graves, S.; Mason, T. G., Formation of Concentrated Nanoemulsions by Extreme Shear. Soft Materials 2004, 2 (2-3), 109-123.

25. Lee, L.; Norton, I. T., Comparing droplet breakup for a high-pressure valve homogeniser and a Microfluidizer for the potential production of food-grade nanoemulsions. Journal of Food Engineering 2013, 114 (2), 158-163.

26. Rodgers, T. L.; Cooke, M.; Hall, S.; Pacek, A.; Kowalski, A., Rotor-stator mixers. Chem Eng Trans 2011, 24, 1411-1416.

27. Urban, K.; Wagner, G.; Schaffner, D.; Röglin, D.; Ulrich, J., Rotor-Stator and Disc Systems for Emulsification Processes. Chemical Engineering & Technology 2006, 29 (1), 24-31.

28. Maa, Y.-F.; Hsu, C., Liquid-liquid emulsification by rotor/stator homogenization. Journal of Controlled Release 1996, 38 (2–3), 219-228.

29. Hall, S.; Cooke, M.; El-Hamouz, A.; Kowalski, A. J., Droplet break-up by in-line Silverson rotor–stator mixer. Chemical Engineering Science 2011, 66 (10), 2068-2079.

30. Scholz, P.; Keck, C. M., Nanoemulsions produced by rotor–stator high speed stirring. International Journal of Pharmaceutics 2015, 482 (1–2), 110-117.

31. Hall, S.; Pacek, A. W.; Kowalski, A. J.; Cooke, M.; Rothman, D., The effect of scale and interfacial tension on liquid–liquid dispersion in in-line Silverson rotor–stator mixers. Chemical Engineering Research and Design 2013, 91 (11), 2156-2168.

32. Paul, E. L.; Atiemo-Obeng, V. A.; Kresta, S. M., Handbook of Industrial Mixing.

33. Das, P. K.; Legrand, J.; Morançais, P.; Carnelle, G., Drop breakage model in static mixers at low and intermediate Reynolds number. Chemical Engineering Science 2005, 60 (1), 231-238.

34. Thakur, R. K.; Vial, C.; Nigam, K. D. P.; Nauman, E. B.; Djelveh, G., Static Mixers in the Process Industries—A Review. Chemical Engineering Research and Design 2003, 81 (7), 787-826.

35. Kiss, N.; Brenn, G.; Pucher, H.; Wieser, J.; Scheler, S.; Jennewein, H.; Suzzi, D.; Khinast, J., Formation of O/W emulsions by static mixers for pharmaceutical applications. Chemical Engineering Science 2011, 66 (21), 5084-5094.

36. Farzi, G.; Bourgeat-Lami, E.; McKenna, T. F., Miniemulsions using static mixers: A feasibility study using simple in-line static mixers. Journal of applied polymer science 2009, 114 (6), 3875-3881.

37. Joscelyne, S. M.; Trägårdh, G., Membrane emulsification — a literature review. Journal of Membrane Science 2000, 169 (1), 107-117.

38. Schröder, V.; Behrend, O.; Schubert, H., Effect of Dynamic Interfacial Tension on the Emulsification Process Using Microporous, Ceramic Membranes. Journal of Colloid and Interface Science 1998, 202 (2), 334-340.

39. Peng, S.; Williams, R. A., Controlled Production of Emulsions Using a Crossflow Membrane. Particle & Particle Systems Characterization 1998, 15 (1), 21-25.

40. van der Graaf, S.; Schroën, C. G. P. H.; Boom, R. M., Preparation of double emulsions by membrane emulsification—a review. Journal of Membrane Science 2005, 251 (1–2), 7-15.

41. Solans, C.; Solé, I., Nano-emulsions: Formation by low-energy methods. Current Opinion in Colloid & Interface Science 2012, 17 (5), 246-254.

42. Miller, C. A., Spontaneous Emulsification Produced by Diffusion — A Review. Colloids and Surfaces 1988, 29 (1), 89-102.

43. Taylor, P.; Ottewill, R. H., The formation and ageing rates of oil-in-water miniemulsions. Colloids and Surfaces A: Physicochemical and Engineering Aspects 1994, 88 (2–3), 303-316.

44. Vitale, S. A.; Katz, J. L., Liquid Droplet Dispersions Formed by Homogeneous Liquid−Liquid Nucleation: “The Ouzo Effect”. Langmuir 2003, 19 (10), 4105-4110.

45. Ganachaud, F.; Katz, J. L., Nanoparticles and Nanocapsules Created Using the Ouzo Effect: Spontaneous Emulsification as an Alternative to Ultrasonic and High-Shear Devices. ChemPhysChem 2005, 6 (2), 209-216.

46. Shinoda, K.; Saito, H., The effect of temperature on the phase equilibria and the types of dispersions of the ternary system composed of water, cyclohexane, and nonionic surfactant. Journal of Colloid and Interface Science 1968, 26 (1), 70-74.

47. Israelachvili, J. N., Intermolecular and surface forces: revised third edition. Academic press: 2011.

48. Roger, K.; Cabane, B.; Olsson, U., Formation of 10−100 nm Size-Controlled Emulsions through a Sub-PIT Cycle. Langmuir 2010, 26 (6), 3860-3867.

49. Sonneville-Aubrun, O.; Babayan, D.; Bordeaux, D.; Lindner, P.; Rata, G.; Cabane, B., Phase transition pathways for the production of 100 nm oil-in-water emulsions. Physical Chemistry Chemical Physics 2009, 11 (1), 101-110.

50. Koroleva, M. Y.; Evgenii, V. Y., Nanoemulsions: the properties, methods of preparation and promising applications. Russian Chemical Reviews 2012, 81 (1), 21-43.

51. Whitesides, G. M., The origins and the future of microfluidics. Nature 2006, 442 (7101), 368-373.

52. Manz, A.; Harrison, D. J.; Verpoorte, E. M. J.; Fettinger, J. C.; Paulus, A.; Lüdi, H.; Widmer, H. M., Planar chips technology for miniaturization and integration of separation techniques into monitoring systems: Capillary electrophoresis on a chip. Journal of Chromatography A 1992, 593 (1–2), 253-258.

53. Theberge, A. B.; Courtois, F.; Schaerli, Y.; Fischlechner, M.; Abell, C.; Hollfelder, F.; Huck, W. T. S., Microdroplets in Microfluidics: An Evolving Platform for Discoveries in Chemistry and Biology. Angewandte Chemie International Edition 2010, 49 (34), 5846-5868.

54. Kawakatsu, T.; Kikuchi, Y.; Nakajima, M., Regular-sized cell creation in microchannel emulsification by visual microprocessing method. J Amer Oil Chem Soc 1997, 74 (3), 317-321.

55. Xu, J. H.; Li, S. W.; Tan, J.; Wang, Y. J.; Luo, G. S., Preparation of highly monodisperse droplet in a T-junction microfluidic device. AIChE Journal 2006, 52 (9), 3005-3010.

56. Seo, M.; Nie, Z.; Xu, S.; Mok, M.; Lewis, P. C.; Graham, R.; Kumacheva, E., Continuous Microfluidic Reactors for Polymer Particles. Langmuir 2005, 21 (25), 11614-11622.

57. Dendukuri, D.; Doyle, P. S., The Synthesis and Assembly of Polymeric Microparticles Using Microfluidics. Advanced Materials 2009, 21 (41), 4071-4086.

58. Seo, M.; Paquet, C.; Nie, Z.; Xu, S.; Kumacheva, E., Microfluidic consecutive flow-focusing droplet generators. Soft Matter 2007, 3 (8), 986-992.

59. Hong, Y.; Wang, F., Flow rate effect on droplet control in a co-flowing microfluidic device. Microfluid Nanofluid 2007, 3 (3), 341-346.

60. Yuet, K. P.; Hwang, D. K.; Haghgooie, R.; Doyle, P. S., Multifunctional Superparamagnetic Janus Particles. Langmuir 2010, 26 (6), 4281-4287.

61. Serra, C. A.; Chang, Z., Microfluidic-Assisted Synthesis of Polymer Particles. Chemical Engineering & Technology 2008, 31 (8), 1099-1115.

62. Sugiura, S.; Nakajima, M.; Itou, H.; Seki, M., Synthesis of Polymeric Microspheres with Narrow Size Distributions Employing Microchannel Emulsification. Macromolecular Rapid Communications 2001, 22 (10), 773-778.

63. Sheridon, N. K.; Richley, E. A.; Mikkelsen, J. C.; Tsuda, D.; Crowley, J. M.; Oraha, K. A.; Howard, M. E.; Rodkin, M. A.; Swidler, R.; Sprague, R., The Gyricon rotating ball display. Journal of the Society for Information Display 1999, 7 (2), 141-144.

64. Nisisako, T.; Torii, T.; Takahashi, T.; Takizawa, Y., Synthesis of Monodisperse Bicolored Janus Particles with Electrical Anisotropy Using a Microfluidic Co-Flow System. Advanced Materials 2006, 18 (9), 1152-1156.

65. Nie, Z.; Xu, S.; Seo, M.; Lewis, P. C.; Kumacheva, E., Polymer Particles with Various Shapes and Morphologies Produced in Continuous Microfluidic Reactors. Journal of the American Chemical Society 2005, 127 (22), 8058-8063.

66. Dendukuri, D.; Pregibon, D. C.; Collins, J.; Hatton, T. A.; Doyle, P. S., Continuous-flow lithography for high-throughput microparticle synthesis. Nat Mater 2006, 5 (5), 365-369.

67. Köhler, J. M.; Li, S.; Knauer, A., Why is Micro Segmented Flow Particularly Promising for the Synthesis of Nanomaterials? Chemical Engineering & Technology 2013, 36 (6), 887-899.

68. Visaveliya, N.; Köhler, J. M., Control of Shape and Size of Polymer Nanoparticles Aggregates in a Single-Step Microcontinuous Flow Process: A Case of Flower and Spherical Shapes. Langmuir 2014, 30 (41), 12180-12189.

69. Visaveliya, N.; Köhler, J. M., Role of Self-Polarization in a Single-Step Controlled Synthesis of Linear and Branched Polymer Nanoparticles. Macromolecular Chemistry and Physics 2015, 216 (11), 1212-1219.

70. Hung, L.-H.; Teh, S.-Y.; Jester, J.; Lee, A. P., PLGA micro/nanosphere synthesis by droplet microfluidic solvent evaporation and extraction approaches. Lab on a Chip 2010, 10 (14), 1820-1825.

71. Bally, F.; Garg, D. K.; Serra, C. A.; Hoarau, Y.; Anton, N.; Brochon, C.; Parida, D.; Vandamme, T.;

Hadziioannou, G., Improved size-tunable preparation of polymeric nanoparticles by microfluidic nanoprecipitation. Polymer 2012, 53 (22), 5045-5051.

CHAPTER 3

DEVELOPMENT OF AN ELONGATIONAL-FLOW MICROPROCESS FOR THE PRODUCTION OF SIZE-CONTROLLED NANOEMULSIONS

Preface

From the literature review, it was reported the need for a microfluidic process allowing the production of size-controlled nanoemulsions which could operate at low energy input and could be easily scaled-up. Most of the conventional large scale emulsifiers rely on a shear flow to rupture the dispersed phase large droplets to ultimately nanosize droplets. However, these devices required a large energy input and cannot finely tune the nanodroplets size. On the other hand, elongational flows were demonstrated, at least theoretically by Taylor, as more efficient than shear flows to rupture large droplets into smaller one even for a highly viscous dispersed phase.

Thus, in the next section, a batch microfluidic process for the production of size-tunable nanoemulsions will be described. It is operating on the basis of a reciprocating elongational-flow through an abrupt restriction placed in the flow of an o/w emulsion. Effect of the operating parameters on the nanodroplets size and size distribution will be thoroughly assessed and modelled by an empirical correlation between relevant dimensionless numbers.

This chapter is partially adapted from the two following articles:

(1) Wei Yu, Christophe A. Serra, Ikram Ullah Khan, Shukai Ding, Rigoberto Ibarra Gomez, Michel Bouquey and René Muller, Development of an Elongational-Flow Microprocess for the Production of Size-Controlled Nanoemulsions: Batch Operation, Chem. Eng. J., to be submitted

(2) Wei Yu, Christophe A. Serra, ShuKai Ding, Rigoberto Ibarra Gomez, Michel Bouquey and René Muller, Development of an Elongational-Flow Microprocess for the Production of Size-Controlled Nanoemulsions: Continuous-Flow Operation, Chem. Eng. J., to be submitted

3.1 Batch operation

ABSTRACT

Performances of a newly developed microprocess in producing size-controlled nanoemulsions in the lower nanometers range were assessed. The microprocess comprised an elongational-flow micromixer with a bore size of either 150, 250 or 500 μm. By inducing a reciprocating flow through the restriction of the micromixer, MMA-based nanoemulsions with controlled sizes in the range 50-300 nm were successfully prepared at low pressures (ca. 2.5 bars) in laminar to intermediate hydraulic flow regimes. Effect of process parameters (flow rate through the restriction, number of cycles), micromixer parameters (angle, bore size) and finally composition parameters (weight content of MMA and surfactant, dispersed to continuous phase viscosity ratio) on nanodroplets size and size distribution was thoroughly studied. A unique empirical correlation was extracted from the experimental results and was found to fairly well model the variations of the nanodroplets size with aforementioned parameters.

3.1.1 Introduction

An emulsion is defined as a two-phase system, prepared by mixing two immiscible liquids, in which small globules of one liquid are dispersed uniformly throughout the other liquid.[1] Nanoemulsion, also known as miniemulsion, refers to an emulsion in which globules (droplets) size is typically in the range of tens to hundreds of nanometers. In order to formulate a stable emulsion, it is necessary to consider well the factors which influence emulsion's quality. These factors include the choice of a proper set of components (dispersed and continuous phases, surfactant or combination of surfactants etc.) and their respective concentration, the choice of an efficient mechanism that can rupture the bigger droplets into micro- or nanoscale ones and finally the selection of a proper order for adding each component.[2]

Over the last decades, nanoemulsions have attracted a lot of industrial and academic interests owing to their specific droplet size as well as their long-term physical stability (no apparent flocculation or coalescence)[3] and have found many application in fields such as food,[4] cosmetic,[5] pharmacy,[6] and fuel[7] industries. However several requirements should be considered for the production of nanoemulsions. First, total insolubility between the dispersed and continuous phases is a prerequisite although for practical reasons the dispersed phase may be slightly soluble in the continuous phase. In such situation and in case of non-equal size droplets, the Ostwald ripening phenomenon occurs which is experimentally observed by the growing of the larger particles at the expense of the smaller ones by molecular diffusion across the continuous phase. The driving force of the Ostwald ripening phenomenon is the Laplace pressure difference between small and large droplets. Although suppressing the Ostwald ripening phenomenon can be achieved by several means,[8] it is easiest to add in the dispersed phase a molecule (so-called Ostwald ripening inhibitor) completely immiscible with the continuous phase which purpose is to create an osmotic pressure which balances the Laplace pressure. The second requirement is an excess of an ionic surfactant in the continuous phase characterized by a fast adsorption kinetics so that to guarantee the efficient coating of the new coming surface of the nanoscale droplets during emulsification and to prevent by electrostatic repulsion the shear-induced coalescence.[9] Not to mention the possibility to decrease the interfacial tension and hence to favor the formation of smaller droplets. Generally, the surfactant is dispersed in the continuous phase with the form of micelles. When the new droplets are produced, these micelles dissociate rapidly into single surfactant entities to cover the droplet's surface. The concentration of surfactant must be above the critical micelle concentration (CMC). The third requirement is choosing the proper surfactant, which should not undergo the formation of lyotropic liquid crystalline microemulsion phase. Indeed, systems containing surfactant, water, alcohol and short chain alkane are known to be prone to form these phases.[10] The fourth requirement is using an

emulsification method that allows rupturing the dispersed phase into nanodroplets and thus overcoming the Laplace pressure.

Several conventional methods are available for producing nanoemulsions. They can be classified into two categories: high-energy and low-energy methods.[11,12] High-energy methods include energy inputs which are provided by apparatus such as ultrasound generator, high-pressure homogenizer, rotor-stator mixer, static mixer and membrane. By using these emulsification methods, the nanodroplets can be obtained by energy transfer with the presence of surfactant whose function is to decrease the interfacial tension. Our group has recently developed a new concept of reactor/mixer (called RMX®) which was successfully used to produce nanoemulsions whose size can be controlled in the range 30-100 nm.[13] The working principle of this pneumatic apparatus is based on the reciprocating flow of a crude emulsion through an abrupt contraction which generates a strong elongational flow, known to be more efficient, in contrast to shear flow, to rupture dispersed phase droplets into smaller ones. Although this apparatus operates at moderate pressure (max 6 bars), conversely to the high pressure homogenizer, the flow regime through the restriction is highly turbulent and may lead to local heating which might be detrimental for certain applications. Low-energy methods take advantage of the internal chemical potential of the emulsion components to achieve emulsification. It relies on the formation of emulsion when either its composition or the surrounding conditions are changed.[14] It consists of spontaneous emulsification, phase inversion temperature and phase inversion composition. Very low interfacial tensions are the key factor of these emulsification methods which can be achieved by formulation designs.

On the other hand, microfluidics is the science and technology of systems that process or manipulate small amounts of fluids (10^{-9} to 10^{-18} liters) using microchannels with dimensions of tens to hundreds of micrometres.[15] After one of the first microfluidic device was reported in 1979,[16] microfluidics strongly attracted many scientists due to its bright potential application. Indeed, a number of benefits can be pulled out from

microfluidic technologies compared to large scale technologies. It includes among others, faster heat and mass transfers, the possibility to carry out separations and detections with high resolution and sensitivity by using very small quantities of chemicals or reagents (so-called μTAS), low cost for reagent, time-saving and tiny devices footprint.[17]

The current study aims at developing a microfluidic version of the RMX® which can extent the size of nanodroplets above 100 nm and operate at lower Reynolds numbers, i.e. at smaller energy input to get rid of local heating. To that extent, a novel batch elongational–flow microprocess has been developed to prepare monomer-based nanoemulsions. Effect of process parameters, device geometry and emulsion composition parameters on the nanodroplets size was thus thoroughly investigated.

3.1.2 Materials and procedure

3.1.2.1 Materials

In this study, four components were required to prepare a standard polymerizable nanoemulsion: monomer (15 vol.%), surfactant (2.5 wt.%/Monomer), hydrophobic agent (4 wt.%/Monomer) as an Ostwald-ripening inhibitor and distilled water (85 vol.%). Based on the standard recipe, each component will be varied in order to investigate its influence on the nanodroplets size. Specifically, the monomer was methyl methacrylate (MMA, 99% purity, supplied by Aldrich). The surfactant was sodium dodecyl sulfate (SDS, 99% purity, supplied by Alfa Aesar), the hydrophobic agent was hexadecane (HD, 99% purity; Sigma Aldrich). Distilled water was used throughout the experiment. Poly methyl methacrylate (PMMA) with a high molecular weight (120,000 g mol^{-1}) synthesized in the laboratory by batch free radical polymerization was used in order to increase the viscosity of the dispersed phase of the emulsion when necessary. Locust bean gum (Louis François, Marne la Vallée, France)

was dissolved in the continuous phase of the emulsion to increase its viscosity when necessary.

3.1.2.2 Microprocess

As illustrated in Figure 1A, the emulsification microprocess mainly consisted of two mid pressure syringe pumps (neMESYS Mid Pressure Module, Cetoni), two 25 mL stainless steel syringes (Cetoni) and one PEEK tee (Valco Vici) as the elongational–flow microemulsifier/micromixer, The syringe pumps are operated by the supplier's software and can independently inject or withdraw, work in tandem (withdraw/withdraw, infuse/infuse) or in opposite phase (withdraw/infuse). The micromixer, in turn, consists of several drilled microchannels having a bore size of either 150, 250 or 500 µm. Two of these microchannels are linked to the stainless steel syringes by two PTFE tubings (1.06 mm ID x 1.68 mm OD). A third microchannel is used to recover the nanoemulsion by means of the same kind of PTFE tubing. For some experiences, a 5 mL syringe were also used. As shown in Figure 1B, the angle between the two microchannels linked to the syringes can be varied from 60 to 180°. A total of eight elongational-flow micromixers were tested whose characteristics are given in Table 1.

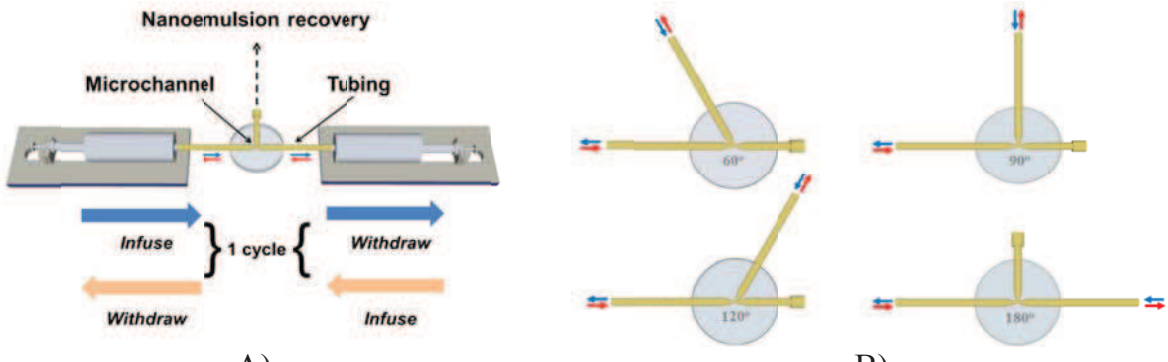

Figure **1**. A): Schematic drawing of the microprocess (not at scale); B) four elongational-flow micromixers with different angles

Table 1. Characteristics of the 8 elongational-flow micromixers investigated

Label	Bore size (D_h in μm)	**Angle** (°)
EFM_500_180	500	180
EFM_250_180	250	180
EFM_150_180	150	180
EFM_500_120	500	120
EFM_500_90	500	90
EFM_250_90	250	90
EFM_150_90	150	90
EFM_500_60	500	60

3.1.2.3 General procedure

Few weight percents of SDS were dissolved in distilled water and hexadecane was dissolved in MMA separately. For some experiments, water and oil phases were viscosified by adding few weight percents of locust bean gum and PMMA respectively. Then the two solutions were separately charged (no premix) into one stainless steel syringe for a total volume of 5 mL. Next, the pumps were switched on and forced to operate at the same flow rate and in opposite phase so that the solution passed from one syringe to the other one through the restriction of the micromixer. A back and forth movement of the pump counts for one cycle. After a prescribed number of cycles (100 to 800), one of the syringes was set to its zero volume position, while the second one was forced to infuse the freshly-prepared nanoemulsion through the recovery microchannel. The duration of one cycle depended upon the flow rate and ranged from 4 to 60 s. The reference conditions are listed in Table 2.

For comparison purpose, nanoemulsions were also prepared using a labscale rotor-stator emulsifier mixer (Ultraturrax T 25 basic, IKA) and equipped with a dispersing element (S 25 N - 8 G). A mixture composed of 12.75 mL of a distilled water/SDS solution and 2.25 mL of a MMA/HD solution was poured into a vial. Six different speeds (6500, 9500, 13500, 17500, 21500 and 24000 RPM) were applied on six independent vials filled with the above mentioned recipe for 10 min.

Table 2. Reference conditions

Micromixer	EFM_250_180
Flow rate, q	50 mL/min
MMA volume fraction, ϕ	15%
Nanoemulsion volume, V	5 mL
SDS concentration, C_{SDS}	2.4 wt.%/MMA
HD concentration, C_{HD}	4 wt.%/MMA
Number of cycles, #	800

3.1.2.4 Characterizations

The nanodroplets diameter and their polydispersity in size (PDI) were characterized by a commercial dynamic light scattering detector (DLS, Zetasizer, Nano Series, Malvern) at a fixed scattering angle of 173°. In order to reach the required turbidity for an accurate measurement and limit the possible coalescence as much as possible, two drops of freshly-prepared nanoemulsions were dispersed into 9 mL of distilled water shortly before the analysis. Approximately 1 mL of the diluted nanoemulsion was injected into the disposable DLS cuvette. Three kinds of average nanodroplets diameters (number-, volume- and intensity-) could be returned automatically by the DLS detector as well as the PDI value. The intensity-average diameter D_{exp} was used

throughout this study. PDI values below 0.2 are usually considered as the feature of monodisperse size distributions.[18] For each sample, DLS measurement was run in triplicate and results are reported in Table S1 for all the conditions investigated. Several samples (up to 5) obtained at different dates were analyzed for the same set of operating parameters. This allowed calculating the coefficient of variation (CV) defined as the ratio of the standard deviation of all average values returned by the DLS measurements and the mean droplet diameter. CV was found to vary from 4% to 1% for the smallest droplets (~50 nm) and the largest ones (~300 nm) respectively. The viscosity of the continuous and dispersed phases was measured with a temperature-controlled capillary viscometer (Schott AVS 360) whose temperature was set to 25°C. Each sample was measured four times and the average value was extracted. The interfacial tension was measured by the rising drop method using a tensiometer (TRK-S, Teclis). The density of all our investigated solutions was measured by weighting 1 mL of the solution sampled with an accurate micropipette (Pipetman P1000, Gilson).

3.1.3 Results and discussion

In the following, a thorough study about the influence of process parameters (number of cycles, flow rate, syringe size), device parameters (bore size, flow geometry) and composition parameters (surfactant concentration, MMA volume fraction, dispersed to continuous phase viscosity ratio) on the nanodroplets size and size distribution was conducted.

3.1.3.1 Effect of bore size, number of cycles, flow rate and micromixer's angle

Whatever the bore size, the variation of D_{exp} with respect to the number of cycles exhibits the same trend (Figure 2); D_{exp} decreases when the number of cycles increases and a plateau value seems to be reached for high numbers of cycles. However when

the flow rate through the restriction is increased, the plateau value decreases and is reached for a smaller number of cycles. Is it noteworthy that for the smaller bore size (150 µm) and the highest flow rate investigated (30 mL/min), the plateau value is obtained just after 100 cycles as the curve is almost flat beyond this point (C). For all data points presented in Figure 2, the PDI was below 0.2 highlighting monodisperse nanoemulsions (see Figure S1), except for the highest bore size (500 µm) operated at the lowest flow rates (65 and 75 mL/min). Moreover for all monodisperse nanoemulsions, no significant variation of the nanodroplets size was observed over a long period of time (at least one month) which indicates that the produced nanoemulsions were stable.

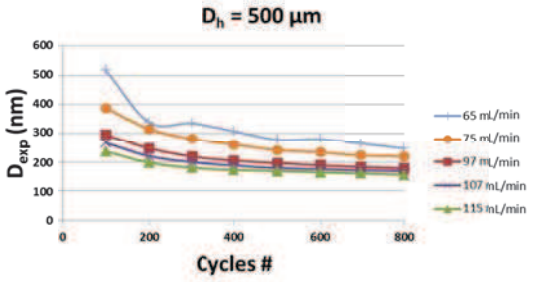

A)

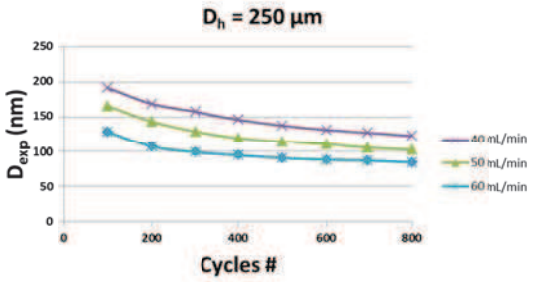

B)

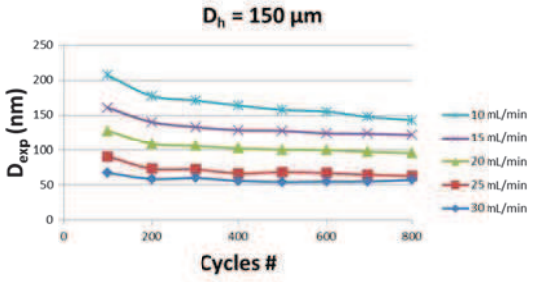

C)

Figure **2**. Variation of nanodroplet size with respect to the number of cycles for different flow rates and three different 180° micromixers: ELM_500_180 (A); ELM_250_180 (B), ELM_150_180 (C).

Given the geometry of the microemulsifier, with a sharp restriction, it is expected that the flow will experience an important elongational strain rate ($\dot{\varepsilon}$) pass the entrance of the restriction which should contribute to the deformation of the droplets and ultimately to their break up into smaller ones. Actually the theory of Taylor summarized by Grace[19] predicts that a droplet can be ruptured when the Capillary number, a dimensionless parameter which compares the viscous and interfacial forces, reaches a threshold value (Critical Capillary Number, Ca_c) which depends only on the dispersed to continuous phase viscosity ratio. For an elongational-flow, the Capillary number is expressed as follow:

Eq. 1

$$Ca = \frac{\eta \dot{\varepsilon} D_d}{2\sigma}$$

where η, D_d and σ denote the viscosity of the emulsion, the droplet diameter and the interfacial tension respectively.

This equation indicates that, for a given viscosity ratio, the droplets can break up when the product $\dot{\varepsilon} D_d$ is such that the Ca_c is reached. Then if the new product (calculated with the new droplet size) is enough to keep the Ca_c or higher, the droplet can be broken up further into smaller droplets and so on. By analogy with polymer melt flows through a die (extrusion) and by assuming that the emulsion is a Newtonian liquid,

Cogswell's analysis[20] leads to the following approximate expression of the elongational strain rate:

Eq. 2

$$\dot{\varepsilon} = \frac{2\,\tau_w\,\dot{\gamma}_w}{3\,\Delta P_e}$$

where τ_w is the shear stress at the wall in the bore microchannel, $\dot{\gamma}_w$ the shear rate and ΔP_e the pressure drop pass the entrance of the restriction.

The shear stress and stress rate are linked together by the Newtonian law of viscosity μ:

Eq. 3

$$\dot{\gamma}_w = \frac{\tau_w}{\mu}$$

Coupling Eq. 2 and Eq. 3 gives:

Eq. 4

$$\dot{\varepsilon} = \frac{2\,\tau_w^{\,2}}{3\,\mu\,\Delta P_e}$$

According to the standard fitting losses approach of fluid mechanics, the pressure drop across the restriction entrance is given by:

Eq. 5

$$\Delta P_e = K_f\,\frac{\rho < u >^2}{2}$$

Eq. 6

$$< u > = \frac{4\,q}{\pi\,D_h^{\,2}}$$

where K_f, ρ, q, $< u >$ and D_h denote the loss coefficient of the restriction (given by Eq. 7), the emulsion density, the flow rate, the mean velocity across the section of the bore microchannel and the diameter of that microchannel.

Eq. 7

$$K_f = 0.45\left[1-\left(\frac{D_h}{D_t}\right)^2\right]$$

Given the size of the PTFE tubing used to connect the microemulsifier (inner diameter D_t = 1.06 mm), K_f is ranging from 0.35 to 0.44 for the 500 and 150 µm bore sizes respectively.

The shear stress in a cylindrical microchannel is expressed by:

Eq. 8

$$\tau_w = \frac{D_h\ \Delta P_h}{4\ L_h}$$

where L_h and ΔP_h are the length and the pressure drop across the length of the bore microchannel.

Expression of ΔP_h depends upon the hydrodynamic regime. For Newtonian fluids flowing in laminar regime inside cylindrical pipes, it is given by the Hagen-Poiseuille law:

Eq. 9

$$\Delta P_h = \frac{128\ \mu\ L_h\ q}{\pi\ D_h^{\ 4}}$$

while in turbulent flow, it can be expressed as a function of the Fanning friction factor (f):

Eq. 10

$$\Delta P_h = \frac{32\ f\ L_h\ \rho\ q^2}{\pi^2\ D_h^{\ 5}}$$

The Fanning factor is usually a function of the Reynolds number and the relative roughness of the pipe. However in case of very high Reynolds numbers, the friction factor depends only upon the relative roughness. Thus it can be considered as a constant with respect to the flow rate and the diameter of the pipe.

Given the Reynolds numbers calculated for all the experiments that were run (see Table S1), the hydrodynamic regime lies somehow between the laminar flow and the turbulent flow. Therefore the pressure drop across the length of the bore microchannel can be written as follows:

Eq. 11

$$\Delta P_h = K_h \, L_h \, \mu^{\gamma} \, D_h^{\beta} \, q^{\alpha}$$

where K_f is a constant, α lies in-between 1 (laminar) and 2 (fully turbulent), β lies in-between -4 (laminar) and -5 (fully turbulent) and γ lies in-between 0 (fully turbulent) and 1 (laminar).

After replacing the expressions of ΔP_e and τ_w in Eq. 4 and rearranging, one gets:

Eq. 12

$$\dot{\varepsilon} = \frac{\Delta P_h^{\,2} \, \pi^2 \, D_h^{\,6}}{192 \, \mu \, L_h^{\,2} \, K_f \, \rho \, q^2}$$

Finally by considering the expression of ΔP_h, one obtains the following relationship:

Eq. 13

$$\dot{\varepsilon} = \frac{\pi^2 \, K_h^{\,2}}{192 \, K_f \, \rho} \, \mu^{2\gamma-1} \, D_h^{\,2\beta+6} \, q^{2\alpha-2}$$

Given the values of α, β and γ, Eq. 13 shows that $\dot{\varepsilon}$ will be higher when q is increased and when D_h is decreased. Accordingly to the Grace theory, it will result in the formation of smaller droplets. This complies well with the effect of the flow rate and bore diameter on the experimental nanodroplets size observed in Figure 2.

As for the effect of the number of cycles (i.e. operating time), it is believed that at least after 100 cycles the droplet breaking-up mechanism is such that two subdroplets are formed from the rupture of a mother droplet. The evidence of small PDIs (< 0.2) all along the operating time (see Figure S1) supports the assumption that the two subdroplets have approximatively the same size. Hence several cycles are required to

gradually decrease the nanodroplets size till equilibrium between the rupture and the coalescence is reached.

Figure 3A presents the variation of the nanodroplets size obtained after 800 cycles with respect to the flow rate for the 8 micromixers investigated. As previously mentioned when discussing the results displayed in Figure 2, one can clearly see the effect of the bore size on the size of the nanodroplets (upper curve of each of the 3 sets of curves); the lower the former, the smaller is the latter. But one can also see the interesting effect of the geometry of the micromixer. While it seems that 180° or 120° micromixers on one hand and 90° or 60° micromixers on the second hand produced the same nanodroplets size, there is a noticeable difference when the angle shifts from obtuse to acute; the latter giving rise whatever the micromixer bore size to lower nanodroplets size. It is believed that pass 90°, the elongated droplets in the bore microchannel may rotate and/or experience more shear rate which favors their rupture into smaller droplets. Data of Figure 3A for the three 180° micromixers where replotted as a function of the velocity through the bore, result is displayed in Figure 3B. Surprisingly, all the data point fall down on a master curve. This indicates that the velocity through the bore microchannel is the key parameter that controls the size of the nanodroplets; it will be used in the following for the correlations.

In summary, it can be concluded that nanoemulsions with well controlled sizes in the range 50-300 μm can be easily obtained with this elongational-flow microprocess. Moreover, for a given recipe (constant composition parameters), the nanodroplets size can be conveniently adjusted either by tuning the flow rate or by choosing a specific microemulsifier (angle and bore size).

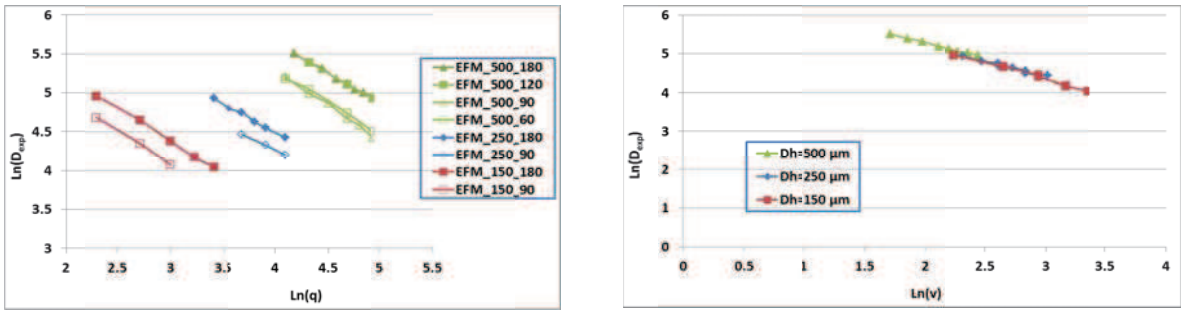

A) B)

Figure **3**. Logarithmic variation of the nanodroplets size with respect to the flow rate for the 8 micromixers investigated (A) and with respect to the velocity through the bore for the three 180° micromixers (B); all other parameters are kept to their reference value.

3.1.3.2 Effect of viscosity ratio and MMA volume fraction

Effects of both continuous phase and dispersed phase viscosities on nanodroplets size were investigated through the continuous to dispersed phase viscosity ratio (η_d/η_c). To increase this ratio, few weight percents of PMMA (from 0 to 15 %, see Table S2) were added to the oil phase. To lower down this ratio, the viscosity of the continuous phase was increased by adding few weight percents of a water-soluble polysaccharide thickening agent extracted from the carob tree[21] (Locus bean gum, from 0 to 0.1 %, see Table S2). Thus, in the investigated experiments, the viscosity ratio ranged from 0.37 to 14.20. Note that the reference condition (see Table 2 and Table S1) corresponds to a viscosity ratio of 0.66. The results are displayed in Figure 4A. As the viscosity ratio increases, the nanodroplets size increases. One can consider that, as the dispersed phase viscosity is increased (high η_d/η_c), it will be more difficult to elongate the droplets and ultimately to break them up because of their higher viscous stress.[22] On this opposite, the higher the viscosity of the continuous phase (low η_d/η_c), the higher is the shear imposed on the droplets which favors their breaking. In Grace's theory, pure shear flows cannot give rise to droplets breakup for viscosity ratios greater than 4. However, previous results show that elongational flows can. Therefore, with viscosity

ratios up de 14, the above results definitely highlight the elongational feature of our microemulsifiers.

One application of such monomer-based nanoemulsions is the preparation of latexes for which the solid content is an important industrial parameter (e.g. paint industry). Thus, in some additional experiments, we varied the volume fraction of MMA from its reference value (15 %) up to 50 %. As seen in Figure 4B, when the MMA volume fraction increases, the nanodroplets size increases too. It is noteworthy that only a two-fold increase is observed when the volume fraction reaches 50 %. One should consider the amount of SDS in the final emulsion which has decreased due to the smaller fraction of aqueous phase (concentration of SDS in water solution was 2.4wt.%/MMA calculated for 15% MMA volume fraction) while the number of MMA droplets increases with its volume fraction. As a consequence and apart from the inherent increase in droplet collisions for more concentrated nanoemulsions, the newly formed nanodroplets are covered by less SDS. This is detrimental to their stabilization and more coalescence may also occur.

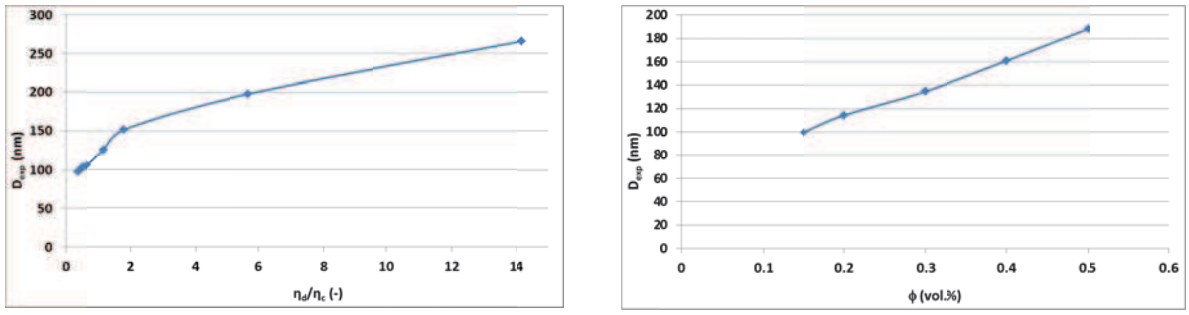

A) B)

Figure **4**. Variation of nanodroplet size with respect to the dispersed to continuous flow rates ratio η_d/η_c (A) and the MMA volume fraction ϕ (B); all other parameters are kept to their reference value.

3.1.3.3 Effect of surfactant concentration and surface tension

In the present study, sodium dodecyl sulfate (SDS) was used as the surfactant and its concentration was given by its weight ratio with respect to the monomer. The effect of this concentration was investigated for two different flow rates (40 and 50 mL/min) and two different number of cycles (100 and 800). As illustrated in Figure 5A, the nanodroplets diameter decreases when the surfactant concentration increases and then seems to reach a plateau pass a concentration of 2.4 wt.%. Given the size of the nanodroplets (100 nm) obtained for the reference condition (solid diamonds) and assuming a SDS to MMA molecular coverage of 1.2 nm^2,[23] the coverage fraction is estimated to be equal to about 100% if the SDS molecules are further assumed to be all located at the MMA/water interphase. This fraction falls down to 49% for a concentration of SDS of 0.5 wt.% at a flow rate of 40 mL/min (solid triangles) which is still enough to ensure the stability of the nanoemulsion.[24] It is noteworthy that the size of the nanodroplets can be controlled to a certain extent by tuning the process parameters (flow rate and number of cycles) even for extremely low amounts of surfactant (e.g. 0.5 wt.%) in contrast to other conventional emulsifiers where the size is usually controlled by the amount of surfactant. This may represent a real benefit for certain applications where a low surfactant concentration is required (e.g. in biomedical applications). The decrease in nanodroplets size with respect to the SDS concentration observed in the first part of the curves of Figure 5A can be explained by considering the variation of the surface tension with respect to SDS concentration. As seen in Figure 5B and as expected, the surface tension decreases with an increase in the SDS concentration. Since the Capillary number is inversely proportional to the surface tension (Eq. 1), this dimensionless parameter increases when the SDS concentration is increased. As a consequence the critical capillary Ca_c can be reached for smaller products $\dot{\varepsilon} D_d$. This means that for a given flow rate (i.e. same $\dot{\varepsilon}$, Eq. 13) the nanodroplets size would be smaller.

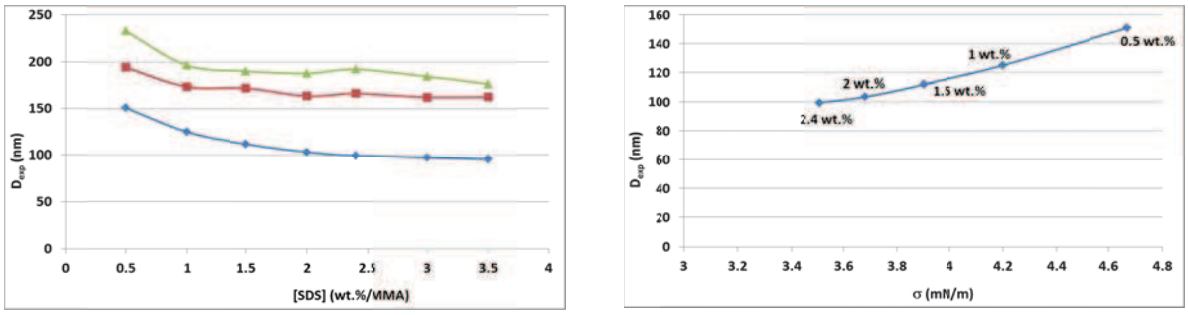

A) B)

Figure **5**. Variation of nanodroplet size with respect to the concentration of SDS for different values of the flow rate and numbers of cycles (-▲-: FR = 40 mL/min, Cycles = 800, - ■-: FR = 50 mL/min, Cycles = 100; -♦-: FR = 50 mL/min, Cycles = 800) (A) and with respect to the surface tension, labels indicate the SDS concentration with respect to MMA (B); all other parameters are kept to their reference value.

3.1.3.4 Comparison with a rotor-stator mixer

In this section we will compare our elongation-flow micromixer against a rotor-stator mixer and will assess the effect of a premixing on the nanodroplets size obtained with our device. Figure 6A presents the classical trend of nanodroplets size variation with respect to the rotor speed (RPM) of the conventional shear emulsifier. The droplet size decreases rapidly with the RPM and ultimately reaches a plateau. The higher the RPM, the higher is the shear force imposed on the droplets and thus the smaller they are. Yuh-Fun Maa and Chung Hsu also found the same trend by using the same kind of rotor-stator mixer.[25] After 10 minutes with the rotor-stator mixer at the highest speed of 24,000 RPM, a nanoemulsion with droplets diameter of 246 nm was obtained. Then 5 mL were collected and injected into one of the syringe of our elongational-flow microprocess for further mixing at different number of cycles. The results are displayed in Figure 6B (solid diamonds). This figure also shows the results obtained directly with the elongational-flow micromixer (solid squares), i.e. without any premixing with the rotor-stator device. It is observed that the elongational-flow microemulsifier allows significantly decreasing the size of the nanodroplets by 100 nm quite rapidly within only 100 cycles, highlighting the superiority of our microemulsifier compared to the shear device. One can also remark that starting from

a premixing generates slightly lower nanodroplets sizes at low number of cycles. However pass 400 cycles, the final droplets diameter seems to be independent on the mixing state of the material loaded to the syringe. This indicates that the quality of the nanoemulsion obtained with the microemulsifier is moderately affected by the mixing state of the raw aqueous/oil solution.

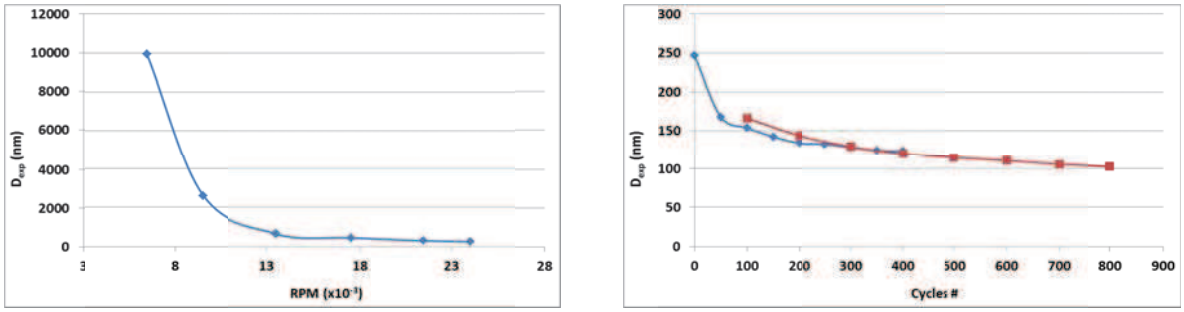

A) B)

Figure **6**. Variation of nanodroplet size with respect to the rotational speed of the rotor-stator mixer (A); variation of droplet size with respect to the number of cycles in elongational-flow micromixer (B) alone (-■ -) or after 10 minutes with rotor-stator mixer at 24,000 RPM (-♦ -); all other parameters are kept to their reference value.

3.1.3.5 Empirical correlations

As seen in Figure 3B, the nanodroplets diameter seems to follow a power law with respect to the velocity through the bore. And from the shape of the curves, the same stands also for the viscosity ratio (Figure 4A), the MMA volume fraction (Figure 4B) and the surface tension (Figure 5B). Therefore, for each of the aforementioned operating parameters, the nanodroplets diameter should follow the following empirical correlation:

Eq. 14 $D_{th} = K X^{\alpha}$

where D_{th} is the empirical nanodroplets diameter, X an operating, device or composition parameter (see Table 3) and *K* & *a* the two correlation coefficients. To determine these coefficients, the experimental nanodroplets diameter (D_{exp}) was plotted again X in a logarithmic plot (see supporting information) and the mean square error (MSE) calculated with Eq. 15 was minimized by applying the excel solver macro on the number of available data (N). Results are presented in Table 3. From the supporting information figures and values of the MSE, it is indeed observed that the nanodroplets diameter follow a power law. It is noteworthy that *a* exponent value is the same whatever the elongational-flow micromixer angle investigated while the K value shifts from 929.43 for 180° and 120° to 643.6 for 90° and 60°. This complies with the trend observed in Figure 3A where the latter always give the smaller nanodroplets diameter.

Eq. 15

$$MSE = \frac{1}{N}\sum_{i=1}^{N}(D_{th,i} - D_{exp,i})^2$$

Then, the same method was applied to get a single empirical correlation that predicts the variation of the nanodroplets diameter with respect to all investigated parameters. However, 90° and 60° angle micromixers were excluded from this correlation as their K value different significantly from that of 180° and 160° micromixers (Table 3). Thus the following correlation was obtained and was found to fairly well predict the nanodroplets diameter as seen in Figure 7A.

Eq. 16

$$D_{th} = 387\, v^{-0.75}\, \eta_d/\eta_c^{0.33}\, \phi^{0.5}\, \sigma^{1.5}$$

Table 3. Parameters of Eq. 14 evaluated with experimental data obtained at 800 cycles

Parameter X	*K* (S.I.)	Exponent *a*	Number of data, N	MSE (nm^2)	Figure in SI
Viscosity ratio (η_d/η_c)	124.01	0.29	8	15.37	S2
Surface tension (σ)	14.25	1.52	5	3.57	S3
MMA volume fraction (ϕ)	267.07	0.53	5	12.61	S4
Velocity through bore (v) for 180° and 120° elongational-flow micromixers	929.43	-0.79	22	51.25	S5
Velocity through bore (v) for 90° and 60° elongational-flow micromixers	643.60	-0.79	13	18.19	S6

Usually empirical correlations are expressed in terms of dimensionless numbers for it gives a broader applicability range to the correlations. Indeed there are virtually an infinity of combinations among the parameters defining a given dimensionless number that gives to this number the same value. Dimensionless numbers are widely used in Chemical Engineering because they always have a physical meaning related to the comparison of two distinct phenomena. To that extend, one has performed a dimensional analysis following the Buckingham method[26] to extract from the many independent parameters defining our process (listed in Table S3) the most relevant dimensionless numbers. Apart from the viscosity ratio and MMA volume fraction already mentioned – whose physical meanings are obvious –, one should consider the Reynolds number (Eq. 17) which is the ratio of inertial forces to viscous forces, the

Weber number (Eq. 18) which compares the inertial forces and interfacial forces and the Contraction Factor (CF, Eq. 19) defined as the ratio between the cross-section of the syringe over the cross-section of bore. Given the small difference (~1%) in dispersed and continuous liquid phase densities (Table S2), the density ratio can be neglected in this study in contrast to gas-liquid flows. One has also to define a dimensionless number for the nanodroplets empirical diameter (D^*_{th}), one has arbitrarily decided to define this number as the ratio of D_{th} and D_S, the syringe diameter (Eq. 20). Finally a new dimensionless empirical correlation was found (Eq. 23) which also predicted fairly well the nanodroplets diameter as seen in Figure 7B.

Eq. 17
$$Re = \frac{\rho \, v \, D_h}{\eta}$$

Eq. 18
$$We = \frac{\rho \, v^2 \, D_h}{\sigma}$$

Eq. 19
$$CF = \left(\frac{D_S}{D_h} \right)^2$$

Eq. 20
$$D^*_{th} = \frac{D_{th}}{D_S}$$

where ρ and η represent the density and viscosity of the nanoemulsion. Nanoemulsion density can be evaluated considering the volume fraction of the two phases accordingly to Eq. 21. Different models are proposed in the literature[27,28,29,30,31] for evaluating the nanoemulsion viscosity. We have chosen to use the model proposed by Dukler *et al.*[29,30] also based on the volume fraction of the two phases (Eq. 22).

Eq. 21
$$\rho = \phi \, \rho_d + (1-\phi) \, \rho_c$$

Eq. 22 $\eta = \phi \eta_d + (1-\phi) \eta_c$

Eq. 23 $D^*_{th} = 2.56 \times 10^{-11} Re^{-9/4} \eta_d/\eta_c^{1/3} \phi^{1/2} We^{-3/2} CF^{1/3}$

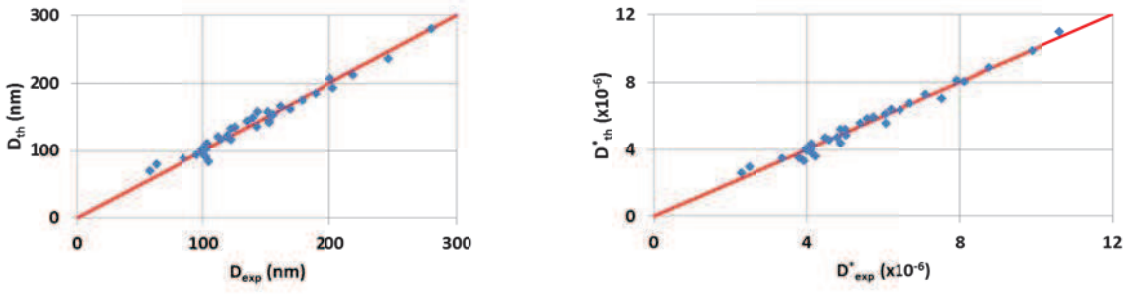

A) B)

Figure **7**. Variation of the non dimensionless (A) and dimensionless (B) empirical nanodroplets diameter as returned by Eq. 16 (MSE = 68.54 nm²) and Eq. 23 (MSE = 7.43×10^{-2}) versus the respective non dimensionless (D_{exp}) and dimensionless (D^*_{exp}) experimental diameter over 36 data points.

In the above correlation (Eq. 23), the experiment performed with a smaller syringe (entry 27 of Table S3) was not considered as the obtained nanodroplets diameter could not be adequately predicted by the equation despite the presence of the contraction factor. It is believed that this originates from the many restrictions in series located between the syringe and the bore. Indeed a 1.06 mm ID PTFE tubing links the syringe and the elongational-flow micromixer whose geometry exhibits besides additional restrictions (Figure S9). Therefore a simple contraction factor based on the syringe and bore cross-sections is unlikely to represent the complex flow pattern experienced by the nanoemulsion during the emulsification process.

The obtained dimensionless empirical correlation differs noticeably from the one we have obtained with a pneumatic elongational-flow emulsification process of larger scale[32] (Eq. 24).

Eq. 24 $D^*_{th} = 8.06x10^{-9}\ Re^{-1.39}\ We^{-1.39}\ \eta_d/\eta_c^{0.45}\ CF^{1.76}$

In the latter, exponents of Re and We were of same absolute value but opposite sign which allowed combining them into the Capillary number. This difference is attributed to the values of the Reynolds and Weber numbers which are in the current study much smaller. In previous work, the process operated in turbulent flow with Re above 5,500 while for this microprocess the laminar and intermediate regimes are predominant with Re values mostly lower than 5,000 (see Table S1). Also, We did not exceed 34 in this study while it was greater than $2.6x10^5$ in previous work. So due to the high flow velocity through the bore provided by the pneumatic pistons of our larger scale emulsifier, the inertial forces were predominant and thus the nanodroplets diameter was only influenced by the viscous and interfacial forces. However, in our current microemulsifier, all three forces are of same importance and therefore the nanodroplets diameter is a function of both Reynolds and Weber numbers. Another difference concerns the size of the nanoemulsion produced and the range of nanodroplets diameters over which are valid the empirical correlations. Indeed, the microprocess allows producing bigger droplets (from 50 to 300 nm vs. 30 to 110 nm for the larger scale emulsifier) while ensuring a better control on the nanodroplets diameters above 60 nm with experimental diameters closer to their empirical values (Figure 7A and Figure S8). To summarize, the larger scale emulsifier should be considered for the production of nanoemulsions in the size range 30 to 60 nm while the current microemulsifier is well adapted for the production of nanodroplets whose diameter is ranging from 50 to 300 nm.

3.1.4 Summary

Elongational-flow micromixers with bore sizes of 150, 250 and 500 µm were successfully used for the production of monodisperse MMA-based nanoemulsions

whose size could be conveniently controlled within the range 50 to 300 nm by simply adjusting the process parameters (flow rate through the restriction, number of cycles) or the micromixer parameters (angle, bore size). The results complied with the expression of the elongational strain rate that was derived from the Cogswell approach in laminar flow for Newtonian fluids. Dispersed to continuous phase viscosity ratios up to 14 as well as dispersed phase volume fractions up to 50% were investigated and easily processed. Compared to a conventional rotor-stator device, our microemulsifier allowed the production of nanoemulsions with much lower and controlled sizes. Finally a correlation between different dimensionless groups (Reynolds and Weber numbers, viscosity ratio, dispersed phase volume fraction and contraction factor) was extracted from the experimental data to predict fairly well the variation of the nanodroplets size with respect to the operating parameters.

This work clearly demonstrated the superior efficiency of elongational flows compared to pure shear flows in producing size-controlled nanoemulsions in the low nanometers range. To that extent we believe that our microprocess would be an interesting alternative to the conventional labscale shear emulsifiers with the additional advantage of using a quite small amount of dispersed phase (less than 1 mL) for cases of expensive or synthesized materials. Moreover, the developed microprocess operates at low pressures (< 2.5 bars) and low Reynolds numbers which should definitely limit any local heating and thus should prevent material degradation. However, given its small footprint, the whole system can be easily temperature controlled (water bath or oven). Finally, the monomer-based nanoemulsions could be polymerized to give colloidal suspensions of polymeric nanoparticles with a given size that may find ultimately applications in a wide range of fields. Also, the developed batch microprocess could be easily extended to a continuous-flow microprocess. For those two perspectives, works are already going on.

In this section an elongational-flow batch microfluidic process was successfully developed for the production of size-tunable nanoemulsions. However this process was characterized by a low mass yield which could be increased if the system operates in continuous-flow mode. Thus in the next section, the original batch design was modified to allow the continuous production of nanoemulsions. Hence the influence of a new operating parameter, the inlet flow rate, on the nanodroplets size and size distribution should be considered.

3.1.5 Supporting information

Experimental data

Table **S1**. Experimental nanodroplets diameter obtained after 800 cycles for the different conditions investigated

Entry	Investigated parameter	Droplet diamter Dexp (nm)	PDI (-)	Bore diameter Db (µm)	Flow rate FR (mL/min)	Re (-)	Surface tension σ (mN/m)	Dispersed phase viscosity ηd (mPa.s)	Continuous phase viscosity ηc (mPa.s)	Dispersed phase density ρd (kg/m^3)	Continuous phase density ρc (kg/m^3)	MMA volume fraction ϕ (-)	Synringe diameter Ds (mm)
1	v	139	-	250	30	2865	3.51	0.61	0.92	893.5	996.4	0.15	25.02
2		122	-	250	35	3343	3.51	0.61	0.92	893.5	996.4	0.15	25.02
3		120	0.144	250	40	3820	3.51	0.61	0.92	893.5	996.4	0.15	25.02
4		103	-	250	45	4298	3.51	0.61	0.92	893.5	996.4	0.15	25.02
5		102.6	0.128	250	50	4775	3.51	0.61	0.92	893.5	996.4	0.15	25.02
6		84	0.146	250	60	5730	3.51	0.61	0.92	893.5	996.4	0.15	25.02
7		143	0.128	150	10	1592	3.51	0.61	0.92	893.5	996.4	0.15	25.02
8		122	0.101	150	15	2388	3.51	0.61	0.92	893.5	996.4	0.15	25.02
9		95	0.135	150	20	3183	3.51	0.61	0.92	893.5	996.4	0.15	25.02
10		62	0.168	150	25	3979	3.51	0.61	0.92	893.5	996.4	0.15	25.02
11		57	0.198	150	30	4775	3.51	0.61	0.92	893.5	996.4	0.15	25.02
													25.02
12		247	0.227	500	65	3104	3.51	0.61	0.92	893.5	996.4	0.15	25.02
13		219	0.179	500	75	3581	3.51	0.61	0.92	893.5	996.4	0.15	25.02
14		203	0.181	500	85	4059	3.51	0.61	0.92	893.5	996.4	0.15	25.02
15		178	0.111	500	97	4632	3.51	0.61	0.92	893.5	996.4	0.15	25.02
16		168	0.099	500	107	5109	3.51	0.61	0.92	893.5	996.4	0.15	25.02
17		155	0.106	500	115	5491	3.51	0.61	0.92	893.5	996.4	0.15	25.02
18	ηd/ηc	102.6	0.128	250	50	4775	3.51	0.66	0.92	893.5	996.4	0.15	25.02
19		125.6	0.108	250	50	4783	3.51	1.08	0.92	904.7	996.4	0.15	25.02
20		151.7	0.118	250	50	4784	3.51	1.66	0.92	905.1	996.4	0.15	25.02
21		198.1	0.198	250	50	4787	3.51	5.22	0.92	910	996.4	0.15	25.02
22		266.1	0.288	250	50	4793	3.51	13.05	0.92	917.8	996.4	0.15	25.02
23		103.6	0.133	250	50	4823	3.51	0.61	1.13	893.5	1008	0.15	25.02
24		105.6	0.125	250	50	4831	3.51	0.61	1.27	893.5	1010	0.15	25.02
25		98	0.113	250	50	4819	3.51	0.61	1.65	893.5	1007.1	0.15	25.02
26	CF	143.4	0.128	150	10	1592	3.51	0.61	0.92	893.5	996.4	0.15	25.02
27		168	0.105	150	10	1592	3.51	0.61	0.92	893.5	996.4	0.15	7.98
28	σ	151	0.13	250	50	4775	4.67	0.61	0.92	893.5	996.4	0.15	25.02
29		125.1	0.122	250	50	4775	4.2	0.61	0.92	893.5	996.4	0.15	25.02
30		112	0.132	250	50	4775	3.9	0.61	0.92	893.5	996.4	0.15	25.02
31		103.56	0.115	250	50	4775	3.68	0.61	0.92	893.5	996.4	0.15	25.02
32		99.6	0.128	250	50	4775	3.51	0.61	0.92	893.5	996.4	0.15	25.02
33	ϕ	99.6	0.128	250	50	4775	3.51	0.61	0.92	893.5	996.4	0.15	25.02
34		114.3	0.129	250	50	4750	3.51	0.61	0.92	893.5	996.4	0.20	25.02
35		134.7	0.119	250	50	4700	3.51	0.61	0.92	893.5	996.4	0.30	25.02
36		161	0.121	250	50	4650	3.51	0.61	0.92	893.5	996.4	0.40	25.02
37		188.3	0.173	250	50	4600	3.51	0.61	0.92	893.5	996.4	0.50	25.02

v: velocity through bore; CF: contraction factor, σ: surface tension, ϕ: MMA volume fraction

Physical properties

Table **S2**. Composition and physical properties of the different formulations investigated

Phase	PMMA wt.%/MMA	HD wt.%/MMA	Locust bean gum wt.%/water	SDS wt.%/MMA	Density, ρ g/mL	Viscosity, η mPa.s
Aqueous continuous phase (4.25 mL; 85 vol.%)	-	-	0	0.5	0.996	0.92
	-	-	0	1	0.996	0.92
	-	-	0	1.5	0.996	0.92
	-	-	0	2	0.996	0.92
	-	-	0	2.4	0.996	0.92
	-	-	0	3	0.996	0.92
	-	-	0	3.5	0.996	0.92
	-	-	0.025	2.4	1.008	1.13
	-	-	0.05	2.4	1.010	1.27
	-	-	0.1	2.4	1.007	1.65
MMA dispersed Phase (0.75 mL; 15 vol.%)	0	4	-	-	0.893	0.61
	2	4	-	-	0.905	1.08
	4	4	-	-	0.905	1.66
	10	4	-	-	0.910	5.22
	15	4	-	-	0.918	13.05

Parameters

Table **S3**. List of independent parameters and corresponding units describing the whole process

Parameter	Symbol	Unit
Velocity through bore	v	m/s
or	or	or
Flow rate*	q	m^3/s
Dispersed phase viscosity	η_d	Pa.s
Continuous phase viscosity	η_c	Pa.s
Dispersed phase density	ρ_d	Kg/m^3
Continuous phase density	ρ_c	Kg/m^3
Bore diameter	D_h	m
Syringe diameter	D_S	m
Nanodroplets size	D_{exp}	m
Surface tension	σ	N/m
MMA volume fraction	ϕ	-

* These two parameters are not independent but linked together through the section of the bore, i.e. the bore diameter

PDI

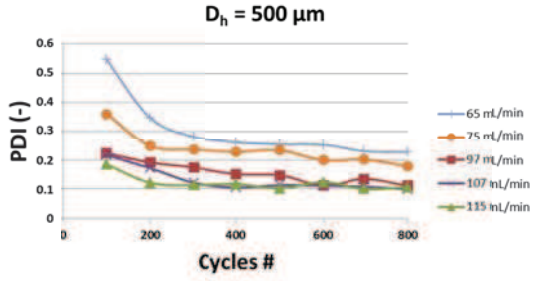

A)

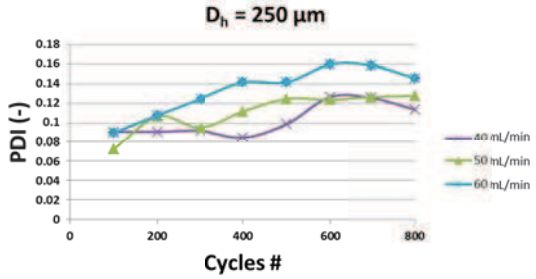

B)

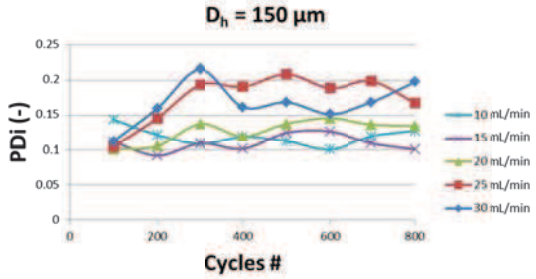

C)

Figure **S1**.Variation of PDI with respect to the number of cycles for different flow rates and three different 180° micromixers: ELM_500_180 (A); ELM_250_180 (B), ELM_150_180 (C).

Correlations

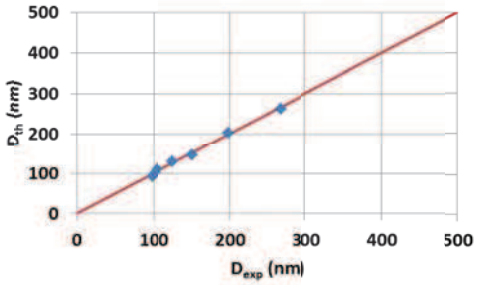

Figure **S2**. Variation of the empirical nanodroplets diameter returned by the empirical correlation (Eq. 1, main text) for viscosity ratio (ηd/ηc) versus experimental diameter.

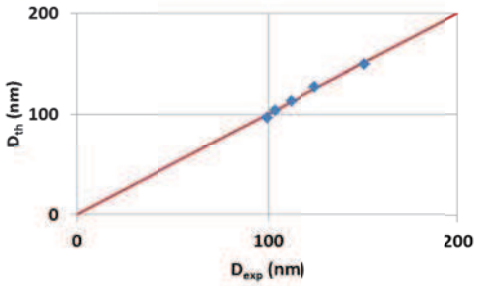

Figure **S3**. Variation of the empirical nanodroplets diameter returned by the empirical correlation (Eq. 1, main text) for surface tension (σ) versus experimental diameter.

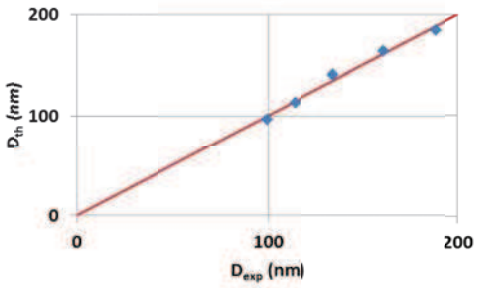

Figure **S4**. Variation of the empirical nanodroplets diameter returned by the empirical correlation (Eq. 1, main text) for MMA volume fraction (ϕ) versus experimental diameter.

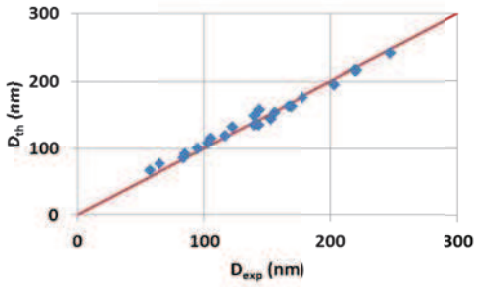

Figure **S5**. Variation of the empirical nanodroplets diameter returned by the empirical correlation (Eq. 1, main text) for the velocity (v) through the bore in case of 180° and 120°elongational-flow micromixers versus experimental diameter.

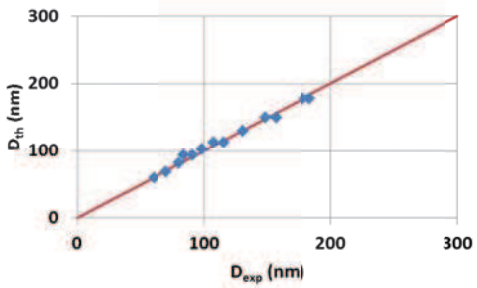

Figure **S6**. Variation of the empirical nanodroplets diameter returned by the empirical correlation (Eq. 1, main text) for the velocity (v) through the bore in case of 90° and 60°elongational-flow micromixers versus experimental diameter.

Effect of syringe's size

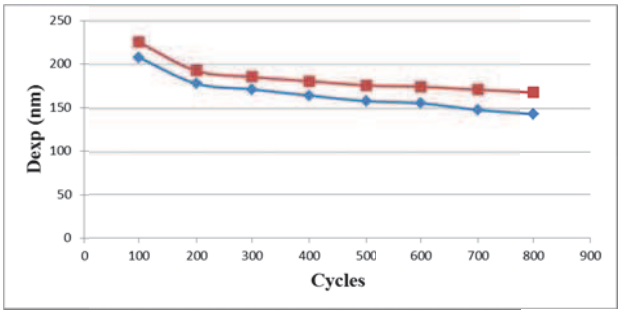

Figure **S7**. Variation of nanodroplets size with respect to the number of cycles for two different syringe's diameters (D_s): - ■-: 8 mm, -♦-: 25 mm.

Correlation for the pneumatic-driven large scale emulsifier

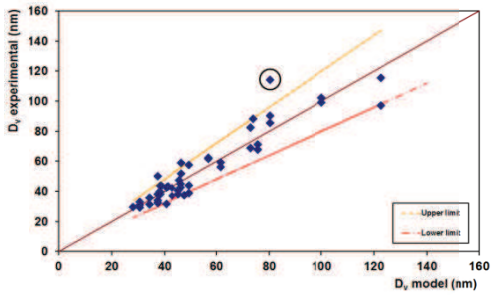

Figure **S8**. Variation of the empirical nanodroplets diameter versus experimental diameter for the pneumatic-driven large scale emulsifier. Upper and lower lines correspond to ± 20% for the model prediction

Schematic drawing of EFM_250_180

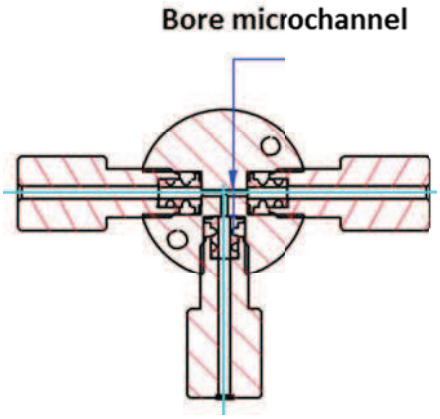

Figure **S9**. Cut view of the EFM_250_180 micromixer (adapted from the manufacturer's drawing, VICI website).

3.1.6 References

1. Remington, J. P.; Troy, D. B.; Beringer, P., Remington: The science and practice of pharmacy. Lippincott Williams & Wilkins: 2006; Vol. 1.

2. Mason, T. G.; Wilking, J. N.; Meleson, K.; Chang, C. B.; Graves, S. M., Nanoemulsions: formation, structure, and physical properties. Journal of Physics: Condensed Matter 2006, 18 (41), R635.

3. Izquierdo, P.; Esquena, J.; Tadros, T. F.; Dederen, C.; Garcia, M. J.; Azemar, N.; Solans, C., Formation and Stability of Nano-Emulsions Prepared Using the Phase Inversion Temperature Method. Langmuir 2002, 18 (1), 26-30.

4. Silva, H. D.; Cerqueira, M. Â.; Vicente, A. A., Nanoemulsions for food applications: development and characterization. Food and Bioprocess Technology 2012, 5 (3), 854-867.

5. Sonneville-Aubrun, O.; Simonnet, J. T.; L'Alloret, F., Nanoemulsions: a new vehicle for skincare products. Advances in Colloid and Interface Science 2004, 108–109 (0), 145-149.

6. Shah, P.; Bhalodia, D.; Shelat, P., Nanoemulsion: A pharmaceutical review. Systematic Reviews in Pharmacy 2010, 1 (1), 24.

7. Koc, A. B.; Abdullah, M., Performance and NOx emissions of a diesel engine fueled with biodiesel-diesel-water nanoemulsions. Fuel Processing Technology 2013, 109 (0), 70-77.

8. Webster, A. J.; Cates, M. E., Osmotic Stabilization of Concentrated Emulsions and Foams. Langmuir 2001, 17 (3), 595-608.

9. Ouzineb, K.; Graillat, C.; McKenna, T. F., Study of compartmentalization in the polymerization of miniemulsions of styrene and butyl methacrylate. Journal of Applied Polymer Science 2004, 91 (1), 115-124.

10. Tlusty, T.; Safran, S. A., Microemulsion networks: the onset of bicontinuity. Journal of Physics: Condensed Matter 2000, 12 (8A), A253.

11. Solans, C.; Izquierdo, P.; Nolla, J.; Azemar, N.; Garcia-Celma, M. J., Nano-emulsions. Current Opinion in Colloid & Interface Science 2005, 10 (3–4), 102-110.

12. Sajjadi, S., Nanoemulsion Formation by Phase Inversion Emulsification: On the Nature of Inversion. Langmuir 2006, 22 (13), 5597-5603.

13. Souilem, I.; Muller, R.; Holl, Y.; Bouquey, M.; Serra, C. A.; Vandamme, T.; Anton, N., A Novel Low-Pressure Device for Production of Nanoemulsions. Chemical Engineering & Technology 2012, 35 (9), 1692-1698.

14. McClements, D. J., Edible nanoemulsions: fabrication, properties, and functional performance. Soft Matter 2011, 7 (6), 2297-2316.

15. Whitesides, G. M., The origins and the future of microfluidics. Nature 2006, 442 (7101), 368-373.

16. Terry, S. C.; Jerman, J. H.; Angell, J. B., A gas chromatographic air analyzer fabricated on a silicon wafer. Electron Devices, IEEE Transactions on 1979, 26 (12), 1880-1886.

17. Manz, A.; Harrison, D. J.; Verpoorte, E. M. J.; Fettinger, J. C.; Paulus, A.; Lüdi, H.; Widmer, H. M., Planar chips technology for miniaturization and integration of separation techniques into monitoring systems: Capillary electrophoresis on a chip. Journal of Chromatography A 1992, 593 (1–2), 253-258.

18. Farzi, G.; Bourgeat-Lami, E.; McKenna, T. F. L., Miniemulsions using static mixers: A feasibility study using simple in-line static mixers. Journal of Applied Polymer Science 2009, 114 (6), 3875-3881.

19. Grace†, H. P., DISPERSION PHENOMENA IN HIGH VISCOSITY IMMISCIBLE FLUID SYSTEMS AND APPLICATION OF STATIC MIXERS AS DISPERSION DEVICES IN SUCH SYSTEMS. Chemical Engineering Communications 1982, 14 (3-6), 225-277.

20. Cogswell, F. N., Converging flow of polymer melts in extrusion dies. Polymer Engineering & Science 1972, 12 (1), 64-73.

21. Garcia-Ochoa, F.; Casas, J. A., Viscosity of locust bean (Ceratonia siliqua) gum solutions. Journal of the Science of Food and Agriculture 1992, 59 (1), 97-100.

22. Jafari, S. M.; Assadpoor, E.; He, Y.; Bhandari, B., Re-coalescence of emulsion droplets during high-energy emulsification. Food Hydrocolloids 2008, 22 (7), 1191-1202.

23. Piirma, I.; Chen, S.-R., Adsorption of ionic surfactants on latex particles. Journal of Colloid and Interface Science 1980, 74 (1), 90-102.

24. Landfester, K., Recent developments in miniemulsions — formation and stability mechanisms. Macromolecular Symposia 2000, 150 (1), 171-178.

25. Maa, Y.-F.; Hsu, C., Liquid-liquid emulsification by rotor/stator homogenization. Journal of Controlled Release 1996, 38 (2–3), 219-228.

26. Buckingham, E., On physically similar systems; illustrations of the use of dimensional equations. Physical Review 1914, 4 (4), 345-376.

27. Mcadams, W. H., Heat Transmission: 3d Ed. McGraw-Hill: 1954.

28. Cicchitti, A.; Lombardi, C.; Silvestri, M.; Soldaini, G.; Zavattarelli, R. Two-phase cooling experiments: pressure drop, heat transfer and burnout measurements; Centro Informazioni Studi Esperienze, Milan: 1959.

29. Dukler, A. E.; Wicks, M.; Cleveland, R. G., Frictional pressure drop in two-phase flow: A. A comparison of existing correlations for pressure loss and holdup. AIChE Journal 1964, 10 (1), 38-43.

30. Dukler, A. E.; Wicks, M.; Cleveland, R. G., Frictional pressure drop in two-phase flow: B. An approach through similarity analysis. AIChE Journal 1964, 10 (1), 44-51.

31. Beattie, D. R. H.; Whalley, P. B., A simple two-phase frictional pressure drop calculation method. International Journal of Multiphase Flow 1982, 8 (1), 83-87.

32. Souilem, I.; Serra, C. A.; Muller, R.; Holl, Y.; Bouquey, M.; Sutter, C., Dimensional analysis of a novel low-pressure device for the production of size-tunable nanoemulsions. AIChE Journal 2015, 61 (1), 23-30.

3.2 Continuous-flow operation

ABSTRACT

A low energy input continuous-flow emulsification microprocess with a productivity of up to 1 kg/d was developed to produce size-controlled oil-in-water MMA-based nanoemulsions whose nanodroplets diameter ranged from 100 to 250 nm. Effective emulsification was promoted by the strong elongational strain rate pass the restriction of a micromixer composed of a microchannel whose characteristic dimension was either 150, 250 or 500 μm. Both effects of the reciprocating flow rate (RFR) through the restriction of the micromixer and the inlet flow rate (IFR) across the micromixer were assessed. Nanodroplets size decreased when the microchannel dimension and IFR were decreased or when increasing the RFR; this latter parameter playing a crucial role in controlling the droplet size. Finally, highly concentrated nanoemulsions containing up to 50% in volume fraction of the oil phase were produced with a slight increase in droplet size (50 nm).

3.2.1 Introduction

In recent years, many scientists were attracted by nanoemulsions because of their high benefits and potential applications in a various fields. To name a few, in the beverage industry, oil-in-water nanoemulsion containing lycopene (a natural antioxidant) in the oil phase were considered to prevent its undesirable oxidation before consumption. Moreover, nanoemulsions of oil/lycopene droplets having a size lower than 100 nm are transparent while the direct adjunction of lycopene in aqueous beverage makes it turbid and thus not appropriate for sale.[1] In the cosmetic industry and specially for skincare products, nanoemulsions are widely used because of the possibility to tune their textures to meet consumers requirements by simply adding gelling or thickening agents.[2] Nanoemulsions are also considered in drug delivery due to their capacity to encapsulate hydrophobic drugs but also to protect them from enzymatic degradation

and hydrolysis during their transportation through the parenteral environment.[3] Additionally, nanoemulsions help in reducing the frequency and dosage of drug treatment as nanoemulsions can guarantee the drug release under a sustained and controllable mode over relative long periods. Apart from the aforementioned fields, nanoemulsions are also widely used food[4] and dairy product[5] industries. Hence, several approaches to prepare a suitable nanoemulsion were developed.

These approaches can be classified into two categories depending on the amount of raw input energy required to emulsify a dispersed phase into nanodroplets homogenously distributed within the continuous phase. Methods that require mechanical shear (rotor-stator mixers), pressure to flow (static mixers and membrane devices) or to hydrodynamically shear (high-pressure homogenizer) the continuous and dispersed phases, and sound waves (ultrasound generator) are part of the high-energy methods. On the opposite, low-energy methods take advantage of the internal chemical potential of the emulsion components to achieve the emulsification. This happens for specifically formulated systems when its composition or the surrounding conditions are changed.[6] Example of the main low-energy methods include spontaneous emulsification, phase inversion temperature and phase inversion composition.

However, if the aforementioned methods are quite efficient to produce small quantities (tens to few hundreds of milliliters) on a laboratory scale, few can be used to produce large volumes that can meet industry requirement. Main limitations include the control of the droplets size along with their size distribution (ultrasound generator) and the large quantity of surfactant (a pretty high cost molecule) in combination with a strict control of the temperature and component concentrations[7] (low-energy methods). Only the high-pressure homogenizer[8] and rotor-stator mixers[9] are commonly used on an industrial scale. However both are usually operated in discontinuous mode which induces inherent variability in between the different batches. Furthermore, these two methods require an extensive energy (i.e. a high cost) to produce nanoemulsions; high-

pressure homogenizers usually operate are 2,000 bars.[10] Thus there is a need to develop new methods that could achieve the production of well size-controlled nanoemulsions in continuous-flow mode and at a low energy input.

In a previous work,[11] our group has developed a scalable low pressure (ca. 2.5 bars) elongational-flow microprocess operating in batch mode that can produce size-controlled nanoemulsions in the size range 50-300 nm. In the present paper, we will demonstrate how the use of our microemulsifier can be extended to the continuous-flow production of size-controlled nanoemulsions.

3.2.2 Materials and procedure

3.2.2.1 Materials

The standard recipe used to produce nanoemulsions of different sizes comprised a hydrophobic liquid (15 vol.%) as the main dispersed phase, a surfactant (2.4 wt.%/Monomer), a hydrophobic agent as the Ostwald-ripening inhibitor (4 wt.%/Monomer) and distilled water (85 vol.%) as the main continuous phase. Specifically, the hydrophobic liquid was the methyl methacrylate monomer (MMA, 99% purity; supplied by Aldrich). The surfactant was sodium dodecyl sulfate (SDS, 99% purity, supplied by Alfa Aesar), the hydrophobic agent was hexadecane (HD, 99% purity; Sigma Aldrich). Distilled water was used throughout the experiment.

3.2.2.2 Description of the continuous-flow microprocess

The continuous-flow microprocess was developed by slightly modifying our original batch microprocess.[11] The latter was composed of two mid pressure syringe pumps (neMESYS Mid Pressure Module, Cetoni), two 25 mL stainless steel syringes (Cetoni) and one PEEK tee (Valco Vici) as the elongational–flow microemulsifier/micromixer, The syringe pumps were operated by the supplier's software and can independently

inject or withdraw, work in tandem (withdraw/withdraw, infuse/infuse) or in opposite phase (withdraw/infuse). The micromixer, in turn, consisted of several drilled microchannels having a bore size of either 150, 250 or 500 μm. Two of these microchannels were linked to the stainless steel syringes by two PTFE tubings (1.06 mm ID x 1.68 mm OD). The last one was used to recover the nanoemulsion at the end of operation. To run the microprocess continuously, the PEEK tee micromixer was replaced by a 4 ports cross-assy PEEK micromixer (Valco Vici, see Figure S17) of different microchannels bore sizes (150, 250 or 500 μm). Two opposite ports were connected to the stainless steel syringes. The third port was connected to the feeding line composed of four PTFE tubings (1.06 mm ID x 1.68 mm OD), a check valve (Cetoni), a T-junction (P-728-01, Upchurch Scientific) and two plastic syringes of 50 mL and 20 mL for the continuous and dispersed phase respectively. Both syringes were mounted on two syringe pumps (PHD 2000, Harvard Apparatus) in order to deliver continuously the oil and water phases with the requested flow rate ratio (i.e. the requested volume fraction of MMA and distilled water). The last port of the cross-assy PEEK micromixer was connected to the outlet line by means of standard PTFE tubings (1.06 mm ID x 1.68 mm OD). This outlet line was equipped with a metering valve (SS-SS1, Swagelok) which purpose was to increase the pressure in the outlet line so that the flow rate matched the inlet one (i.e. the sum of both oil and water phase flow rates). A T-junction (SS-100-3, Swagelok) was also used in order to mount a pressure gauge (PTU-S-AG400-31AD, Swagelok) to monitor the pressure in the outlet line. Finally the nanoemulsion was collected in a vial via a small stainless steel capillary (SS-T1-S-014-6ME, Swagelok) connected to the metering valve (Figure 1).

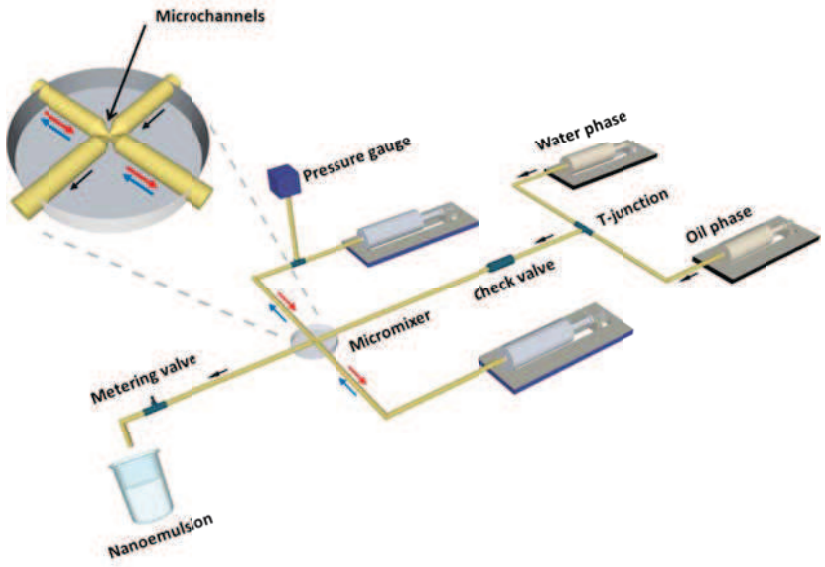

Figure 8. A): Schematic drawing (not at scale) of the continuous-flow microprocess for producing size-controlled nanoemulsions.

3.2.2.3 Emulsification procedure

The water and oil phases were prepared by dissolving the surfactant (SDS, 2.4 wt.%/MMA) and the Ostwald-ripening inhibitor (HD, 4 wt.%/MMA) in the distilled water and MMA phases respectively. Then each of the two phases was filtered (Chromacol 30-SF-50(N), 30MM SYR FILTER NYLON 5.0UM) to remove any insoluble that can potential block the elongational–flow micromixer. Then 4.25 mL of the SDS/water solution was charged into one stainless steel syringe followed by 0.75 mL of the HD/MMA solution in same syringe using a micropipette (Pipetman P1000, supplied from Gilson). So the water and oil phases were not premixed but rather laid side-by-side in the stainless syringe while the second one was kept empty before any run. In some experiments, these 5 mL were changed when investigating the effect of the original volume charged into the stainless steel syringe. Later, the 50 mL and 20 mL plastic syringes were loaded with pure SDS/water and pure HD/MMA solutions respectively. Then the two feeding pumps were switched on to purge the whole system from air bubbles. The individual flow rates of these syringe pumps were set such a way that the volume fraction of oil phase in the emulsion was equal to 15% and the

total inlet flow rate entering the elongational-flow micromixer ranged from 0.05 to 0.75 mL/min. In some experiments, the individual flow rates were adjusted to reach volume fractions of oil phase up to 50% for a constant total flow rate of 0.25 mL/min. Afterwards, the emulsifying pumps were switched on and forced to operate in opposite phase (withdraw/infuse) at same flow rate (later called reciprocating flow rate, RFR, to distinguish with the inlet flow rate, IFR) which was varied from 25 to 136 mL/min depending on the bore size of the elongational-flow micromixer. Finally, samples of the nanoemulsion collected at the exit of the outlet line were taken at regular time intervals to follow the size of the droplets with time.

3.2.2.4 Characterization

The nanodroplets diameter and polydispersity in size (PDI) were characterized by a commercial dynamic light scattering detector (Zetasizer, Nano Series, Malvern) at a fixed scattering angle of 173°. In order to reach the required turbidity for an accurate measurement and limit the possible coalescence as much as possible, two drops of freshly-prepared nanoemulsions were dispersed into 9 mL of distilled water shortly before the analysis. Approximately 1 mL of the diluted nanoemulsion was injected into the disposable DLS cuvette. Three kinds of average nanodroplets diameter (number-, volume- and intensity-) could be returned automatically by the DLS detector as well as the PDI value. The intensity-average diameter D_{exp} was used throughout this study. PDI values below 0.2 are usually considered as the feature of monodisperse size distributions[12] For each sample, DLS measurement was run in triplicate. During each measurement, 10 to 30 scans were performed automatically. Experiments and measurements shown in the present study were performed at room temperature. Several samples (up to 5) obtained at different dates were analyzed for the same set of operating parameters. This allowed calculating the coefficient of variation (CV) defined as the ratio of the standard deviation of all average values returned by the DLS

measurements and the mean droplet diameter. CV was found to vary from 4% to 1% for the smallest droplets (54 nm) and the largest ones (234 nm) respectively.

3.2.3 Results and discussion

The effect of different operating parameters (emulsification time, reciprocating and inlet flow rates, initial volume charged in the stainless steel syringe and ratio of reciprocating to inlet flow rates) on the droplet size was thoroughly studied. The mechanism of droplet formation in such elongational-flow micromixer was deeply explained in our previous paper on the batch microprocess.[11] In brief, the emulsion flowing from one stainless steel syringe to the other one and *vice versa* experiences a sharp decrease in channel diameter pass the restriction - from 25 mm (inner diameter of the stainless syringe) down to either 150, 250 or 500 μm (in the reciprocating microchannel). This induces a large elongational strain rate and so a high Capillary number which is proportional to the product of the droplet diameter by the elongational strain rate. From the theory of Taylor summarized by Grace,[13] a droplet can undergo a rupture into smaller droplets when the Capillary number reaches a critical value. Then, if the combination of elongational strain rate and newly formed droplet diameter is sufficient to still keep the Capillary number above the critical value, the droplets can rupture into even smaller ones and so on. In the present study, one can wonder about the effect of the inlet flow rate and for instance if the cross flow of a raw emulsion through the micromixer will detrimentally affect the emulsification induced by the reciprocating flow rate.

3.2.3.1 Effect of operating time, bore size, reciprocating and inlet flow rates

Figure 9 presents the variation of the nanodroplets size with respect to the operating time for the batch mode (IFR=0 mL/min) and the continuous flow-mode for different inlet flow rates and three different microchannel bore sizes.

It is first observed that nanodroplets with diameters ranging from 100 to 250 nm and narrow size distributions (PDI<0.2, see Figure S18) can be produced continuously. The smaller size was obtained with the smallest bore size (150 μm) while the larger one was produced with the largest microchannel (500 μm). This size range can probably be extended towards even smaller diameters by applying a reciprocal flow rate higher than 30 mL/min.

One also notes that the nanodroplets size decreases with the operating time but reaches a plateau value that is obtained more rapidly as the inlet flow rate is increased. This trend can be readily explained if one assumes that the droplets rupture into two subdroplets. As seen in Figure S18, the PDIs of the nanoemulsions produced at different operating times stay below 0.2 which may significate that the two subdroplets have approximatively the same size. Hence time is required to gradually decrease the nanodroplets size till equilibrium between the rupture and the coalescence is reached (plateau zone). On the other hand, the inlet flow also experiences a restriction when entering the micromixer (see Figure S17). As explained above, the higher the flow rate through this restriction (i.e. the higher the inlet flow rate or the lower the size of the restriction), the higher is the elongational strain rate and the better chance the droplet will have to rupture into smaller ones. This means that the inlet microchannel probably contributes to the emulsification by rupturing chunks of dispersed phase into droplets hence speeding up the whole emulsification process. Therefore the transient regimes observed in Figure 9 are shorter when the inlet flow rate is increased.

Finally one observes that the continuous-flow microprocess will always produce larger nanodroplets in comparison with the batch microprocess. The nanodroplets size is

getting besides higher and higher as the inlet flow rate is increased. Indeed, injecting a fresh raw mixture of oil and water phases in an emulsion stream being refined by the reciprocating flow will decrease the time spent by this emulsion in the microemulsifier. This is a situation much comparable to the batch mode in case the operating time is reduced. As seen in the batch curves of Figure 9, the result is the production of bigger droplets. Then, the higher the inlet flow rate, the smaller the residence time of the emulsion in the microemulsifier and the higher the nanodroplets droplet size. However this effect seems to be amplified by the bore size. For a microchannel size of 250 and 500 μm, one observes (Figure 9A&B) that, for short operating times and for the smallest IFR tested (0.25 mL/min), the nanodroplets size obtained with the batch mode and the continuous-flow mode are quite comparable. However this is not the case at all for the smallest bore size (Figure 9A) as the difference in nanodroplets size reaches almost 80 nm. This can be explained by considering the ratio of RFR to IFR which for the same IFR of 0.25 mL/min is equal to 120, 200 and 544 for the bore sizes of 150, 250 and 500 μm respectively. This means that for the smallest bore size, the inlet flow rate is less negligible before the reciprocating flow rate than in the two other cases. Therefore one can wonder if the RFR to IFR ratio is not a key parameter.

To get a deeper insight in the interplay between the inlet flow rate (IFR) and the reciprocating flow rate (RFR), experiments were performed by keeping constant the RFR to IFR ratio and by varying the two flow rates accordingly. As seen in Figure 10, the nanodroplets size and PDI decrease when both RFR and IFR increase. Thus the flow rate ratio does not seem to be a key parameter in controlling the size of the nanoemulsion. However, from previous experiments (Figure 9) one has seen that the nanodroplets size increases when IFR increases. Therefore to explain the results presented in Figure 10 one has to consider that the RFR is playing a crucial role which surpasses the one played by the IFR.

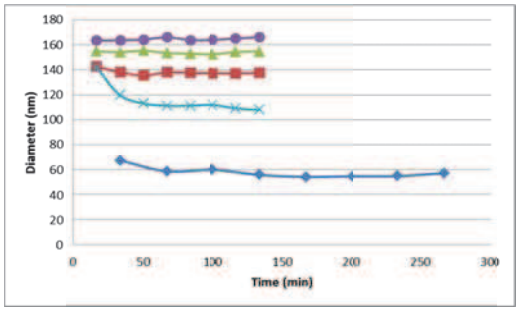

A).

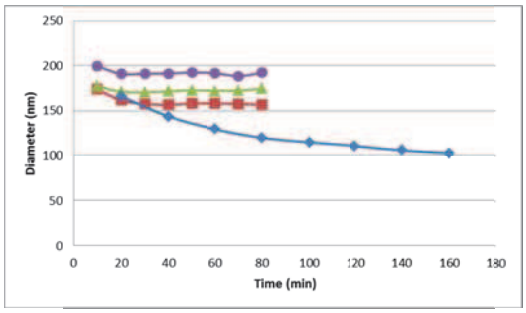

B)

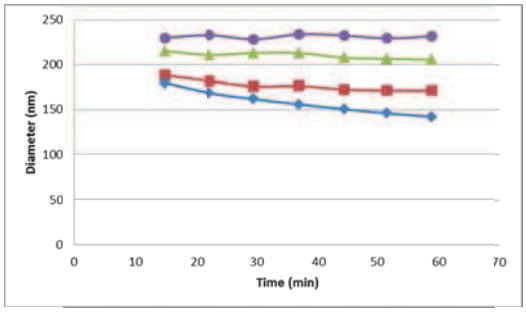

C)

Figure **9**. Variation of the nanodroplets size with operating time for a bore size of 150 µm (A), 250 µm (B) and 500 µm(C) and for different inlet flow rates (-♦-: 0 mL/min, - X-: 0.05 mL/min, - ■-: 0.25 mL/min, -▲-: 0.5 mL/min, -●-: 0.75 mL/min); reciprocating flow rate was set to 30 mL/min (A), 50 mL/min (B) and 136 mL/min (B).

Thus the effect of the reciprocating flow rate (RFR) was studied in a set of experiments for which it was increased stepwise from 40 to 60 mL/min once the steady state was reached. Results presented in Figure 11 show that the nanodroplets size and PDI decrease when EFR increases. It was demonstrated in our previous work on the batch microprocess[11] that the elongational strain rate is directly proportional to the square of the reciprocating flow rate, so the higher the EFR, the lower can be the

nanodroplets size. However the most relevant result is the possibility offered by the developed continuous-flow microprocess to fairly well tuned the nanodroplets size by simply adjusting the reciprocating flow rate while maintaining a given emulsion mass productivity, i.e. a constant inlet flow rate.

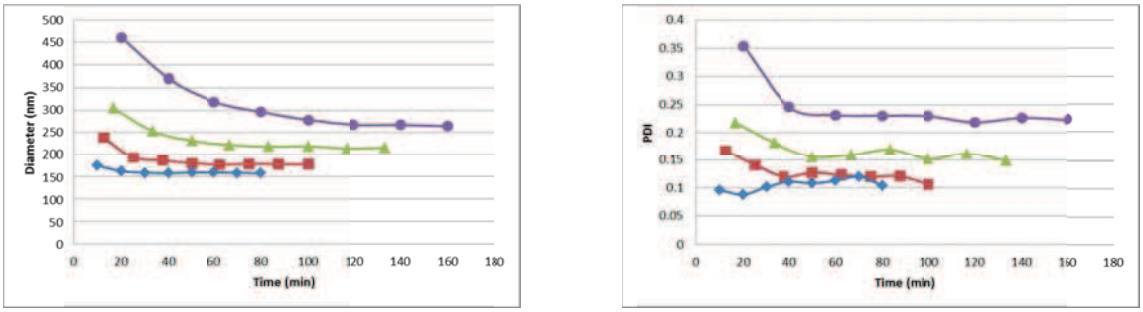

A) B)

Figure **10**. Variation of the nanodroplets size (A) and PDI (B) with respect to operating time for a bore size of 250 µm and for a constant reciprocating to inlet flow rate ratio of 200 obtained with different combinations of reciprocating flow rate (RFR) and inlet flow rate (IFR) (-♦-: RFR:IFR = 50:0.25 mL/min, - ■-: RFR:IFR = 40:0.2 mL/min, -▲-: RFR:IFR = 30:0.15 mL/min, -●-: RFR:IFR = 25:0.125 mL/min).

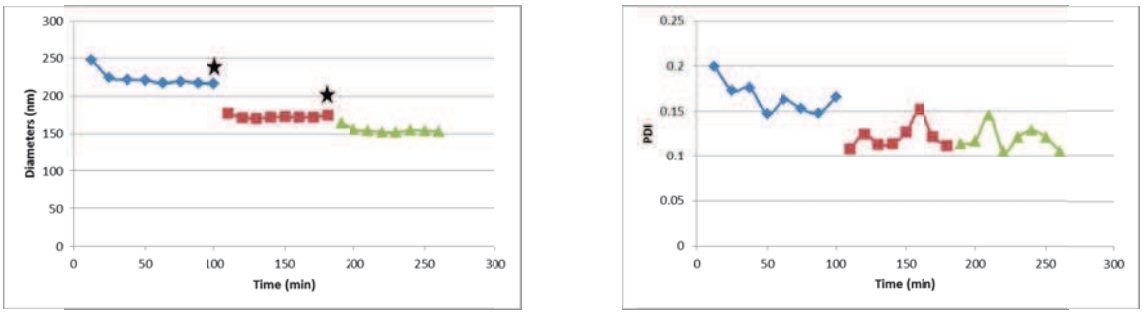

A) B)

Figure **11**. Variation of the nanodroplets size (A) and PDI (B) with respect to the operating time for a bore size of 250 µm, an inlet flow rate of 0.25 mL/min and a stepwise decrease of the reciprocating flow rate (-♦-: 40 mL/min, - ■-: 50 mL/min, -▲-: 60 mL/min). Stars indicate when the reciprocating flow rate was increased.

3.2.3.2 Effect of the initial emulsion volume charged in the stainless steel syringe

For a given reciprocating flow rate, the higher the initial emulsion volume charged in the stainless steel syringe, the longer is the duration of one cycle (i.e. the duration of a back and forth movement of the reciprocating syringe pumps). Therefore, one may expect that in case of variation of this initial emulsion volume, the droplet size might vary. However Figure 12 shows surprisingly that when the steady state is reached, the droplet size is same whatever the initial emulsion volume. Only the transient regime seems to be affected by such volume. The lower the volume, the shorter is the transient regime or in other words the faster the steady state is reached. For the reciprocating flow rate used in this set of experiments (50 mL/min), the durations of one cycle for an initial emulsion volume of 5, 10 and 15 mL were equal to 12, 24 and 36 s respectively. These durations were 200 times shorter than the durations (40, 80 and 120 min) required to inject the same volumes when the inlet flow rate was set to 0.25 mL/min. Therefore, in such conditions the initial emulsion volume has no effect on droplet size. However it is expected that it would not be the case when both durations will be of same order of magnitude, i.e. when the initial emulsion volume would be largely increased. Thus, under the conditions tested, it seems that the droplet size is only affected by the reciprocating (Figure 11) and inlet (Figure 9) flow rates. This means that the microprocess can still operate quite efficiently with small initial emulsion volumes which is a real benefit as the hold-up volume will be reduced.

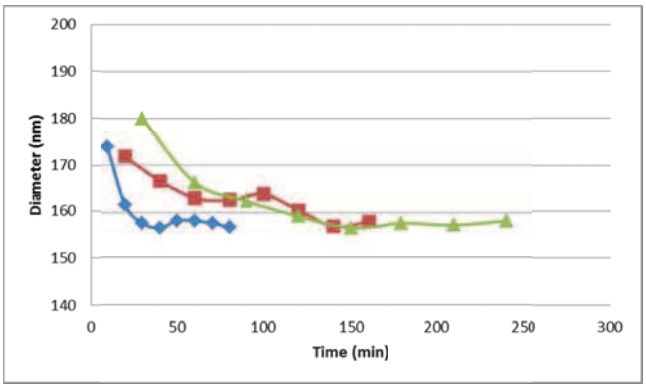

Figure **12**. Variation of the nanodroplets size with respect to operating time for a bore size of 250 µm, a reciprocating flow rate of 50 mL/min, an inlet flow rate of 0.25 mL/min and for different volumes of total emulsion initially charged in the stainless steel syringe and (-♦-: 5 mL, - ■-: 10 mL, -▲-: 15 mL).

3.2.3.3 Effect of MMA volume fraction

The MMA volume fraction is another important factor that can affect the nanodroplets size. In this last set of experiments, one made variation of the MMA volume fraction in the feed line (from 15% to 50%) by lowering the flow rate of the water phase and increasing that of the oil phase while maintaining the overall inlet flow rate constant (0.25 mL/min). Figure 13 shows the variation of the nanodroplets size with respect to MMA volume fraction. The nanodroplets size was found to increase consistently with oil phase volume fraction. Two different explanations can be proposed to account for this trend. Firstly, as the MMA volume fraction increases, the concentration of SDS in the emulsion decreases because of the volume of water phase is reduced. Indeed, the concentration of SDS in water was kept equal to 3.6 mg per gram of water which corresponds to 2.4 wt.%/MMA calculated for a 15% MMA volume fraction (reference recipe). As a consequence, the interfacial tension increases which results in larger MMA droplets as it was shown in our previous work.[11] Secondly, the emulsion gets more concentrated in MMA when its volume fraction increases and so the chance of droplets collision. As the amount of surfactant was reduced, the number of SDS molecules at the surface of MMA droplets is decreased which favor coalescence and thus the formation of bigger droplets with a larger PDI as seen in Figure 13. Finally it

is noteworthy that only a 50 nm increase in nanodroplets size was reported between low (15%) and high (50%) solid content. This demonstrates the high efficiency of the developed continuous-flow process to produce highly concentrated size-controlled nanoemulsions.

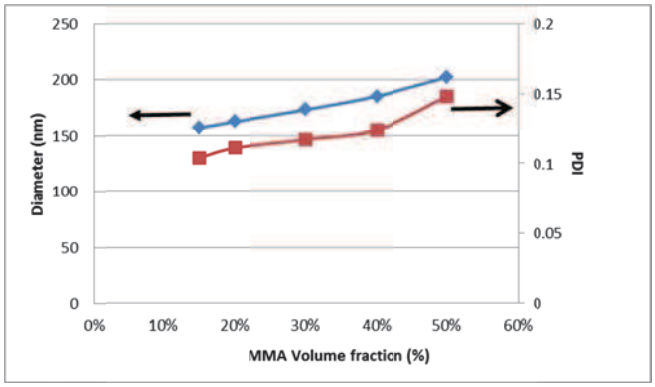

Figure **13**. Variation of the nanodroplets size (-♦-) and PDI (- ■-) with respect to volume fraction of oil phase for an operating time of 80 min (bore size: 250 µm; reciprocating flow: 50 mL/min, inlet flow rate: 0.25 mL/min).

3.2.4 Summary

Continuous-flow production of monodispersed and size-controlled oil-in-water MMA-based nanoemulsions in the size range 100-250 nm was successfully achieved by means of an elongational-flow micromixer. The reciprocating flow rate (RFR) through the microchannel of the micromixer is the key parameter in controlling the nanodroplets size: the higher the RFR, the smaller are the droplets. The diameter of the microchannel plays also an important role in the final nanoemulsion size; reducing the dimension of the microchannel produces smaller droplets but induces a higher operating pressure (up to 7 bars). Compared to the batch version, the inlet flow which crosses the micromixer induces an increase in the nanodroplets size; the higher the inlet flow rate (IFR), the bigger are the droplets. However the steady state in droplet size is reached more rapidly when IFR is high; within about 15 minutes compared to more than one hour for the batch mode. Finally highly concentrated nanoemulsions

with a solid content up to 50% were easily produced with a slight increase in nanodroplets size (+50 nm) compared to the reference nanoemulsion of 15% oil phase volume fraction. The developed low pressure microprocess was able to produce up to 1 kg per day of nanoemulsion but it should be easily scaled up to attain higher mass productivities and meet the requirements for a small commercial production.

3.2.5 Supporting information

Schematic drawing of the 4 ports elongational-flow micromixer

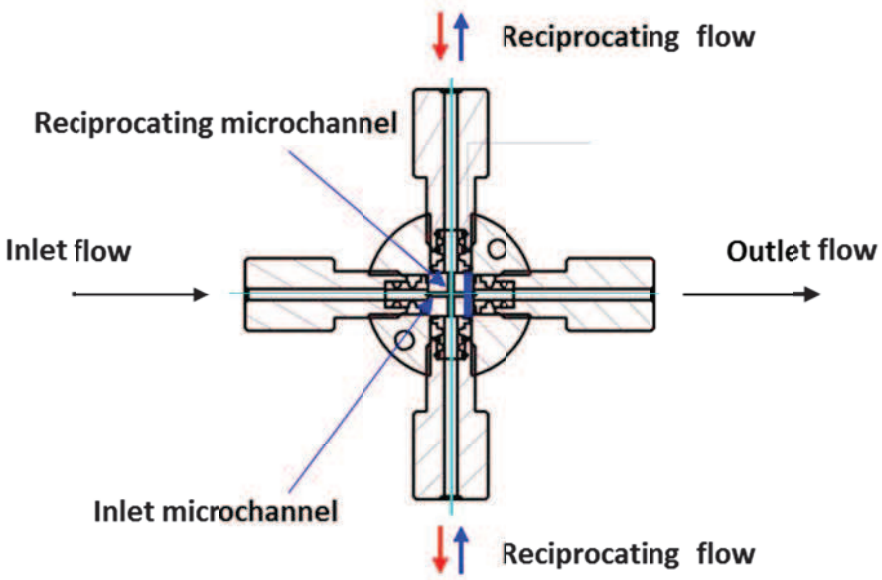

Figure **S1**. Cut view of 4 ports elongational-flow micromixer (adapted from the manufacturer's drawing, VICI website).

PDI

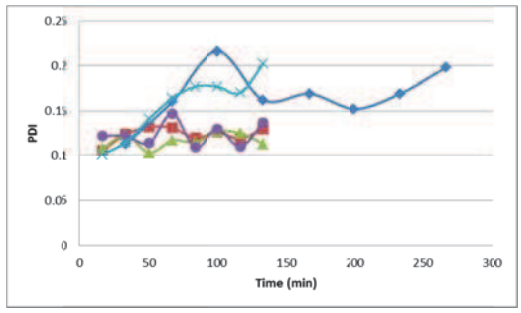

A)

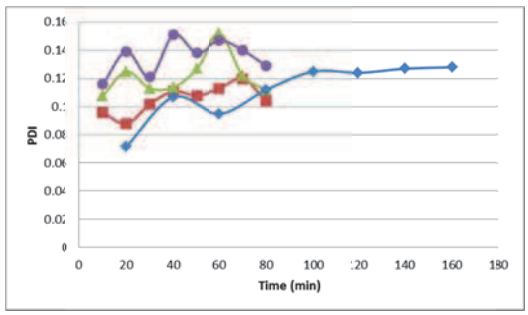

B)

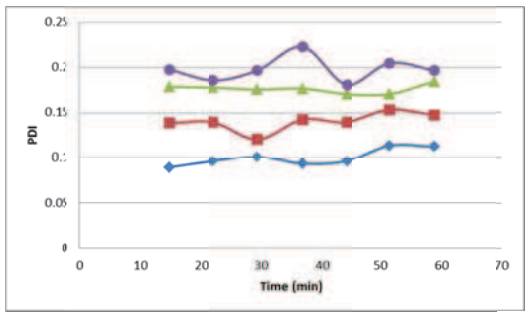

C)

Figure **S2**. Variation of PDI with operating time for a bore size of 150 µm (A), 250 µm (B) and 500 µm(C) and for different inlet flow rates (-♦-: 0 mL/min, - X-: 0.05 mL/min, - ■-: 0.25 mL/min, -▲-: 0.5 mL/min, -●-: 0.75 mL/min); reciprocating flow rate was set to 30 mL/min (A), 50 mL/min (B) and 136 mL/min (B).

3.2.6 References

1. Kim, S. O.; Ha, T. V. A.; Choi, Y. J.; Ko, S., Optimization of Homogenization–Evaporation Process for Lycopene Nanoemulsion Production and Its Beverage Applications. *Journal of Food Science* **2014,** *79* (8), N1604-N1610.

2. Sonneville-Aubrun, O.; Simonnet, J. T.; L'Alloret, F., Nanoemulsions: a new vehicle for skincare products. *Advances in Colloid and Interface Science* **2004,** *108–109*, 145-149.

3. Lovelyn, C.; Attama, A. A., Current state of nanoemulsions in drug delivery. *Journal of Biomaterials and Nanobiotechnology* **2011,** *2* (05), 626.

4. Silva, H. D.; Cerqueira, M. Â.; Vicente, A. A., Nanoemulsions for food applications: development and characterization. *Food and Bioprocess Technology* **2012,** *5* (3), 854-867.

5. Wilde, P.; Corredig, M., Emulsions and nanoemulsions using dairy ingredients. *Dairy-derived ingredients: food and nutraceutical uses* **2009**, 539-564.

6. McClements, D. J., Edible nanoemulsions: fabrication, properties, and functional performance. *Soft Matter* **2011,** *7* (6), 2297-2316.

7. Seekkuarachchi, I. N.; Tanaka, K.; Kumazawa, H., Formation and Charaterization of Submicrometer Oil-in-Water (O/W) Emulsions, Using High-Energy Emulsification. *Industrial & Engineering Chemistry Research* **2006,** *45* (1), 372-390.

8. Peshkovsky, A. S.; Bystryak, S., Continuous-flow production of a pharmaceutical nanoemulsion by high-amplitude ultrasound: Process scale-up. *Chemical Engineering and Processing: Process Intensification* **2014,** *82*, 132-136.

9. Jafari, S. M.; He, Y.; Bhandari, B., Production of sub-micron emulsions by ultrasound and microfluidization techniques. *Journal of Food Engineering* **2007,** *82* (4), 478-488.

10. Tadros, T.; Izquierdo, P.; Esquena, J.; Solans, C., Formation and stability of nano-emulsions. *Advances in Colloid and Interface Science* **2004,** *108–109*, 303-318.

11. Yu, W.; Serra, C. A.; Khan, I. U.; Ding, S.; Gomez, R. I.; Bouquey, M.; Muller, R., Development of an Elongational-Flow Microprocess for the Production of Size-Controlled Nanoemulsions: Batch Operation. *Chem. Eng. J. submitted*.

12. Farzi, G.; Bourgeat-Lami, E.; McKenna, T. F. L., Miniemulsions using static mixers: A feasibility study using simple in-line static mixers. *Journal of Applied Polymer Science* **2009,** *114* (6), 3875-3881.

13. Grace, H. P., Dispersion phenomena in high viscosity immiscible fluid systems and application of static mixers as dispersion devices in such systems. *Chemical Engineering Communications* **1982,** *14* (3-6), 225-277.

CHAPTER 4
APPLICATION TO THE SYNTHESIS OF MULTI-SCALE AND MULTI-DOMAIN POLYMERIC MICROPARTICLES

Preface

In previous chapter an elongational-flow microprocess was developed for the production of size-tunable nanoemulsions. If the dispersed phase of the o/w nanoemulsion is composed of a polymerizable compound (monomer), then the nanoemulsion could be turned into a colloidal suspension of polymer nanoparticles upon miniemulsion polymerization of the monomer. On the other hand, capillaries-based microfluidic droplet generators were proved to be quite efficient tools for the production of monodispersed polymer microparticles with controlled sizes and morphologies (e.g. Janus or core-shell structures). Thus, this chapter aims at bringing these two "worlds" (nanoparticles and microparticles) in order to prepare composite and hybrid multi-scale and multi-domain particles. In such objects, polymer nanoparticles obtained from the aforementioned polymerizable nanoemulsions and noble metal nanoparticles will be selectively embedded into different domains of a polymeric microparticle.

This chapter is partially adapted from the following article:

(1) Wei Yu, Christophe A. Serra, Meriem Er-Rafik, Marc Schmutz, Isabelle Kraus, Shukai Ding, Michel Bouquey and René Muller, Development of an Elongational-Flow Microprocess for the Production of Size-Controlled Nanoemulsions: Application to the Preparation of Monodispersed Polymer Nanoparticles and Composite Polymeric Microparticles, Chem. Eng. J., to be submitted

4.1 Composite microparticles

ABSTRACT

A three step microfluidic process is proposed for the production of composite plain and core-shell polymeric microparticles doped with polymer nanoparticles. These monodispersed microparticles were prepared by means of capillaries-based microfluidic droplet generators from a dispersed phase obtained after the thermally-induced or UV-initiated miniemulsion polymerization of size-controlled o/w monomer(s)-based nanoemulsions produced in a novel elongational-flow microemulsifier. Nanodroplets and polymer microparticles sizes were conveniently varied by tuning the different process parameters, namely the reciprocating flow rate through the emulsifier microchannel and number of cycles for the former and flow rates of all immiscible phases for the latter. As such, 300 μm plain poly(acrylamide) microparticles and 300 μm poly(acrylamide) core – poly(tri(propylene glycol) diacrylate) shell microparticles of 500 μm containing either 230 nm poly(tri(propylene glycol) diacrylate-co-methyl methacrylate) or 360 nm poly(tri(propylene glycol) diacrylate) nanoparticles embedded into the poly(acrylamide) matrix were successfully prepared. This microfluidic process represents a facile route to the synthesis of multi-scale and multi-domain composite polymeric microparticles.

4.1.1 Introduction

Polymer nanoparticles are defined as particulate dispersions or solid particles of polymeric materials which size is ranging from 10 to 1,000 nm.[1] Due to their specific size and the resulting extremely high surface to volume ratio ($3x10^7$ m^2/m^3 for a particle of 100 nm in diameter), polymeric nanoparticles attract a growing interest and have already found various applications in fields like drug delivery, sensing, contrast agents etc.[2]

Two different approaches can be considered to prepare polymer nanoparticles depending upon whether an emulsification step is carried out.[3] The first approach consists in a one-step procedure involving a preformed polymer solubilized in an adequate solvent. Two main different methods work out this approach. In the first method, so-called solvent displacement method or nanoprecipitation[4], the polymer solution is put into contact with a non-solvent of the polymer. In case the polymer solvent is miscible in the non-solvent, a fast diffusion of the former into the latter leaves the polymer in a supersaturated state which ultimately precipitates to form nanoparticles. An adequate surfactant is however required which helps in the stabilization of the nanoparticles and prevent aggregation. This method is quite easy to process, low energy consuming and wildly applicable without much additives.[5] However, the primary drawback of this nanoprecipitation method is that a low polymer concentration (typically around 1 wt.%) is required to enable a good control on the particle size. Nonetheless this method was successfully intensified toward higher polymer concentrations (up to 5 wt.%) by employing microfluidic devices.[6,7]The spray-drying technique composes the second method and is widely used in biomedical and pharmaceutical applications especially in drug delivery when dried polymer nanoparticles are required for further applications.[8]The working principle consists in atomizing the polymer solution into small droplets that are then put into contact with a hot gas to evaporate the polymer solvent and form solid polymer nanoparticles which are eventually recovered by a cyclone unit.

The second approach consists in a two-step procedure which implies at first the emulsification of either a polymer or a monomer solution into nanodroplets followed by either the removal of the solvent of the polymer from the polymer solution droplets or by the free radical polymerization of the monomer droplets. The two most common techniques employed in the first method involve the so-called solvent diffusion and solvent evaporation procedure. Both have in common to precipitate the polymer by removing its solvent, like in the case of former nanoprecipitation method of first approach, either by using a high vapor pressure solvent (e.g. dichloromethane,

chloroform or ethyl acetate) that can be evaporated easily upon applying a slight vacuum or by employing a solvent which is miscible with the continuous phase of the emulsion. In the second method, an emulsion of monomers droplets in a suitable continuous phase has to be prepared. One distinguishes between different emulsion types depending upon the size of the droplets. Droplets with sizes ranging from 10 to 100 nm are called microemulsions and are usually thermodynamically stable, miniemulsions (also referred to as nanoemulsions) are characterized by droplets sizes ranging from 100 nm to 1 μm while emulsions with bigger droplets sizes are so-called macroemulsions. Then one has to apply in a second step a suitable polymerization technique to get the polymer nanoparticles. Depending upon the size range of the nanoparticles to be prepared, one distinguishes between three main different techniques: miniemulsion, micromeulsion and standard emulsion polymerization techniques[9]. The latter[10] usually requires the following components: water as the main phase, a monomer with low solubility in water, a water-soluble initiator and a surfactant. The radial polymerization is initiated in the surfactant micelles and the monomer diffuses from the micron-size monomer droplets through the water phase to feed the growing particles. The typical polymer nanoparticles size achieved with such technique is around 500 nm. The miniemulsion polymerization[11] differs from the standard emulsion polymerization by the size of the monomer droplets which ranges from 50 to 300 nm and also by the locus of the polymerization which takes place directly inside the monomer nanodroplets. An oil-soluble or water-soluble surfactant and an Ostwald ripening inhibitor are required besides the water and a poorly water-soluble monomer. Miniemulsion polymerization usually provides polymer nanoparticles which size is bigger than the original monomer droplets size, ranging from 100 to 500 nm. Finally in comparison with the previous technique, microemulsion polymerization[12] requires a much higher quantity of surfactant such as to decrease to almost zero the interfacial tension between the water and oil phases. To that extent, very small nanoparticles can be prepared with sizes typically below 100 nm. Most of the time, the polymerization is triggered by heating the reactive medium

in conjunction with the use of thermal initiators. However few examples of photo-initiated polymerization in dispersed media were reported. Chemtob and coll.[13] successfully used a microfluidic photoreactor for the production of different (meth)acrylate and thiol-ene polymers via miniemulsion photopolymerization. Over the thermally-induced polymerization, photopolymerization displays a couple of advantages such as ambient temperature reaction, fast reaction rates, spatial and temporal control, and the possibility to use energy-saving lamps. All of the aforementioned emulsion polymerization techniques require the preparation of an emulsion in which the monomer is dispersed in the continuous phase. Several methods are available for producing nanoemulsions. They can be classified into two categories: high-energy and low-energy methods.[14,15] High-energy methods include energy inputs which can be reached by ultrasound generator, high-pressure homogenizer, rotor-stator mixer, static mixer and membrane. By using these emulsification methods, the nanodroplets can be obtained by energy transfer with the presence of surfactant whose function is to decrease the interfacial tension. Low-energy methods take advantage of the internal chemical potential of the emulsion components to achieve emulsification. They rely on the spontaneous formation of emulsion when either its composition or the surrounding conditions are changed.[16] Example of the main low-energy methods include spontaneous emulsification, phase inversion temperature and phase inversion composition. Very low interfacial tensions are the key factor of these emulsification methods which can be achieved by formulation designs. Alternatively, less conventional microfluidic devices can be employed for the production of nanoemulsion with the added advantage of a better control of the nanodroplets size and size distribution. Koehler and coll.[17] succeeded to produce poly(methyl methacrylate) nanoparticles in a single-step microcontinuous flow process. Nanodroplets of methyl methacrylate were generated by the shear force caused by the tangential flow of a continuous phase (water) at the surface of a microhole plate through which the dispersed phase was pumped. The plate was photolithographically fabricated and contained 16x48 holes of 20 μm in diameter. Then downstream upon

collection in a heated beaker, the nanodroplets were thermally polymerized. Highly monodispersed spherical nanoparticles in the size range 700 to 600 nm were synthesized with an ionic surfactant (SDS) which size could be easily varied by adjusting the surfactant concentration.

Polymeric microparticles are defined as spherical or non-spherical particles with a size in the micrometer range (typically from 1 μm to 1000 μm).[18] Polymeric microparticles are essential not only for fundamental research but also for a wide range of applications including drug delivery,[19] paints and catalysis.[20] A couple of approaches have been employed to produce polymeric microparticles including suspension polymerization, spray drying, emulsion/solvent evaporation, phase separation and grinding.[19] However all these approached do not provide a straightforward control of the final particle size, not the mention the usual large particle size distribution they induce.[21] A new approach to prepare uniform polymeric microparticles has been recently promoted by microfluidic techniques.[22] Over conventional processes, microfluidic-assisted processes provide the possibility to accurately control the size of the microparticles, their size distribution, as well as their shape, morphology and composition.[23] Thus, microfluidic techniques enable to control the formation of spherical particles, non-spherical particles like plugs and disk or fibers.[23,24,25,26,27]

Multi-scale and multi-domain composite polymeric microparticles represent complex morphologically particles containing subdomains composed of polymer materials of lower scales. Examples of multi-domain include core-shell or Janus particles for which at least two different domains of usually two different polymer matrices are present in the same microparticle. Polymeric microparticles doped with polymer nanoparticles are an example of multi-scale particles as they present at least two domains which differ by one or more decades in size. Manipulation and storage of nanoparticles may be hazardous for human health[28] and their encapsulation into higher scales objects that can be safely manipulated such as multi-scale polymer microparticles represents one solution to this problem.

The current study aims at preparing size-tunable plain and core-shell polymeric microparticles doped with polymer nanoparticles by following a straightforward three step microfluidic procedure. Monomer(s)-based nanoemulsions will be firstly produced in an elongational-flow emulsification microdevice and then polymerized by thermally-induced or UV-initiated minimelusion polymerization to give rise to size-controlled colloidal suspensions of polymer nanoparticles. Later these nanosuspensions will be emulsified into single or core-shell microdroplets in different capillaries-based microfluidic droplet generators. Downstream to their formation, droplets will be polymerized online by UV light to finally give the multi-scale and multi-domain polymeric microparticles selectively doped with lower scale polymer nanoparticles.

4.1.2 Materials and procedure

4.1.2.1 Materials

To produce the polymerizable nanoemulsions, we used an oil phase composed of a monomer, a hydrophobic agent (4 wt.%/Monomer) as an Ostwald-ripening inhibitor and either an organic-soluble photo- or thermal initiator (2.5 or 0.5 wt.%/Monomer respectively). The water phase comprised a surfactant (2.5 wt.%/Monomer) and distilled water. Specifically, the monomer was either methyl methacrylate (MMA, 99% purity, supplied by Aldrich) or tri(propylene glycol) diacrylate (TPGDA, supplied by Aldrich) or a mixture of MMA:TPGDA 50:50 wt.%. Note that TPGDA is bearing two double bonds and so can play the role of a crosslinker. The surfactant was sodium dodecyl sulfate (SDS, 95% purity, supplied by Sigma Aldrich), the hydrophobic agent was hexadecane (HD, 99% purity, supplied by Sigma Aldrich), the organic-soluble photo initiator was 1-hydroxycyclohexyl phenyl ketone (HCPK, 99% purity, supplied by Aldrich) and the organic-soluble thermal initiator was Azobisisobutyronitrile (AIBN, 98% purity, supplied by Merck).

For the production of plain microparticles or the core phase of core-shell microparticles, the above nanoemulsions were firstly polymerized an then admixed with a hydrophilic monomer (Acrylamide, AC, 97% purity, 40 wt.%/Water in the colloidal suspension, supplied by Aldrich), a water-soluble photoinitiator (Genocure DMHA, 5 wt.%/AC, supplied by Rahn), and a crosslinker (N,N'-methylene-bisacrylamide, MBA, 99% purity, 10 wt.%/AC monomer, supplied by Sigma Aldrich).

When producing the core-shell microparticles, the shell phase was composed of pure TPGDA admixed with a surfactant (span 80, 3.5 wt.%/TPGDA, supplied by Fluka) and a photoinitiator (HCPK, 99% purity, 3.5 wt.%/TPGDA, supplied by Aldrich).

In the synthesis of plain and core-shell microparticles, the carrier fluid was composed of silicon oil (500 cSt, supplied by Aldrich) and a distilled water solution admixed with 2 wt.% of methyl cellulose (supplied by Alfa Aesar) to increase the viscosity (4,000 cSt,) respectively.

4.1.2.2 Elongational-flow emulsification microprocess for the production of size-controlled nanoemulsions

As illustrated in Figure 1, the emulsification microprocess mainly consisted in two mid pressure syringe pumps (neMESYS Mid Pressure Module, Cetoni), two stainless steel syringes and one PEEK tee (Valco Vici) as the elongational–flow microemulsifier/micromixer, The syringe pumps were operated by the supplier's software and can independently inject or withdraw, work in tandem (withdraw/withdraw, infuse/infuse) or in opposite phase (withdraw/infuse). The micromixer consisted in several drilled microchannels having a bore size of either 150, 250 or 500 μm. Two of these microchannels were linked to two 25 mL stainless steel syringes (Cetoni) by two PTFE tubing (1.06 mm ID x 1.68 mm OD). A third microchannel was used to recover the nanoemulsion in a glass vial by means of the same kind of PTFE tubing.

The polymerizable nanoemulsions were prepared at first following the procedure described elsewhere.[29] In brief, a total of 5 mL composed of the oil phase (15 vol.%) and the water phase (85 vol.%) was directly charged (no premix) into one stainless steel syringe. Then the pumps were switched on and forced to operate in opposite phase at the same reciprocating flow rate. A back and forth movement of the pump counts for one cycle. After a prescribed number of cycles (100 to 800), one of the syringes was set to its zero volume position, while the second one was forced to infuse the freshly-prepared nanoemulsion through the recovery microchannel. Once recovered, the nanoemulsions were first diluted with fresh SDS/water solution at a dilution rate ranging from 0 to 95%.

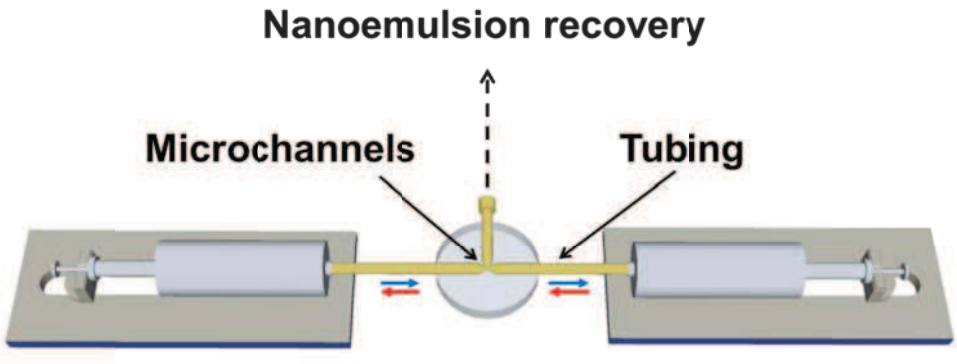

Figure 1. Schematic drawing (not at scale) of the elongational-flow emulsification microprocess.

4.1.2.3 Polymerization of the nanoemulsions

The (diluted) nanoemulsions obtained from previous step were converted into stable colloidal suspensions of polymeric nanoparticles by hardening the nanodroplets of the emulsion oil phase considering two different approaches: either by UV-initiated or thermal polymerization. In the first approach (Figure 2A), a plastic syringe (20 mL, HSW) was filled with the produced (diluted) nanoemulsion and charged in a syringe pump (PHD 2000, Harvard Apparatus) whose flow rate was set to 0.025 mL/min. Thus, the nanoemulsion was forced to flow inside a PTFE tubing (1.06 mm ID×1.68

mm OD) co-axially arranged in a wider stainless steel tube (4 mm ID) of 22 cm length. At both ends, the latter was equipped with a T-junction (Swagelok) in which was set one of the two light guides of an UV source (Lightningcure LC8, Hamamatsu) operating at λ = 365 nm; a wavelength corresponding to the maximum of absorbance of the photoinitiator added into the oil phase. Given the flow rate and the length of the stainless steel tube, the residence time of the nanoemulsion under the UV light was about 7 minutes. For some experiments, the PTFE tubing was replaced by a fused silica capillary (100 µm ID × 165 µm OD, Polymicro Technologies). In the second approach (Figure 2B), the glass vial containing the (diluted) nanoemulsion was left overnight in an over which temperature was set to 70°C.

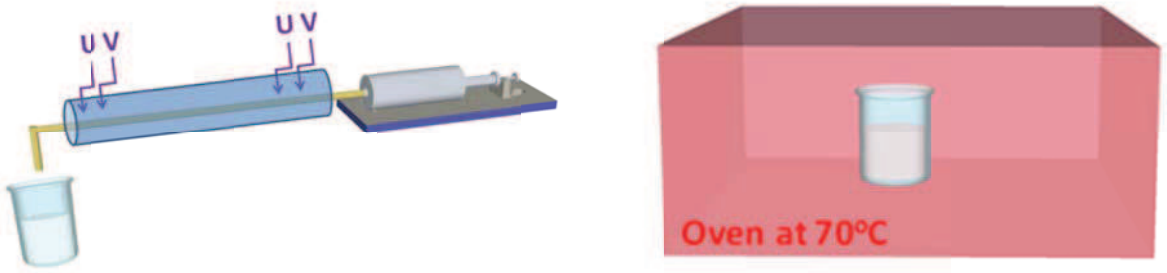

A) B)

Figure 2 Schematic drawing of two methods to produce colloidal suspension: A) polymerization by UV irradiation; B) thermal polymerization in an oven (not to scale).

4.1.2.4 Capillary-based microfluidic devices for the production of composite polymeric microparticles

Once the produced colloidal suspensions of polymeric nanoparticles obtained in the previous step were admixed with an appropriate monomer, photoinitiator and possibly crosslinker (see section 4.1.2.1), they were used as the dispersed or inner phase of capillaries-based microfluidic droplet generators (Figure 3).

Thus polymeric microparticles containing thousands of polymer nanoparticles embedded in the polymer matrix (Figure 3A1) were produced using the one capillary device of Figure 3A2 originally developed for the production of plain microparticles.[30] The device was composed of a hydrophilic fused silica capillary (100 μm ID × 165 μm OD, Polymicro Technologies) aligned along the main axis of a 1/16" T-junction (Upchurch Scientific). The dispersed phase composed of a polymerizable colloidal suspension of polymeric nanoparticles (see section 4.1.2.1) was delivered by a syringe pump (PHD 2000, Harvard Apparatus). The continuous phase was delivered through the port perpendicular to the main axis of the T-junction by another syringe pump (PHD 2000, Harvard Apparatus). Both phases exited the T-junction through a PTFE tubing (1.6 mm ID × 3.2 mm OD, Fisher Bioblock Scientific). At the capillary tip, the two phases got in contact and droplets of dispersed phase were spontaneous formed whose size can be conveniently varied by adjusting the continuous and dispersed phases flow rates.[30] Downstream, a portion of the PTFE tubing was placed under the same previous UV source to promote the polymerization of the microparticles' matrix. The nanoparticles-doped plain polymer microparticles were collected in a beaker at the exit of the PFE tubing. Finally the microparticles were washed three times with petroleum ether to remove any traces of the PDMS oil and left dried at room temperature overnight.

Nanoparticles-doped core-shell polymer microparticles (Figure 3B1) were prepared similarly with a co-axial capillaries-based microfluidic droplet generator (Figure 3B2) originally developed for the production of polymer core – polymer shell microparticles.[31] One hydrophilic fused silica capillary (100 μm ID × 165 μm OD, Polymicro Technologies) was placed inside another wider hydrophilic fused silica capillary (530 μm ID × 670 μm OD, Polymicro Technologies) so as to produce double droplets whose core and shell were composed of the inner and middle phase solutions respectively (see section 2.1). The droplet generator featured two T-junctions to allow the feeding of the outer phase on one hand and the middle and inner phases on the other hand. Each phase was pumped through the system by a syringe pump (PHD

2000, Harvard Apparatus). Given the hydrophobic nature of the shell phase, the outer phase was composed of a viscous aqueous solution (see section 2.1). Downstream, core and shell phase of double droplets were hardened par photopolymerization using same UV arrangement. Once collected, the core-shell microparticles were washed 3 times with fresh distilled and dried overnight at room temperature.

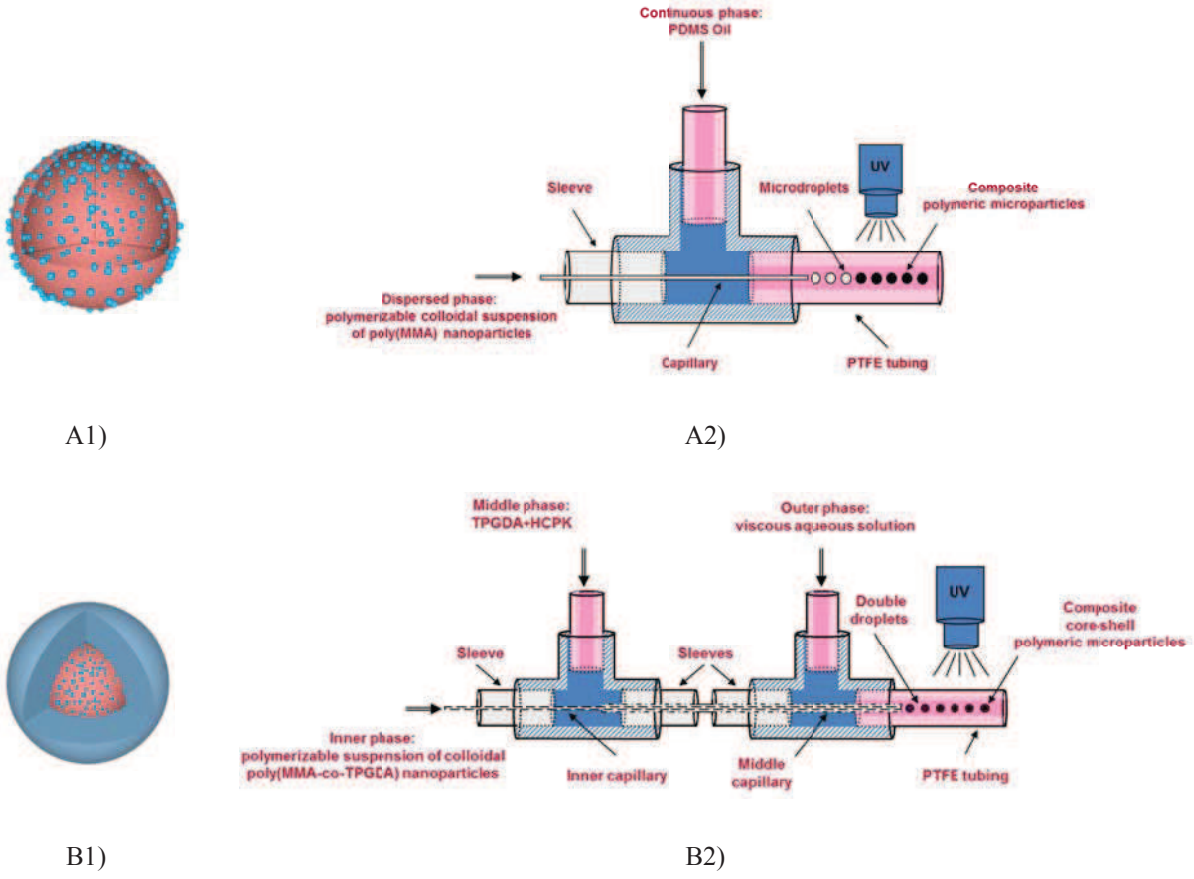

Figure 3. Schematic drawings of capillaries-based microfluidic devices (A2, B2) for producing composite plain polymer microparticles (A1) or core-shell microparticles (B1) respectively.

4.1.2.5 Characterization

Interfacial tensions between the different oil phases (MMA, MMA-co-TPGDA) and water phase were measured by the rising drop method using a tensiometer (TRK-S, Teclis). The nanodroplets and nanoparticles diameters and their respective

polydispersity in size (PDI) were characterized by a commercial dynamic light scattering detector (DLS, Zetasizer, Nano Series, Malvern) at a fixed scattering angle of 173°. In order to reach the required turbidity for an accurate measurement and limit the possible coalescence as much as possible, two drops of freshly-prepared nanoemulsions or colloidal suspensions were dispersed into 9 mL of distilled water shortly before the analysis. Approximately 1 mL of the diluted sample was injected into the disposable DLS cuvette. Three kinds of average diameters (number-, volume- and intensity-) could be returned automatically by the DLS detector as well as the PDI value. The intensity-average diameter D_{exp} was used throughout this study. PDI values below 0.2 are usually considered as the feature of monodispersed size distributions.[32] For each sample, DLS measurement was run in triplicate. During each measurement, 10 to 30 scans were automatically performed by the DLS apparatus.

To visualize shape and size of the produced nanoparticles, a 400 carbon lacey film (Ted Pella) is rendered hydrophilic with a glow discharge treatment (Elmo Cordouan) then a 5 µL drop is deposited onto the grid and the film is blotted and plunged-freezed with a home automatic freezing machine. The humidity and T° are controlled at > 80% and 23°C respectively. The grid is then transferred onto a Gatan 626 cryoholder and observed under low dose conditions in a Tecnai G2 under 200kV. Images are recorded with an Eagle 2k2k ssCCD camera (FEI).

Formation of the microdroplets at capillary(ies) tip(s) was visualized and recorded with a microscope (Eclipse 80i, Nikon) equipped with a CCD camera (Pike F-032B, Allied Technology) to check that droplet were formed in the dripping regime.[30] The camera captured up to 200 fps at a full resolution of 648 × 488 pixels. Scanning Electron Microscopy (XL FEG/SFEG/Sirion, JSM 6380, JEOL or VEGA 3 LMV, TESCAN) was used to observe the surface, morphology and cross section of the microparticles. The cross section was obtained after cutting with a sharp razor blade the microparticles to reveal their inner structure.

4.1.3 Results and discussion

4.1.3.1 Nanoemulsions and colloidal suspensions

The developed elongational-flow microprocess allowed the easy and straightforward production of monodispersed monomer-based nanoemulsions whose size can be conveniently tuned from 60 to 280 nm. As shown in Table 1, the control in size is achieved by adjusting any of the following process parameters: reciprocating flow rate (entry 6&7), number of cycles (entry 5&7 or 6&9 or 1&2) and microchannel size (entry 7&8). Smaller nanodroplets were obtained when the former two parameters are increased or when the latter is decreased. In a previous study,[29] we have shown that the higher the elongational strain rate ($\dot{\varepsilon}$) imposed by the sharp restriction of the micromixer, the smaller are the nanodroplets. Moreover we have demonstrated that $\dot{\varepsilon}$ is proportional to the reciprocating flow rate and inversely proportional to the microchannel size. As for the effect of the number of cycles, PDI values below 0.2 for cycles above 100 made us to hypothesize that the droplet break-up mechanism proceeded via a rupture into two subdroplets of almost same size. Therefore, several passages through the restriction (i.e. more cycles) are required to gradually decrease the nanodroplets size till equilibrium between the rupture and the coalescence is reached.

Table 1 also shows that an oil phase composed of either pure TPGDA or a mixture of MMA and TPGDA (50 wt.%) gives different nanoemulsion sizes (entry 9&10) when processed with the same parameters. This can be readily interpreted considering the difference in interfacial tensions between the two aforementioned oil phases; a larger nanodroplets size was obtained, as expected, with the highest interfacial tension.

Table 1. Size of produced nanodroplets and related operating conditions

Entry	Oil phase	Reciprocating flow rate	Number of cycles	Microchannel size	Interfacial tension	Nanodroplets size*	Nanodroplets PDI*	Nanoparticles size*	Nanoparticles PDI*
		mL/min	(-)	(µm)	(mN/m)	(nm)	(-)	(nm)	(-)
1	MMA	30	100	150	3.51	84	0.156	125[£]	0.035[£]
2		30	800	150		74	0.198	87[£]	0.089[£]
3		50	800	250		94	0.115	137[£]	0.047[£]
4	TPGDA -co- MMA	30	800	150	3.02	56	0.139	184[£]	0.032[£]
5		30	800	150		56	0.139	130[$]	0.077[$]
6		20	100	150		162	0.068	215[$]	0.157[$]
7		30	100	150		92	0.134	164[$]	0.100[$]
8		30	100	250		278	0.202	262[$]	0.280[$]
9		20	200	150		149	0.082	227[$]	0.168[$]
10	TPGDA	20	200	150	5.78	249	0.210	361[$]	0.218[$]

* retuned by DLS measurements. £ obtained by thermal polymerization at 70°C. $ obtained by UV polymerization.

MMA-based nanoemulsions (Table 1, entry 1 to 3) were successfully polymerized by thermal polymerization at 70°C to give colloidal suspensions that were stable over several weeks. Size and PDI of the obtained nanoparticles are reported in Table 1. It is observed that the nanoparticles size is consistently bigger that the size of the nanodroplets they originated from. The size difference ranges from 13 to 43 nm. Note that the coefficient of variation over 3 to 5 samples was found to be ranging from 2% to 3% which means that the error in measuring the size of the nanodroplets is around 3 nm. Thus these differences are significate and may be explained by two possible concomitant phenomena. It is likely that a portion of the whole nanodroplets may not have been nucleated and/or the increase in the temperature up to 70°C may have destabilized the nanoemulsions. As a result, non-nucleated droplets may have served as reservoirs for the polymerizing ones,[33] and/or coalescence may have occurred. Figure 4 shows cryo-TEM pictures of two nanosuspensions (Table 1, entry 1&2) and

clearly demonstrates that one can also readily control the size of the final nanoparticles. One observes round shaped particles with size ranging from 20 nm up to 100 nm (Figure 4a) and from 20 nm up to 200 nm (Figure 4b) for 800 and 100 cycles respectively. These sizes are pretty much in agreement with those returned by the DLS measurements 87 and 125 nm.

When the nanoemulsions were polymerized by UV irradiation (Table 1, entry 5 to 10), a strong increase in nanoparticles' diameter is observed, from 53 nm to 128 nm. The mother nanoemulsion used prior to polymerization was an already quite turbid and concentrated solution (in oil content) which when flowing in the irradiated PTFE tubing led to two phenomena[34] i) the incident UV light energy was reduced when penetrating through the nanoemulsion due to multiple diffusion (a non-elastic phenomenon) induced by the high concentration of nanodroplets, ii) UV light penetration depth was also highly reduced by the diffusion. As a consequence, it is expected that only the nanodroplets located close to the wall of the tubing will received enough energy to promote the dissociation of the photoinitiator and hence initiate the polymerization. Non-nucleated nanodroplets will thus serve as monomer reservoirs for the polymerizing ones. We replaced the 1.06 mm ID PTFE tubing by a 100 μm ID fused silica capillary with the hope to nucleate much more nanodroplets by reducing drastically the medium thickness to be irradiated. Unfortunately the system got clogged quite rapidly.

To limit the increase in size after polymerization triggered either by UV irradiation of by heating the reactive medium, we developed an approach consisting in the dilution of the nanoemulsion in order to reduce the concentration of the nanodroplets and avoid as much as possible the multiple diffusion as well as to limit the coalescence. Results obtained with TPGDA/MMA-based nanoemulsions (Table 1, entry 4&5) are presented in Figure 5. The strategy was quite effective and required a dilution factor of 95% to recover the original size of the mother nanodroplets in case of UV-initiated polymerization and more than 100% for the case of thermal polymerization. However

this latter case is quite impractical since a higher dilution rate is required. Hence UV-initiated polymerization seems to be the more appropriate method to guarantee that the microparticles size could be controlled by adjusting the process parameters of the elongational-flow microprocess (i.e. by controlling the mother nanoemulsion size). Nonetheless both methods allowed the production of size-controlled nanoparticles.

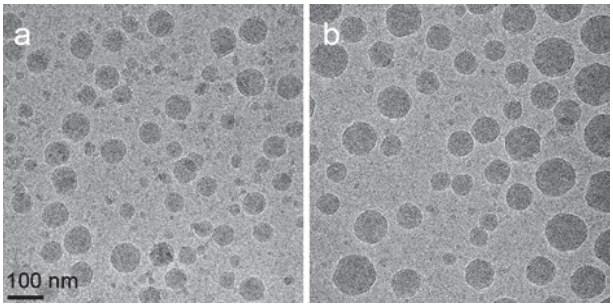

Figure 4. Cryo-TEM micrographs of two poly(MMA) nanoparticles obtained by thermal polymerization of MMA-based nanoemulsions produced with 800 (a) or 100(b) cycles (Table 1, entry 1&2).

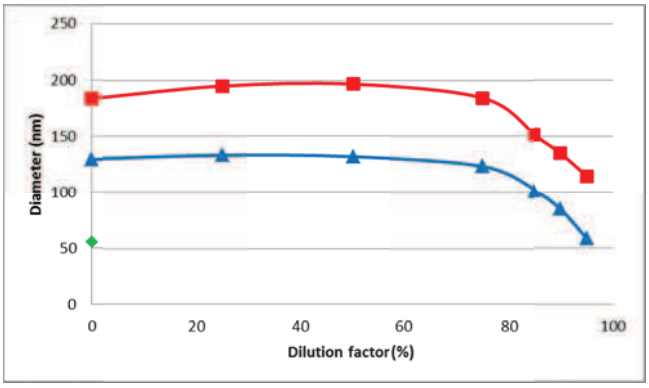

Figure 5. Variation of the nanoparticles size according to the dilution rate of the original TPGDA-co-MMA nanoemulsion (-♦-) when polymerized either by UV irradiation (-▲-) or thermal polymerization (-■-). Operating conditions correspond to entry 4&5 of Table 1.

4.1.3.3 Composite polymer microparticles

The synthesized composite plain polymer microparticles (Figure 3A1) were based on the nanoemulsions that were hardened by UV irradiation through the PTFE tubing (Table 1, entry 9&10). By means of the capillary-based droplet generator of Figure 3A2, plain microparticles were successfully prepared with narrow size distribution. Microparticles produced with such microfluidic device have sizes that can be precisely controlled from low 100 μm up to 600 μm by several parameters including the capillary dimension (inner diameter), the dispersed phase flow rate (Q_d), the continuous phase flow rate (Q_c) and the viscosity of the continuous phase.[35] In biref, increasing the dispersed phase flow rate or decreasing the continuous phase flow rate results in larger microdroplets that produce larger microparticles. In opposite, smaller dispersed phase flow rate or higher continuous phase flow rate results into smaller microparticles. The formation of the droplets results from the competition between the shear force imposed by the flow of the continuous phase on the growing droplet at the tip of the capillary and the interfacial force. This result in the formation of droplets of same volume at constant frequency (raging from few Hz to few kHz). The extreme narrow size distribution is thus a specific advantage of microfluidic systems over more conventional methods like the suspension polymerization method. Indeed, the coefficient of variation of the particle size distribution achieved by microfluidic droplet generators is typically lower than 5%.[23] At high flow rate of the continuous phase and large values of Q_c/Q_d, a transition from dripping mode to jetting mode could occur.[36] In jetting mode the dispersed phase is elongated and rupture into smaller microdroplets but the presence of satellite droplets of even lower sizes increases largely the coefficient of variation of the particle size distribution.[30] The microparticles presented in Figure 6A&D were prepared from the TPGDA-co-MMA and pure TPGDA nanoemulsions respectively under the following conditions: flow rate of the continuous phase (PDMS oil) 240 μL/min, flow rate of the dispersed phase (polymerizable colloidal suspension) 2.0 μL/min. Both microparticles exhibited an averaged diameter of 300 μm. SEM micrographs confirmed the presence of

poly(TPGDA-co-MMA) and poly(TPGDA) nanoparticles on the surface of the microparticles (Figure 6B&E) and in their inner structure (Figure 6D&F). The presence of the nanoparticles at the surface of the microparticles may originate from the elimination of the water phase originally present in the microparticles. Indeed, the matrix of the microparticles consisted in a hydrogel of poly(acrylamide) due to the presence of water in the polymerizable colloidal suspension which served as the dispersed phase for the production of the microparticles. However due the SEM sample preparation procedure which involved vacuum, the water was removed and the microparticles matrix appeared solid.

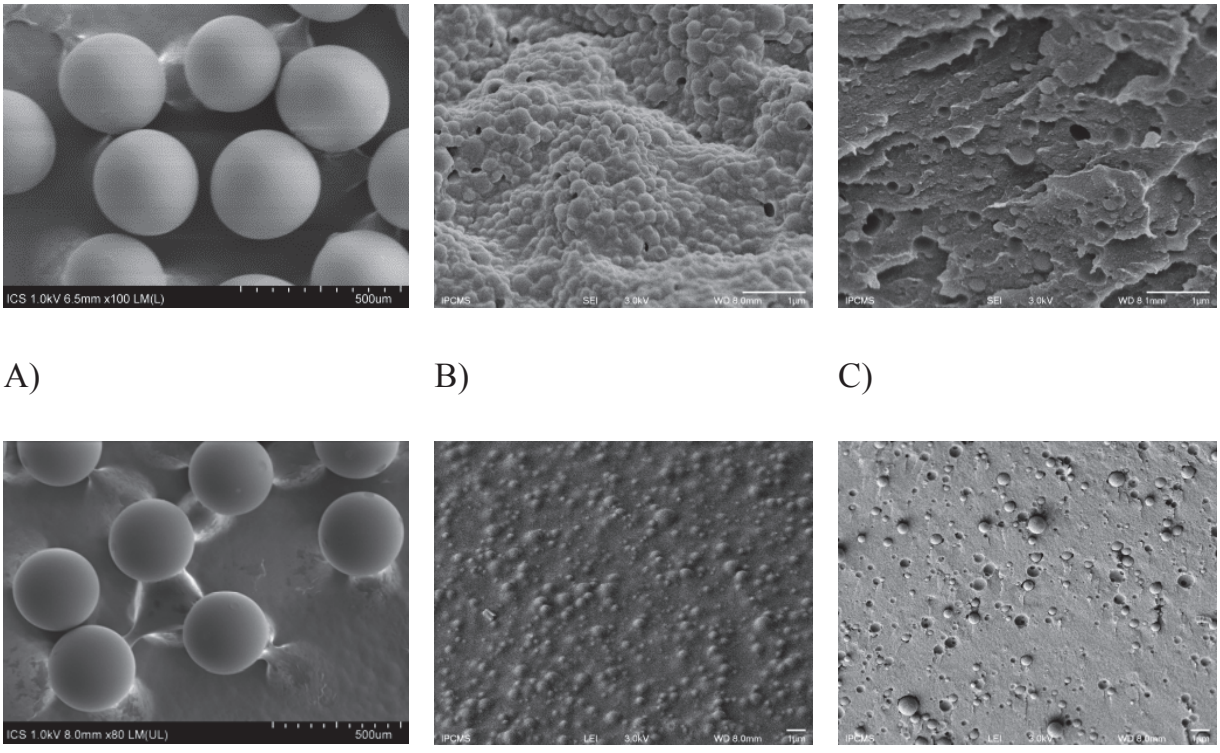

A) B) C)

D) E) F)

Figure 6. SEM micrographs of poly(acrylamide) plain microparticles doped with either poly(TPGDA-co-MMA) or poly(TPGDA) nanoparticles obtained after UV irradiation: overview of microparticles (A,D), their surface (B,E) and their inner structure (C,F). Operating conditions: Q_c = 240 µL/min, Q_d = 2.0 µL/min.

Composite core-shell microparticles were obtained from the co-axial capillaries-based microfluidic droplet generator of (Figure 3B2) and from the TPGDA-co-MMA based nanoemulsion (Table 1, entry 9). These microparticles were produced under the following conditions: flow rate of the continuous phase (viscous aqueous solution, Qo) 130 µL/min, flow rate of the middle phase (TPGDA solution, Qm) 4 µL/min, flow rate of the inner phase (polymerizable colloidal suspension, Qi) 1.5 µL/min. The final size of the microparticles depends on the combination of the three phases flow rate namely the outer, middle and inner phases. As demonstrated in a previous work,[31] the final overall microparticles size depends on the ratio of outer to middle phase flow rates while the shell thickness (or core size) is mainly affected by the flow rate ratio of the middle and inner phases respectively. Under the tested operating conditions, the SEM micrograph of Figure 7A revealed 500 µm microparticles having a truly core-shell structure with a core size of about 300 µm. The gap observed between the shell and core was induced by the elimination of water from the hydrogel poly(acrylamide) core during the SEM preparation procedure (vacuum) and caused the core to shrink. Figure 7B shows the inner structure of the core after being sectioned with a sharp razor blade. It reveals the presence of many poly(TPGDA-co-MMA) nanoparticles embedded in the core matrix.

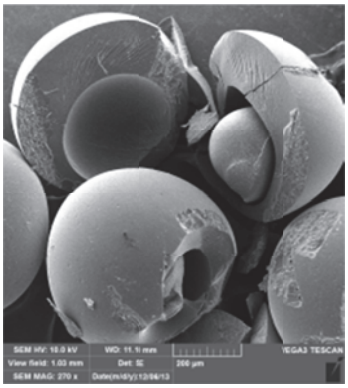
A)

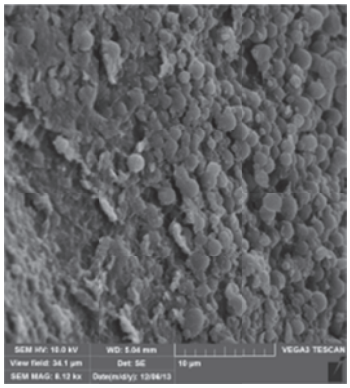
B)

Figure 7. SEM micrographs of core-shell microparticles having a diameter of 500 µm (A) and core matrix doped with 227 nm poly(TPGDA-co-MMA) nanoparticles (B). Process parameters: Q_o = 130 µL/min, Q_m = 4 µL/min, Q_i = 1.5 µL/min.

4.1.4 Summary

We have demonstrated that composite multi-scale and multi-domain polymeric microparticles doped with lower scale polymer nanoparticles can be easily produced using a straightforward three steps microfluidic procedure. First, monomer(s)-based nanoemulsions with narrow size distributions were produced by means of an elongation-flow emulsification microprocess. Nanodroplets size were easily varied in the range 56 to 278 nm by tuning the operating conditions; namely the reciprocating flow rate through the micromixer and the number of cycles. Second, colloidal suspensions of polymeric nanoparticles were obtained from the thermally-induced of UV-initiated polymerization of former nanoemulsions. Upon polymerization, nanoparticles size ranged from 87 to 360 nm and had a bigger size than the nanodroplets size they originate from but remained monodispersed in size as proved by DLS measurements. Last step involved the addition of a proper hydrophilic monomer, crosslinker and UV photoinitiator to the colloidal suspensions before to emulsify the resulting mixture in capillaries-based microfluidic droplets generators to produce monodispersed single or double droplets. Upon online UV polymerization, performed downstream to the formation of the droplets, nanoparticles-doped plain and core-shell polymer microparticles of 300 μm and 500 μm in diameter respectively with narrow size distributions were obtained. SEM micrographs revealed that polymeric nanoparticles were effectively embedded in either the matrix of the plain microparticles or in the 300 μm core matrix of the core-shell microparticles. As shown in a previous work, the size of the plain microparticles can be conveniently varied by tuning the dispersed and continuous phases flow rate ratio while the overall core-shell microparticles size depends on the flow rate ratio of the outer and middle phases. As for the size of the core (or shell thickness), it can be varied by changing the flow rate of the inner phase.

Such kind of polymer microparticles morphologies are quite challenging to produce with conventional batch processes. Thus it is believed that the microfluidic approach developed during this work will represents in the future a new and facile route to the synthesis of even more complex multi-scale and multi-domain microparticles, e.g. nanoparticles-doped core-multishell or janus microparticles, which may find application in drug, cell or gene delivery, sensorics or functional optical materials.

In this section plain and core-shell polymeric microparticles doped with polymer nanoparticles obtained from the miniemulsion polymerization of monomer-based nanoemulsions produced in our newly developed batch elongational-flow microprocess were prepared. Such microparticles represent a nice example of composite multi-scale and multi-domain objects. On the other hand, hybrid multi-scale and multi-domain objects bear the promise of a bright future as their specific morphology composed or organic and inorganic compounds of different scales could find many applications in sensorics or theranostics to name a few. Hence the next section is devoted to the preparation of highly morphologically complex polymeric microparticles incorporating in specific domains not only polymer nanoparticles but also noble metal nanoparticles obtained by the direct UV-initiated reduction of their corresponding salts.

4.1.5 References

1. Nagavarma, B.; Yadav, H. K.; Ayaz, A.; Vasudha, L.; Shivakumar, H., Different techniques for preparation of polymeric nanoparticles—a review. Asian J. Pharm. Clin. Res 2012, 5 (3), 16-23.

2. Mohanraj, V.; Chen, Y., Nanoparticles–A Review. Tropical Journal of Pharmaceutical Research 2006, 5 (1), 561-573.

3. Allouche, J., Synthesis of Organic and Bioorganic Nanoparticles: An Overview of the Preparation Methods. In Nanomaterials: A Danger or a Promise?, Brayner, R.; Fiévet, F.; Coradin, T., Eds. Springer London: 2013; pp 27-74.

4. Bally, F.; Garg, D. K.; Serra, C. A.; Hoarau, Y.; Anton, N.; Brochon, C.; Parida, D.; Vandamme, T.; Hadziioannou, G., Improved size-tunable preparation of polymeric nanoparticles by microfluidic

nanoprecipitation. Polymer 2012, 53 (22), 5045-5051.

5. Hornig, S.; Heinze, T.; Becer, C. R.; Schubert, U. S., Synthetic polymeric nanoparticles by nanoprecipitation. Journal of Materials Chemistry 2009, 19 (23), 3838-3840.

6. Anton, N.; Bally, F.; Serra, C. A.; Ali, A.; Arntz, Y.; Mely, Y.; Zhao, M.; Marchioni, E.; Jakhmola, A.; Vandamme, T. F., A new microfluidic setup for precise control of the polymer nanoprecipitation process and lipophilic drug encapsulation. Soft Matter 2012, 8 (41), 10628-10635.

7. Bally, F.; Serra, C. A.; Brochon, C.; Anton, N.; Vandamme, T.; Hadziioannou, G., A Continuous-Flow Polymerization Microprocess with Online GPC and Inline Polymer Recovery by Micromixer-Assisted Nanoprecipitation. Macromolecular Reaction Engineering 2011, 5 (11-12), 542-547.

8. Li, X.; Anton, N.; Arpagaus, C.; Belleteix, F.; Vandamme, T. F., Nanoparticles by spray drying using innovative new technology: The Büchi Nano Spray Dryer B-90. Journal of Controlled Release 2010, 147 (2), 304-310.

9. Slomkowski, S.; Alemán, J. V.; Gilbert, R. G.; Hess, M.; Horie, K.; Jones, R. G.; Kubisa, P.; Meisel, I.; Mormann, W.; Penczek, S., Terminology of polymers and polymerization processes in dispersed systems (IUPAC Recommendations 2011). Pure and Applied Chemistry 2011, 83 (12), 2229-2259.

10. Chern, C., Emulsion polymerization mechanisms and kinetics. Progress in polymer science 2006, 31 (5), 443-486.

11. Schork, F. J.; Luo, Y.; Smulders, W.; Russum, J.; Butté, A.; Fontenot, K., Miniemulsion Polymerization. In Polymer Particles, Okubo, M., Ed. Springer Berlin Heidelberg: 2005; Vol. 175, pp 129-255.

12. Pavel, F. M., Microemulsion polymerization. Journal of dispersion science and technology 2004, 25 (1), 1-16.

13. Lobry, E.; Jasinski, F.; Penconi, M.; Chemtob, A.; Croutxe-Barghorn, C.; Oliveros, E.; Braun, A. M.; Criqui, A., Continuous-flow synthesis of polymer nanoparticles in a microreactor via miniemulsion photopolymerization. RSC Advances 2014, 4 (82), 43756-43759.

14. Solans, C.; Izquierdo, P.; Nolla, J.; Azemar, N.; Garcia-Celma, M., Nano-emulsions. Current Opinion in Colloid & Interface Science 2005, 10 (3), 102-110.

15. Sajjadi, S., Nanoemulsion formation by phase inversion emulsification: on the nature of inversion. Langmuir 2006, 22 (13), 5597-5603.

16. McClements, D. J., Edible nanoemulsions: fabrication, properties, and functional performance. Soft Matter 2011, 7 (6), 2297-2316.

17. Koehler, J.; Moeller, F.; Schneider, S.; Guenther, P.; Albrecht, A.; Gross, G., Size-tuning of monodisperse PMMA nanoparticles by micro-continuous-flow polymerization using a silicon micro-nozzle array. Chemical Engineering Journal 2011, 167 (2), 688-693.

18. Campos, E.; Branquinho, J.; Carreira, A. S.; Carvalho, A.; Coimbra, P.; Ferreira, P.; Gil, M. H., Designing polymeric microparticles for biomedical and industrial applications. European Polymer Journal 2013, 49 (8), 2005-2021.

19. Guan, J.; Ferrell, N.; James Lee, L.; Hansford, D. J., Fabrication of polymeric microparticles for drug delivery by soft lithography. Biomaterials 2006, 27 (21), 4034-4041.

20. Dendukuri, D.; Hatton, T. A.; Doyle, P. S., Synthesis and Self-Assembly of Amphiphilic Polymeric Microparticles. Langmuir 2007, 23 (8), 4669-4674.

21. Anton, N.; Jakhmola, A.; Vandamme, T. F., Trojan microparticles for drug delivery. Pharmaceutics 2012, 4 (1), 1-25.

22. Steinbacher, J. L.; McQuade, D. T., Polymer chemistry in flow: New polymers, beads, capsules, and fibers. Journal of Polymer Science Part A: Polymer Chemistry 2006, 44 (22), 6505-6533.

23. Serra, C. A.; Chang, Z., Microfluidic-Assisted Synthesis of Polymer Particles. Chemical Engineering & Technology 2008, 31 (8), 1099-1115.

24. Nisisako, T.; Torii, T.; Higuchi, T., Novel microreactors for functional polymer beads. Chemical Engineering Journal 2004, 101 (1–3), 23-29.

25. Subramaniam, A. B.; Abkarian, M.; Stone, H. A., Controlled assembly of jammed colloidal shells on fluid droplets. Nature materials 2005, 4 (7), 553-556.

26. Jeong, W.; Kim, J.; Kim, S.; Lee, S.; Mensing, G.; Beebe, D. J., Hydrodynamic microfabrication via “on the fly” photopolymerization of microscale fibers and tubes. Lab on a Chip 2004, 4 (6), 576-580.

27. Dendukuri, D.; Tsoi, K.; Hatton, T. A.; Doyle, P. S., Controlled Synthesis of Nonspherical Microparticles Using Microfluidics. Langmuir 2005, 21 (6), 2113-2116.

28. Ramachandran, G., Assessing nanoparticle risks to human health. William Andrew: 2011.

29. Yu, W.; Serra, C. A.; Khan, I. U.; Ding, S.; Gomez, R. I.; Bouquey, M.; Muller, R., Development of an Elongational-Flow Microprocess for the Production of Size-Controlled Nanoemulsions: Batch Operation. Chem. Eng. J. submitted.

30. Serra, C.; Berton, N.; Bouquey, M.; Prat, L.; Hadziioannou, G., A predictive approach of the influence of the operating parameters on the size of polymer particles synthesized in a simplified microfluidic system. Langmuir 2007, 23 (14), 7745-7750.

31. Chang, Z.; Serra, C. A.; Bouquey, M.; Prat, L.; Hadziioannou, G., Co-axial capillaries microfluidic device for synthesizing size-and morphology-controlled polymer core-polymer shell particles. Lab on a Chip 2009, 9 (20), 3007-3011.

32. Farzi, G.; Bourgeat-Lami, E.; McKenna, T. F. L., Miniemulsions using static mixers: A feasibility study using simple in-line static mixers. Journal of Applied Polymer Science 2009, 114 (6), 3875-3881.

33. Schork, F. J.; Luo, Y.; Smulders, W.; Russum, J. P.; Butté, A.; Fontenot, K., Miniemulsion polymerization. In Polymer Particles, Springer: 2005; pp 129-255.

34. Jasinski, F.; Lobry, E.; Lefevre, L.; Chemtob, A.; Croutxe-Barghorn, C.; Allonas, X.; Criqui, A., Acrylate nanolatex via self-initiated photopolymerization. Journal of Polymer Science Part A: Polymer Chemistry 2014, 52 (13), 1843-1853.

35. Bouquey, M.; Serra, C.; Berton, N.; Prat, L.; Hadziioannou, G., Microfluidic synthesis and assembly of reactive polymer beads to form new structured polymer materials. Chemical Engineering Journal 2008, 135, Supplement 1 (0), S93-S98.

36. Seo, M.; Nie, Z.; Xu, S.; Mok, M.; Lewis, P. C.; Graham, R.; Kumacheva, E., Continuous Microfluidic Reactors for Polymer Particles. Langmuir 2005, 21 (25), 11614-11622.

4.2 Composite/Hybrid microparticles

4.2.1 Introduction

Microfluidics is the science and technology of systems that process or manipulate small amounts of fluids (10^{-9} to 10^{-18} liters) using microchannels with dimensions of tens to hundreds of micrometers.[1] It is an interdisciplinary field which has largely contributed to the development of flow chemistries.[2] Use of microfluidic devices allowed to explore the possibility to run chemical reactions in new operating windows (higher T, pressure and reactant concentrations)[3] and to produce organic and inorganic materials with better defined or new properties.[4,5]

Specifically, microfluidic systems have shown the possibility to synthesize and assemble polymeric microparticles with narrow size distribution and various sizes, shapes, morphologies, and compositions.[6,7,8,9] Such polymeric microparticles are usually obtained from the hardening of a monomer-based microdroplet by either thermal-induced of UV-initiated polymerization. Indeed, microfluidic devices are extremely efficient emulsification systems which allow to produce either o/w or w/o size-controlled macroemulsions. Moreover the droplet size distribution is usually extremely narrow as its coefficient of variation is typically lower than 5%.[10] Photopolymerization is usually preferred over thermal-induced polymerization for a couple of reasons: i) this a quite efficient method for hardening the liquid monomer droplet into a solid polymer material within few tens of seconds[11], ii) it can easily be implemented in flow and such can fix rapidly non-thermodynamically stable droplet morphologies before relaxing phenomena can occur.

Two different categories of microfluidic devices have been reported for the emulsification of a polymerizable liquid.[10] In the first one both continuous and dispersed fluids flow inside microchannels while in the second one the continuous phase flow inside a tube and the dispersed phase inside a capillary of small dimensions. The emulsification mechanism, which is quite similar for these 2

categories, proceeds from the break-up of a liquid thread into droplets when the to-be dispersed phase is sheared by the continuous and immiscible phase. Three microchannel-based devices are commonly found: the terrace-like microchannel device, the T-junction microchannel device and the flow focusing microchannel device (FFD). The terrace-like microchannel device[12,13] consists of a main channel in which flows the continuous phase. Several microchannels deliver the dispersed phase at the top and from both sides of the main channel. Then terraces located just below the microchannels allow the break-up of the dispersed phase thread. In T-junction microchannel devices,[14,15] the to-be dispersed phase is delivered through a microchannel perpendicular to a main channel in which flows the continuous phase. Depending on the flow rates of the continuous and dispersed phase, the break-up is observed at the junction of the two microchannels or further downstream. FFDs are based on the principle of hydrodynamic focusing.[16] The dispersed phase flows in a central microchannel while the continuous phase is delivered through two side channels. In front of the central channel, a small orifice or a restriction allows the continuous phase to pinch the dispersed liquid thread which breaks pass the orifice into droplets. Three capillary-based devices are also commonly found: the co-flow capillary device, the cross-flow capillary device and the flow-focusing capillary device. The characteristic of the co-flow device is that the dispersed phase flows in the same direction as the continuous phase flow.[17,18] In the cross-flow device the dispersed phase flows in a direction perpendicular to that of the continuous phase flow like for the T-junction microchannel device.[19] The characteristic of the flow-focusing device is that the dispersed phase flow is axisymmetrically pinched by the flow of the continuous phase resulting in the elongation of the dispersed phase stream which breaks up into droplets under capillary instabilities.[20] Capillary-based devices has the following advantage over microchannel-based devices: the dispersed phase is flowing in the centerline of the continuous phase and thus could be keep kept away from the device wall where phase inversion may happen in case of the wettability of the dispersed phase is great than that of the continuous phase. Hence, a same capillary-

based devices can produce o/w or w/o emulsions. However they do have some drawback to: they are somehow limited in the flow arrangement and design. Although each device from these two categories has its own characteristics, some general trends can be drawn for the control of the particle size.[6,21,22] Two dimensionless numbers were identified which significantly contribute to the final particle diameter: the Reynolds number (Re) and the capillary number (Ca) which mainly depend upon the fluids density and viscosity, the mean fluids velocity, a characteristic dimension of the flow (usually the channel width) and the interfacial tension between the two immiscible fluids. Thus the particle diameter is primarily a function of the velocities or flow rates of the two phases. Generally an increase in the continuous phase flow rate or a decrease in the dispersed phase flow rate induces a decrease of the mean polymer particle diameter. This diameter is also affected by the interfacial tension; lower interfacial tensions leading to smaller particles. Fluids viscosity plays as well an important role. An increase in the continuous phase viscosity or a decrease in that of the dispersed phase is usually followed by a decrease in the final particle size. Finally it was observed that a reduction in the characteristic dimension of the microsystem, e.g. the channel width for the terrace-like microchannel and T-junction devices, the orifice width for the FFD and the inner capillary diameter for the capillary-based devices, generates smaller particles.

Besides the simple droplet morphology, double droplets, i.e. a droplet in another droplet, can be produced by slight modifications of the aforementioned FFD and co-flow capillary-based device. Thus FFD was modified to accommodate two additional side microchannels[23] so as to deliver at same time three different phases: the inner channel delivering the embedded droplet phase, the middle microchannels the main droplet phase and the outer phase the continuous phase. Same can be obtained with tow co-axially arranged capillaries.[24] Upon polymerization, these double droplets led to the formation of core-sell polymer microparticles whose core and shell sizes can readily be tuned upon varying the flow rates of the three phases.

Microfluidic devices not only present advantages to prepare microscale particles but also nanoscale ones. Recently, preparation of polymeric nanoparticles has been explored using microfluidic devices to control the size[25], mophology[26] and shape[27,28] of the produced nanoparticles. Two methods were mostly developed depending whether a monomer phase or a polymer phase was used as the starting material. The first method is much comparable to the aforementioned method to produce polymeric microparticles. By applying a specific microfluidic device, the monomer phase is emulsified into nanodroplets which are later polymerized. On example of such device was reported by Koehler *et al.*,[29] they fabricated a microhole plate containing 16x48 holes of 20 μm in diameter by photolithographic techniques. The monomer nanodroplets were generated by the shear force caused by the tangential flow of a continuous phase at the surface of a microhole plate through which the dispersed phase was pumped. The second method relies on the so-called solvent displacement method in which a polymer precipitates when its solvent diffuses rapidly in a non-solvent of the polymer. The key point in this method to obtained size-controlled polymer nanoparticles is to promote an extremely fast diffusion of the solvent such as to avoid aggregation and low nanoparticles sizes (down to less than 100 nm). This can be achieved either by producing microdroplets of the polymer solution in a stream of polymer non-solvent by means of microchannel based devices,[30] or by mixing the polymer solvent with its non-solvent in a microstructured mixer such as to produce a staggered stream of the two solutions with lamellae thickness can be as low as 45 μm.[31]

If microfluidic polymer micro and nanoparticles have already found separately applications in many fields such as drug release,[32,33,34] sensorics[35] to name a few, they were scarcely combined to produce new materials like composite/hybrid multi-scale and multi-domain polymeric microparticles. In such objects, polymer nanoparticles and possibly inorganic nanoparticles are selectively embedded into different domains of a polymeric microparticle. These materials could have strong applications in fields such as optical sensors and theranostics.

In this paper, we present a facile microfluidic route to the preparation of core-shell polymer microparticles selectively doped with polymer and metal nanoparticles by following a three-step procedure. Morphological structure and chemical Z-contrast (COMPO) of the microparticles were extensively characterized by SEM and EDXS respectively.

4.2.2 Experimental section

4.2.2.1 Materials

Five components were used to prepare a polymerizable o/w nanoemulsion: monomer (15 vol.%), Ostwald ripening inhibitor (4 wt.%/Monomer), surfactant (2.5 wt.%/Monomer), distilled water (85 vol.%) as well as the organic-soluble photoinitiator (2.5 wt.%/Monomer). Specifically, the oil phase was composed of a mixture containing same weight amount of methyl methacrylate (MMA, 99% purity, supplied by Aldrich) and tri(propylene glycol) diacrylate (TPGDA, supplied by Aldrich), hexadecane (HD, 99% purity, supplied by Sigma Aldrich) as the Ostwald ripening inhibitor and the photoinitiator 1-hydroxycyclohexyl phenyl ketone (HCPK, 99% purity, supplied by Aldrich). Note that TPGDA also acted as a crosslinker due to its two double bonds. The water phase comprised distilled water and sodium dodecyl sulfate (SDS, 95% purity, supplied by Sigma Aldrich) as a surfactant. The double droplets core phase was composed of the above poly(TPGDA-co-MMA) colloidal suspension admixed with a water-soluble photoinitiator (Genocure DMHA, supplied by Rahn, 5 wt.%/water-soluble monomer), a hydrophilic monomer (Acrylamide, 97% purity, supplied by Aldrich, 40 wt.%/water in the colloidal suspension), a crosslinker (N,N'-methylene-bisacrylamide, MBA, 99% purity, 10 wt. %/water-soluble monomer, supplied by Sigma Aldrich) and Tetrachloroauricacid trihydrate ($AuHCl_4 \bullet 3H_2O$, $\geq$ 99.5%, supplied by Roth, 0.17 wt.%/colloidal suspension). The double droplets shell

phase was composed of pure TPGDA, span80 surfactant (3.5 wt.%/TPGDA, supplied by Fluka), HCPK (99% purity, 3.5 wt.%/TPGDA, supplied by Aldrich), diethylene glycol (DEG, 99% purity, 99%, 10 vol.%/Monomer, supplied by Acros) and silver nitrate salt ($AgNO_3$, 0.17 wt.%/Monomer, supplied by VWR). Finally, the carrier fluid during the synthesis of core-shell microparticles was composed of an aqueous solution of 2 wt.% methyl cellulose (supplied by Alfa Aesar). Ascorbic acid (supplied by VWR) and silver nitrate were used for the silver enforcement. Distilled water was used throughout the experiment.

4.2.2.2 First step: preparation of the polymerizable nanoemulsion

Figure 8 depicts the schematic drawing of the elongational-flow microprocess used to produce the polymerizable nanoemulsion. It mainly consisted in two mid pressure syringe pumps (neMESYS Mid Pressure Module, Cetoni), two 25 mL stainless steel syringes and one PEEK tee (Valco Vici) as the elongational-flow microemulsifier/micromixer. The syringe pumps were controlled by the manufacturer's software and were forced to operate in opposite phase (withdraw/infuse) so as to induce a reciprocating flow rate (RFR) of 20 mL/min through the micromixer. A back and forth movement of the pumps counts for one cycle. The micromixer consisted in three drilled microchannels having a bore size of 150 μm. Two of these microchannels were connected to the two 25 mL stainless steel syringes (Cetoni) by two PTFE tubing (1.06 mm ID x 1.68 mm OD). The third microchannel was used to recover the nanoemulsion once the operation was finished. The TPGDA/MMA oil and water phases composing the nanoemulsion were directly charged without premix into one stainless steel syringe for a total volume of 5 mL. Then, the pumps were switched on. After 200 cycles, one pump was switched off in its zero volume position while the second one pumped the freshly prepared nanoemulsion (a milky-like solution) through the recovery microchannel where it was collected for second step.

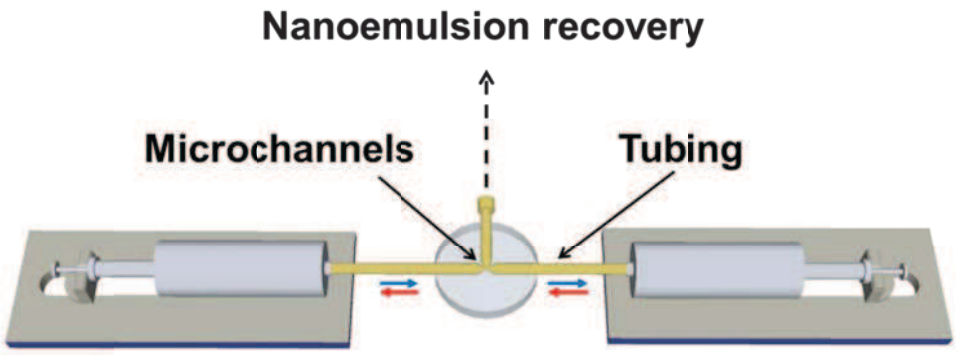

Figure 8 Schematic drawing of the microprocess to prepare the polymerizable nanoemulsion (not at scale).

4.2.2.3 Second step: preparation of the colloidal suspension derived from the polymerizable nanoemulsion

The freshly-prepared nanoemulsion was polymerized by UV irradiation in a tube-in-tube device shown in Figure 9.4 mL of the above nanoemulsion were charged in a 5 mL plastic syringe (HSW). Then the syringe was placed in the holder of a syringe pump (PHD 2000, Harvard Apparatus) aiming at delivering the nanoemulsion through a 22 cm long PTFE tubing (1.68 mm ID x 3.2 mm OD) at a constant flowrate of 0.025 mL/min. The PTFE tubing was inserted inside a 4 cm ID stainless steel tube equipped at both ends with a T-junction (Swagelok) in which was set one of the two light guides of an UV source (Lightningcure LC8, Hamamatsu) operating at λ = 365 nm; a wavelength corresponding to the maximum of absorbance of the photoinitiator added into the nanoemulsion monomer phase. Given the size of the PTFE tubing and the flow rate, the residence time of the nanoemulsion under the UV irradiation was about 20 min. At the end of the PTFE tubing, the polymerized nanoemulsion, i.e. colloidal suspension of polymer nanoparticles, was collected in a vial.

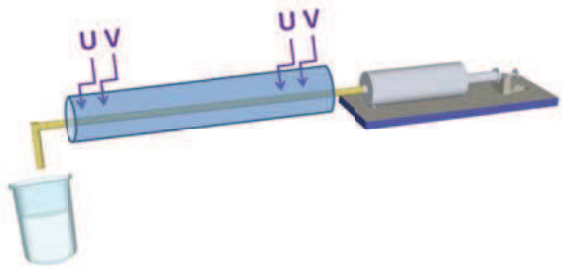

Figure 9 Schematic drawing of the UV-initiated polymerization setup to convert the polymerizable nanoemulsion into a colloidal suspension of polymer nanoparticles (not to scale).

4.2.2.4 Third step: production of core-shell microparticles by a co-axial capillaries-based microfluidic droplet generator

Acrylamide, MBA, Genocure DMHA and gold salt were first added step by step to the freshly prepared nanosuspension under vigorous agitation to form the core phase of the core-shell microparticles. Then, the mixture was left stirred for an additional 10 min protected from ambient UV light by aluminum foil in order to prevent unwanted reduction of the gold salt. Meanwhile, the shell phase was prepared by dissolving the silver salt in DEG and pouring the resulting solution in a mixture of span80, HCPK and TPGDA. The carrier phase was prepared separately by dissolving the methyl cellulose in distilled water. Then all three aforementioned phases were injecting in the co-axial capillaries-based microfluidic droplet generator of Figure 10 by means of three distinct syringe pumps (PHD 2000, Harvard Apparatus) operating at the following flow rates: Q_{core} = 1.5 µL/min, Q_{shell} = 4 µL/min, $Q_{carrier}$ = 130 µL/min. The droplet generator consisted in a set of two 1/16" T-junction (Upchurch Scientific) and 2 co-axially arranged fused silica capillaries (Polymicro Technologies). The inner capillary (100 µm ID × 165 µm OD) served to inject the core phase while the middle capillary (530 µm ID × 670 µm OD) allowed delivering the shell phase. Both capillaries tips were placed in the centerline of another PTFE tubing (1.68 mm ID x 3.2 mm OD). Upon contact at the tips of the 2 capillaries, the three phases gave rise to

the production of core-shell microdroplets. The formation of such double droplets and methods to make variation of overall droplet and core sizes are reported in a previous paper.[24] Two centimeters downstream the double droplet formation, the same UV-arrangement used in second step was utilized to polymerize the microdroplets into core-shell microparticles and to reduce the metal salts. Given the flow rate of the carrier fluid and length of the UV-arrangement (22 cm), the residence time of a droplet under UV light was about 4 seconds. At the end of the UV-arrangement, the microparticles were collected into a beaker and washed with distilled water 3 times to remove the excess methyl cellulose. Then a filter paper was used to separate the microparticles from the aqueous solution. Finally, the microparticles were allowed to dry overnight at room temperature.

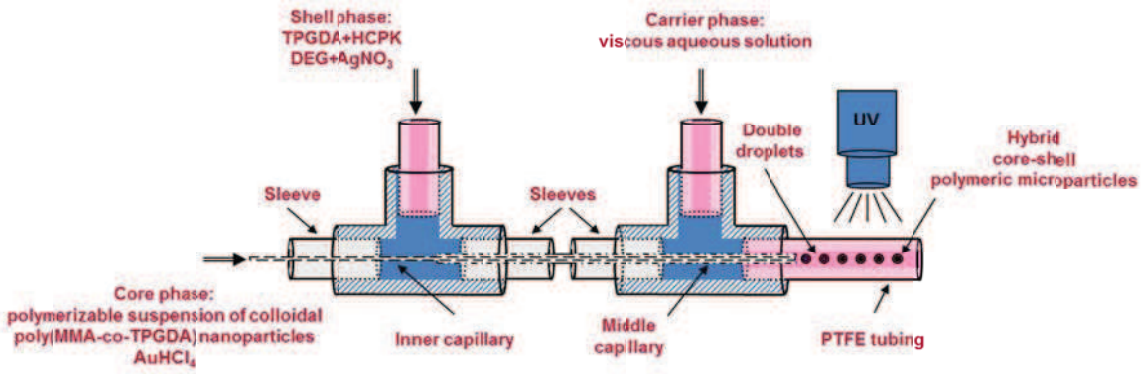

Figure 10 Schematic drawing of the co-axial capillaries-based microfluidic droplet generator for the production of double droplets that were hardened downstream into core-shell microparticles by UV-initiated polymerization.

4.2.2.5 Silver reinforcement

For the silver reinforcement experiment, two different aqueous solutions were prepared; the first one contained 3 mmol/L of ascorbic acid and the second one 2mmol/L of silver nitrate. Then few core-shell microparticles were immersed into 50 µL of the first aqueous solution in a vial. Next, 50 µL of the silver nitrate aqueous

solution was poured into the vial. The reduction of the silver salt was allowed for few minutes under gentle stirring. Finally, the core-shell microparticles were recovered by paper filtration and allowed to dry overnight at room temperature. Upon all these different steps, the particle morphology that was targeted is represented in Figure 11.

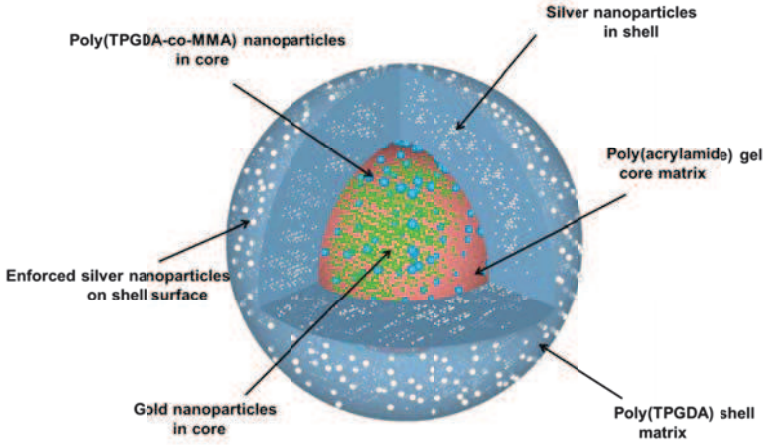

Figure 11 Schematic drawing of a targeted core-shell polymeric microparticle doped with organic and inorganic nanoparticles.

4.2.2.6 Characterization

Composite/Hybrid microparticles were observed by scanning electron microscopy (S4800, Hitachi and JSM-6380, JEOL) to observe their surface and inner structure.[36] For the latter, microparticles were cut into pieces with a sharp razor blade. SEM secondary electron images and back-scattered electrons images in chemical Z-contrast (COMPO) were recorded (JEOL 6700F) and energy dispersive X-rays spectrometry (EDXS) (Thermo-Noran Vantage) was performed to identify the chemical composition. A single microparticle was fixed in a specific holder from Leica and trimmed with a cryotrim diamond knife to have a flat surface rendering the core shell structure visible and EDX analysis. (Ultramicrotom, UCT, Leica).

4.2.3 Results and discussion

Figure 12 shows a snapshot of several composite/hybrid polymer microparticles as prepared following the aforementioned three step procedure. Each microparticle presents a black/reddish central part which is attributed to the gold nanoparticles. Indeed a solution of about 10 nm gold NPs has a red appearance.

Figure 12 Image of dried composite/hybrid core-shell microparticles.

A microparticle was ultramicrotomed to unveal the core-shell structure. Figure 13 is a characteristic SEM mirograph. The small black arrow points to the cut shell. It has a thickness around 100 microns. The poly(TPDGA) appears at low magnification like a continuous phase. The long black arrow indicates the cut retracted core, with a limited core-shell interface pointed by the two arrowheads. The white arrow shows the empty space created by the drying process of the microparticle. Indeed, removing the water from the poly(acrylamide) hydrogel induced the core to shrink and as such appears like a hazelnut.

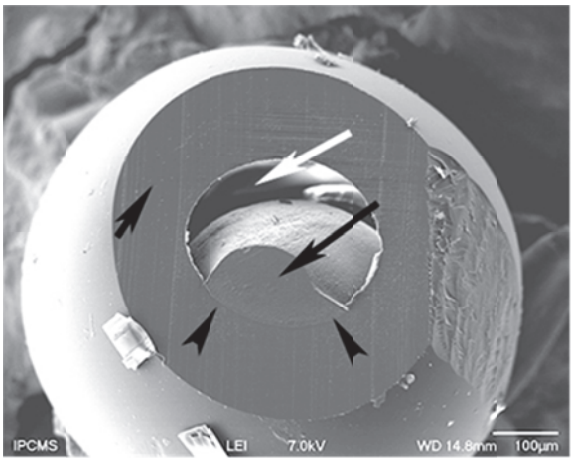

Figure 13 SEM micrograph of a core-shell polymeric microparticle.

A close look at the interface can be seen at high magnification in Figure 14. The small and long black arrows point to the shell and the core, respectively. The parallel strips are a cutting artifact due to the knife clearly seen in the shell region. Empty holes are detected within the shell region (white arrow). They are not seen homogeneously distributed in the shell. We suspect that the aqueous DEG used as a dispersion medium for the silver salt is expelled during the organic TPGDA polymerization process, resulting in drops formation. The drying process has left empty holes. The core region appears granular. To better characterize it, we have fractured a microparticle and observed the inner core region as shown in Figure 15. This preparation step avoids the smearing effect of the knife seen in Figure 14.

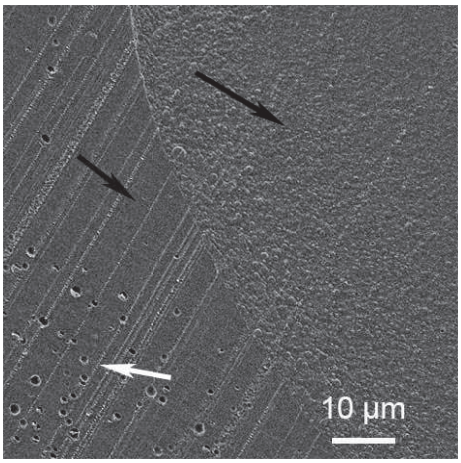

Figure 14 High magnification of the microparticles core-shell interface.

The SEM micrograph of Figure 15 shows the inner structure of the microparticles core and clearly reveals the presence of about 300 nm poly(TPGDA-co-MMA) nanoparticles embedded in the poly(acrylamide) core matrix.

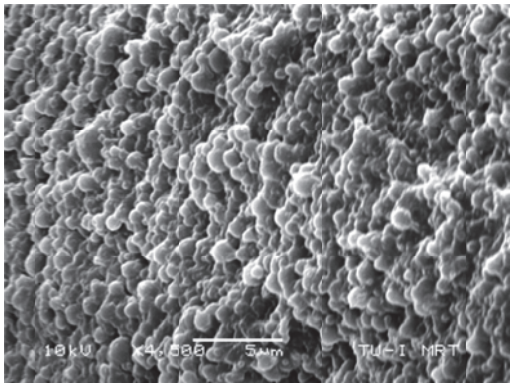

Figure 15 SEM micrograph of the poly(acrylamide) core matrix exhibiting the presence of poly(TPGDA-co-MMA) nanoparticles.

In Figure 16, compo image of the shell region shows the presence of metallic nanoparticles (black arrows). The majority of NPs are located in the vicinity of the empty holes. This corroborates our assumption that DEG has been expelled from the organic matrix during polymerization, leading to the presence of NPs in the holes. The

nature of those NPs is confirmed by X-Rays analysis to be silver (long arrows) or in rare cases gold (short arrows). The unexpected presence of gold NPs inside the shell could be an artefact due to the cutting step.

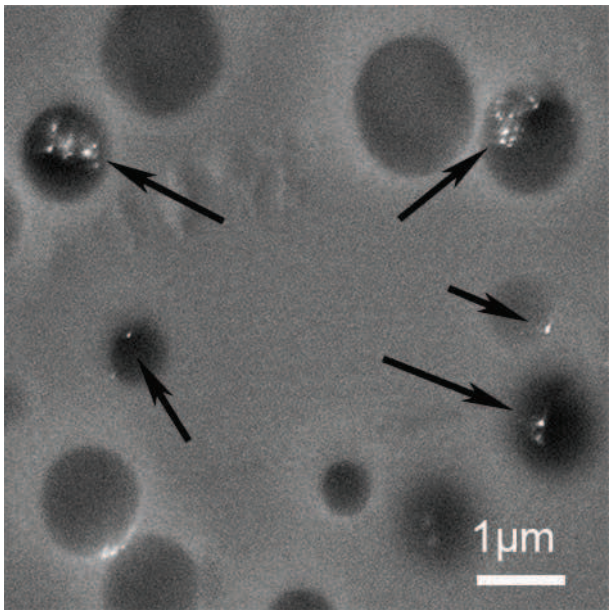

Figure 16 SEM compo image of a shell region.

As for the core, the presence of supposedly metallic NPs is confirmed by compo images (Figure 17). Unfortunately, due to the electron beam sensitive nature of the poly(acrylamide) core matrix, we were not able to perform EDXS analysis before melting of the analyzed region.

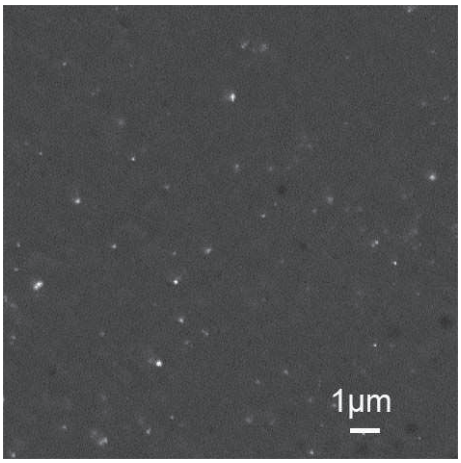

Figure 17 SEM compo image of a core region.

To better confirm the presence of Ag NPs at the microparticles surface, we used silver reinforcement technique. These NPs served as seeds for the synthesis of Ag^0 obtained from the reduction of the silver salt by the ascorbic acid. As a consequence, the large Ag nanoparticles (300 nm) to be seen at the surface of the microparticles (Figure 18) testify of the presence of these original Ag NPs produced during the UV-irradiation of the double microdroplets. One can assume that during the droplet formation, DEG and silver salt present in the shell phase (TPGDA) may have migrated toward the outer surface in contact with the aqueous carrier fluid because of their higher affinity with an hydrophilic compound (water) than with a hydrophobic one (TPGDA).

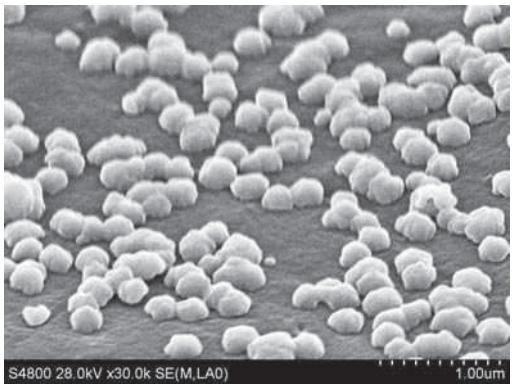

Figure 18 SEM micrograph of the surface of a core-shell polymeric microparticle after silver reinforcement. The silver particles are seen white due to the Z-contrast imaging.

4.2.4 Summary

A new facile microfluidic route to the synthesis of core-shell polymeric microparticles doped with organic and inorganic nanoparticles is presented. The approach follows a three-step procedure. First of all, a TPGDA/MMA oil-in-water nanoemulsion was produced in an elongational-flow microprocess. Then the monomers nanodroplets were polymerized by a continuous-flow UV-initiated miniemulsion polymerization process to give rise to a colloidal suspension of polymer nanoparticles. The nanosuspension was then admixed with a water-soluble monomer (acrylamide) and gold salt. Resulting solution composed the core phase of a co-axial capillaries-based microfluidic droplet generator which produced size-controlled double droplets. The shell phase was composed of a TPGDA, DEG and silver salt mixture. Finally online UV-irradiation allowed the double droplets polymerization and metal salt reduction. Resulting 800 μm core-shell composite/hybrid polymeric microparticles were extensively characterized by scanning electron miscopy and energy dispersive X-rays spectrometry. Analyses revealed the truly core-shell morphology, the presence of poly(TPGDA-co-MMA) nanoparticles of 300 nm in the poly(acrylamide) core along with supposedly gold nanoparticles, the presence of principally silver particles in the inner and outer surfaces of the poly(TPGDA) shell as well as in spherical regions of supposedly DEG compound inside the shell. After a silver reinforcement procedure, bigger silver nanoparticles (300 nm) were revealed at the surface of the microparticles.

4.2.5 References

1. Whitesides, G. M., The origins and the future of microfluidics. *Nature* **2006,** *442* (7101), 368-373.

2. Elvira, K. S.; i Solvas, X. C.; Wootton, R. C., The past, present and potential for microfluidic reactor technology in chemical synthesis. *Nature chemistry* **2013,** *5* (11), 905-915.

3. Illg, T.; Löb, P.; Hessel, V., Flow chemistry using milli-and microstructured reactors—from conventional to novel process windows. *Bioorganic & medicinal chemistry* **2010,** *18* (11), 3707-3719.

4. Abou-Hassan, A.; Sandre, O.; Cabuil, V., Microfluidics in inorganic chemistry. *Angewandte Chemie International Edition* **2010,** *49* (36), 6268-6286.

5. Park, J. I.; Saffari, A.; Kumar, S.; Günther, A.; Kumacheva, E., Microfluidic synthesis of polymer and inorganic particulate materials. *Annual Review of Materials Research* **2010,** *40*, 415-443.

6. Dendukuri, D.; Doyle, P. S., The Synthesis and Assembly of Polymeric Microparticles Using Microfluidics. *Advanced Materials* **2009,** *21* (41), 4071-4086.

7. Engl, W.; Backov, R.; Panizza, P., Controlled production of emulsions and particles by milli- and microfluidic techniques. *Current Opinion in Colloid & Interface Science* **2008,** *13* (4), 206-216.

8. Serra, C. A.; Chang, Z., Microfluidic-assisted synthesis of polymer particles. *Chemical engineering & technology* **2008,** *31* (8), 1099-1115.

9. Steinbacher, J. L.; McQuade, D. T., Polymer chemistry in flow: New polymers, beads, capsules, and fibers. *Journal of Polymer Science Part A: Polymer Chemistry* **2006,** *44* (22), 6505-6533.

10. Serra, C. A.; Chang, Z., Microfluidic-Assisted Synthesis of Polymer Particles. *Chemical Engineering & Technology* **2008,** *31* (8), 1099-1115.

11. Decker, C., The use of UV irradiation in polymerization. *Polymer International* **1998,** *45* (2), 133-141.

12. Sugiura, S.; Nakajima, M.; Itou, H.; Seki, M., Synthesis of polymeric microspheres with narrow size distributions employing microchannel emulsification. *Macromolecular rapid communications* **2001,** *22* (10), 773-778.

13. Sugiura, S.; Nakajima, M.; Seki, M., Preparation of monodispersed polymeric microspheres over 50 μm employing microchannel emulsification. *Industrial & engineering chemistry research* **2002,** *41* (16), 4043-4047.

14. Thorsen, T.; Roberts, R. W.; Arnold, F. H.; Quake, S. R., Dynamic pattern formation in a vesicle-generating microfluidic device. *Physical review letters* **2001,** *86* (18), 4163.

15. Nisisako, T.; Torii, T.; Higuchi, T., Droplet formation in a microchannel network. *Lab on a Chip* **2002,** *2* (1), 24-26.

16. Cristini, V.; Tan, Y.-C., Theory and numerical simulation of droplet dynamics in complex flows—a review. *Lab on a Chip* **2004,** *4* (4), 257-264.

17. Serra, C.; Berton, N.; Bouquey, M.; Prat, L.; Hadziioannou, G., A predictive approach of the influence of the operating parameters on the size of polymer particles synthesized in a simplified microfluidic system. *Langmuir* **2007,** *23* (14), 7745-7750.

18. Panizza, P.; Engl, W.; Hany, C.; Backov, R., Controlled production of hierarchically organized large emulsions and particles using assemblies on line of co-axial flow devices. *Colloids and Surfaces A: Physicochemical and Engineering Aspects* **2008,** *312* (1), 24-31.

19. Quevedo, E.; Steinbacher, J.; McQuade, D. T., Interfacial polymerization within a simplified microfluidic device: capturing capsules. *Journal of the American Chemical Society* **2005,** *127* (30), 10498-10499.

20. Utada, A. S.; Fernandez-Nieves, A.; Stone, H. A.; Weitz, D. A., Dripping to jetting transitions in coflowing liquid streams. *Physical review letters* **2007,** *99* (9), 094502.

21. Garstecki, P.; Fuerstman, M. J.; Stone, H. A.; Whitesides, G. M., Formation of droplets and bubbles in a microfluidic T-junction-scaling and mechanism of break-up. *Lab on a Chip* **2006,** *6* (3), 437-446.

22. Jeong, W. J.; Kim, J. Y.; Choo, J.; Lee, E. K.; Han, C. S.; Beebe, D. J.; Seong, G. H.; Lee, S. H., Continuous Fabrication of Biocatalyst Immobilized Microparticles Using Photopolymerization and Immiscible Liquids in Microfluidic Systems. *Langmuir* **2005,** *21* (9), 3738-3741.

23. Nie, Z.; Xu, S.; Seo, M.; Lewis, P. C.; Kumacheva, E., Polymer particles with various shapes and morphologies produced in continuous microfluidic reactors. *Journal of the American chemical society* **2005,** *127* (22), 8058-8063.

24. Chang, Z.; Serra, C. A.; Bouquey, M.; Prat, L.; Hadziioannou, G., Co-axial capillaries microfluidic device for synthesizing size-and morphology-controlled polymer core-polymer shell particles. *Lab on a Chip* **2009,** *9* (20), 3007-3011.

25. Hung, L.-H.; Teh, S.-Y.; Jester, J.; Lee, A. P., PLGA micro/nanosphere synthesis by droplet microfluidic solvent evaporation and extraction approaches. *Lab on a Chip* **2010,** *10* (14), 1820-1825.

26. Ishizaka, T.; Ishigaki, A.; Suzuki, A.; Suzuki, T. M.; Kawanami, H., A Facile and Continuous Fabrication of Polyimide Hollow Nanoparticles Using a Microfluidic System. *Chemistry Letters* **2012,** *41* (3), 221-223.

27. Visaveliya, N.; Köhler, J. M., Role of Self-Polarization in a Single-Step Controlled Synthesis of Linear and Branched Polymer Nanoparticles. *Macromolecular Chemistry and Physics* **2015,** *216* (11), 1212-1219.

28. Visaveliya, N.; Köhler, J. M., Control of Shape and Size of Polymer Nanoparticles Aggregates in a Single-Step Microcontinuous Flow Process: A Case of Flower and Spherical Shapes. *Langmuir* **2014,** *30* (41), 12180-12189.

29. Koehler, J.; Moeller, F.; Schneider, S.; Guenther, P.; Albrecht, A.; Gross, G., Size-tuning of monodisperse PMMA nanoparticles by micro-continuous-flow polymerization using a silicon micro-nozzle array. *Chemical Engineering Journal* **2011,** *167* (2), 688-693.

30. Hung, L.-H.; Teh, S.-Y.; Jester, J.; Lee, A. P., PLGA micro/nanosphere synthesis by droplet microfluidic solvent evaporation and extraction approaches. *Lab chip* **2010,** *10* (14), 1820-1825.

31. Bally, F.; Garg, D. K.; Serra, C. A.; Hoarau, Y.; Anton, N.; Brochon, C.; Parida, D.; Vandamme, T.; Hadziioannou, G., Improved size-tunable preparation of polymeric nanoparticles by microfluidic nanoprecipitation. *Polymer* **2012,** *53* (22), 5045-5051.

32. Kong, T.; Wu, J.; Yeung, K. W. K.; To, M. K. T.; Shum, H. C.; Wang, L., Microfluidic fabrication of polymeric core-shell microspheres for controlled release applications. *Biomicrofluidics* **2013,** *7* (4), 044128.

33. Khan, I. U.; Serra, C. A.; Anton, N.; Li, X.; Akasov, R.; Messaddeq, N.; Kraus, I.; Vandamme, T. F., Microfluidic conceived drug loaded Janus particles in side-by-side capillaries device. *International journal of pharmaceutics* **2014,** *473* (1), 239-249.

34. Khan, I. U.; Serra, C. A.; Anton, N.; Vandamme, T., Continuous-flow encapsulation of ketoprofen in copolymer microbeads via co-axial microfluidic device: Influence of operating and material parameters on drug carrier properties. *International journal of Pharmaceutics* **2013,** *441* (1), 809-817.

35. Köhler, J. M.; März, A.; Popp, J. r.; Knauer, A.; Kraus, I.; Faerber, J.; Serra, C., Polyacrylamid/silver composite particles produced via microfluidic photopolymerization for single particle-based SERS microsensorics. *Analytical chemistry* **2012,** *85* (1), 313-318.

36. Sawyer, L.; Grubb, D.; Meyers, G. F., *Polymer microscopy*. Springer Science & Business Media: 2008.

CHAPTER 5
CONCLUSION AND PERSPECTIVES

5.1 Context and objectives

Microfluidic devices were proved to be quite efficient systems to produce microdroplets with a high control on their size and size distribution. Polymeric microparticles with different shapes (sphere, high aspect ratios particles) and different morphologies (plain, Janus, core-shell) can be easily produced from the thermally-induced or UV-initiated polymerization of above polymerizable microdroplets.

On the other hand, microfluidic devices were also found recently as excellent candidates to produce monodispersed polymeric nanoparticles either from monomer nanodroplets or by nanoprecipitation of a preformed polymer.

Although both "worlds" (microfluidic nanodroplets and microfluidic micropdroplets) allow producing size controlled polymeric particles at the micro- and nanoscale, they were never readily merged to prepare even more morphologically complex particles like composite/ hybrid multi-scale and multi-domain polymeric microparticles.

In this context, this work aimed at producing such kind of particles by first developing a new scalable and low energy consumption microfluidic process for the production of size-controlled polymerizable nanoemulsions; second by polymerizing the latter to get colloidal suspensions of polymer nanoparticles and third, by using these nanosuspensions as the dispersed phase in different capillaries-based microfluidic droplet generators to finally prepared multi-scale and multi-domain polymeric microparticles doped with polymer nanoparticles and noble metal nanoparticles.

5.2 Results

This work has demonstrated the possibility of producing monodispersed MMA-based nanoemulsions of controlled sizes (50-300 nm) using a newly batch elongational-flow microfluidic process operating at very low pressure (< 8 bars). Its working principle is based on a strong elongational-flow obtained from the reciprocating flow through the sharp restriction (microchannel) of a micromixer placed in the flow of an o/w

emulsion. Compared to several restrictions in series, the microprocess operates at a much lower pressure drop since the latter is only imposed by one transfer through the microchannel. Also compared to more conventional emulsifiers (high pressure homogenizer or rotor-stator devices), the developed microprocess promote an elongational flow which from the early work of Taylor is known to be more efficient, in contrast to shear flow, to rupture dispersed phase droplets into smaller ones even when the dispersed phase is more viscous than the continuous phase. Thus the size control is achieved simply by adjusting the process parameters (flow rate through the restriction, the number of cycles) and the geometric characteristics of the elongational-flow micromixer (angle and diameter of the microchannel) without the need of adjusting the amount of surfactant. A dimensional analysis of the developed microprocess allowed to find a correlation between dimensionless numbers (Re and We in others) that perfectly predicted the nanodroplets size based on various operating parameters - those above mentioned as well as the volume fraction of the dispersed phase (up to 50%), the ratio of the viscosity of the dispersed phase and the continuous phase ($3x10^{-2}$ to 14) and the contraction factor.

With some adjustments, the previously developed microprocess was successfully run continuously to produce up to 1 kg/d of nanoemulsions which sizes were also controlled in the range 100 to 250 nm. The reciprocating flow rate (RFR) through the microchannel of the micromixer was found to be the key parameter in controlling the nanodroplets size: the higher the RFR, the smaller were the droplets. The diameter of the microchannel played also an important role in the final nanoemulsion size; reducing the dimension of the microchannel produces smaller droplets but induced a higher operating pressure (up to 8 bars). Compared to the batch version, the inlet flow which crossed the micromixer induced an increase in the nanodroplets size; this resulted directly from the reduction of the residence time of the emulsion in the micromixer. However the steady state in droplet size was reached more rapidly when the inlet flow rate was high; within about 15 minutes compared to more than one hour for the batch mode.

By using a polymerizable dispersed phase containing a monomer (TPGDA, TPGDA-co-MMA 50:50 or MMA), a thermal (AIBN) or photo (HCPK) initiator and an Ostwald ripening inhibitor (HD), the obtained o/w nanoemulsions were converted into size-controlled colloidal suspensions of polymer nanoparticles in the range 87 to 360 nm by thermally-induced or UV-initiated miniemulsion polymerization. Obtained nanoparticles diameters were found to be higher than the diameters of the nanodroplets they originated from. It was assumed that coalescence was favored during the thermally-induced polymerization by the increase in temperature which somehow destabilized the nanoemulsions. As for the UV-initiated method, the highly turbid medium favored the multiple diffusion which in turn reduced the UV light energy and penetration depth through the sample. Thus only a portion of nanodroplets were initiated and non- initiated one served as reservoir for the growing particles.

Finally the aqueous nanosuspensions of poly(TPGDA-co-MMA or TPGDA) nanoparticles were admixed with a proper combination of hydrophilic monomer (acrylamide), crosslinker (MBA) and water-soluble photoinitiator (DMHA) in order to be used as the dispersed phases of two different capillaries-based microfluidic droplet generators. The produced size-controlled microdroplets were finally photopolymerized online and 300 µm plain as well as 500 µm core-shell composite polymeric microparticles doped with lower scale polymer nanoparticles (227 or 360 nm) were obtained. Composite/hybrid polymeric core-shell microparticles were also synthesized and deeply characterized by SEM and EDXS. Analyses revealed the presence of gold nanoparticles in the core and silver nanoparticles in the shell which were synthesized *in situ* from their salt precursors during microdroplets polymerization.

In summary, this work has demonstrated the high efficiency of a novel low energy microfluidic emulsification device for the production of nanoemulsions which were used for the synthesis of composite/hybrid multi-scale and multi-domain polymeric microparticles.

5.3 Perspectives

Such kind of polymer microparticles morphologies are quite challenging to produce with conventional batch processes. Thus it is believed that the microfluidic approach developed during this work will represents in the future a new and facile route to the synthesis of even more complex multi-scale and multi-domain microparticles, e.g. nanoparticles-doped core-multishell or janus microparticles, which may find application in drug, cell or gene delivery, theranostics, sensorics or functional optical materials.

The batch elongational-flow microprocess could be useful for testing dispersed phases which are expensive or available in small quantities because only 0.5 to 1 mL can be used in contrast to conventional methods that require much larger quantities. As for its continuous version, it could be applied to a small production of emulsions with high added value or served as a benchmark for the design of a larger volume production unit.

Still, some mechanisms are not fully understood. For instance, the mechanism of droplet rupturing and the location where it happens, at the entrance of the microchannel, close to its exit, pass the exit? Questions that could find an answer if a proper transparent micromixer is manufactured in conjunction with the use of a high speed CCD camera to record the droplets rupture. Also computational fluid mechanics and heavy simulations may give some insights.

For the continuous version, it would be interesting to run specific experiments to determine the residence time distribution (RTD) and to assess how it can be influenced by the reciprocating and inlet flow rates and size of the restriction.

TPGDA: tri(propylene glycol) diacrylate
MMA: methyl methacrylate
SEM: Scaning electron microscopy
EDXS: energy dispersive X-rays spectrometry
MBA: N,N'-methylene-bisacrylamide
DMHA: genocure
AIBN: azobisisobutyronitrile
HCPK: 1-hydroxycyclohexyl phenyl ketone
HD: hexadecane

5.4 Scientifique production

5.4.1 Articles

(1) Wei Yu, Christophe A. Serra, Ikram Ullah Khan, Shukai Ding, Rigoberto Ibarra Gomez, Michel Bouquey and René Muller, Development of an Elongational-Flow Microprocess for the Production of Size-Controlled Nanoemulsions: Batch Operation, *Chem. Eng. J.*, to be submitted.

(2) Wei Yu, Christophe A. Serra, ShuKai Ding, Rigoberto Ibarra Gomez, Michel Bouquey and René Muller, Development of an Elongational-Flow Microprocess for the Production of Size-Controlled Nanoemulsions: Continuous-Flow Operation, *Chem. Eng. J.*, to be submitted.

(3) Wei Yu, Christophe A. Serra, Meriem Er-Rafik, Marc Schmutz, Isabelle Kraus, Shukai Ding, Michel Bouquey and René Muller, Development of an Elongational-Flow Microprocess for the Production of Size-Controlled Nanoemulsions: Application to the Preparation of Monodispersed Polymer Nanoparticles and Composite Polymeric Microparticles, *Chem. Eng. J.*, to be submitted.

5.4.2 Conference paper

(1) Yu W., N. Visaveliya, I.U. Khan, C.A. Serra, M. Köhler, R. Muller, Y. Holl and M. Bouquey, Production of size-tunable nanoemulsions in an elongational flow microdevice and its application to the synthesis of multi-scale composite polymeric microparticles, In Proc. of *Microfluidics 2014*, Limerick (Ireland), December 10-12, 2014, 7 pages.

5.4.3 Oral communication

(1) Yu W., N. Visaveliya, I.U. Khan, C.A. Serra, M. Köhler, R. Muller, Y. Holl and M. Bouquey, Production of size-tunable nanoemulsions in an elongational flow microdevice and its application to the synthesis of multi-scale composite polymeric

microparticles, In Proc. of *Microfluidics 2014*, Limerick (Ireland), December 10-12, 2014.

5.4.4 Posters

(1) Wei Yu, Christophe A. Serra, Ikram U. Khan, Microfluidic devices for the production of polymeric microparticles and nanoemulsions*, Polymers at interfaces, Summer School in Soft Matter Science*, Mittelwihr (France), July 7-12, 2013.

(2) Wei Yu, Nikunjkumar Visaveliya, Ikram U. Khan, Christophe A. Serra and Michael Koehler, Production of size-tunable nanoemulsions in an elongational flow microdevice and its application to the synthesis of multi-scale composite polymeric microparticles, in Proc. of *13th International Conference on Microreaction Technology - IMRET13*, Budapest (Hungary), June 23-25, 2014.

(3) Yu W., N. Visaveliya, I.U. Khan, C.A. Serra, M. Köhler, R. Muller, Y. Holl and M. Bouquey, Production of size-tunable nanoemulsions in an elongational flow microdevice and its application to the synthesis of multi-scale composite polymeric microparticles, in Proc. of *Microfluidics 2014*, Limerick (Ireland), December 10-12, 2014.

Wei YU

Développement d'un microprocédé discontinu et continu pour la production de nanoémulsions de tailles contrôlées : application à la préparation de microparticules de polymère composites et hybrides

Résumé

L'objectif de ce travail fut de développer et d'étudier les performances d'un microprocédé basse pression à écoulement élongationnel pour la production de nanoémulsions polymérisables de tailles contrôlées et de distributions de taille étroites. Le diamètre des nanogouttelettes a pu être précisément ajusté dans la gamme 50-300 nm en modifiant simplement les paramètres de procédé : le débit réciproque au travers du micromélangeur, le nombre de cycles et la dimension caractéristique du microcanal. Les nanoémulsions produites furent, dans une seconde étape, polymérisées par voie thermique ou par irradiation UV afin de générer des suspensions colloïdales de nanoparticules de polymère de tailles également contrôlées (87-360 nm). Un monomère, un agent de réticulation ainsi qu'un amorceur thermique ou photochimique appropriés furent par la suite ajoutés au milieu continu de ces nanosuspensions. Les solutions résultantes servirent comme phases dispersées dans des générateurs microfluidiques de gouttelettes à capillaires. Les microgouttelettes de taille contrôlée ainsi produites furent polymérisées en ligne par irradiation UV pour donner lieu à des microsphères ou à des microparticules coeur-écorce composites de polymère toutes deux dopées avec des nanoparticules de polymère. Des microparticules composites et hydrides comportant des nanoparticules d'or dans le coeur et d'argent dans l'écorce furent également obtenues grâce à la réduction photochimique *in situ* des sels précurseurs lors de la photopolymérisation des microgouttelettes. Ce travail a démontré l'efficacité d'un nouveau dispositif microfluidique basse énergie pour la production de nanoémulsions et leur emploi pour la synthèse de matériaux polymères morphologiquement complexes.

Mots-clés : microfluidique, écoulement elongationnel, micromélangeur, gouttelette, microparticule, nanoparticule, polymère, composite, hydride

Résumé en anglais

The aim of this work was to develop and to study the performances of a low pressure elongational-flow microprocess for the production of size-controlled polymerizable nanoemulsions with narrow size distributions. Nanodroplets diameter was easily tuned in the size range 50-300 nm by varying the process parameters, namely the reciprocating flow rate through the micromixer, the number of cycles and the characteristic dimension of the microchannel. Obtained nanoemulsions were in a second step thermally or UV-assisted polymerized to give colloidal suspensions of size-tunable polymer nanoparticles (87-360 nm). Then, a proper monomer, crosslinker and thermal- or photo-initiator were added to the continuous phase of these nanosupensions. The resulting mixtures were used as the dispersed phases of two different capillaries-based microfluidic droplet generators. The produced sizecontrolled microdroplets were finally UV polymerized online and plain as well as core-shell composite polymeric microparticles doped with lower scale polymer nanoparticles were obtained. Composite/hybrid polymeric core-shell microparticles were also synthesized for which gold nanoparticles in the core and silver nanoparticles in the shell were synthesized *in situ* from their salt precursors during microdroplets polymerization. This work has demonstrated the high efficiency of a novel low energy microfluidic emulsification device for the production of nanoemulsions which were used for the synthesis of morphologically complex polymeric materials.

Keywords: microfluidics, elongational-flow, micromixer, droplet, microparticle, nanoparticle, polymer, composite, hybrid